DOCTOR OF PHILOSOPHY

Molecule-inserted silicon nanogaps

Phillips, Laurie

Award date:
2011

Awarding institution:
Bangor University

Molecule-Inserted Silicon Nanogaps

A thesis submitted to the
University of Wales
in candidature for the

Degree of
Philosophiæ Doctor

by

Laurie James Phillips

Supervisor: Professor Geoffrey J. Ashwell

PRIFYSGOL
BANGOR
UNIVERSITY

School of Chemistry
Prifysgol Bangor – Bangor University

2011

Contents

Acknowledgements

I would like to take this opportunity to thank Professor Geoffrey J. Ashwell for giving me the opportunity to do this Ph.D., and to the Engineering and Physical Sciences Research Council for my funding. I am grateful to all my colleagues from the Nanomaterials Group, particularly Dr. Ben Robinson, for their help, advice and friendship during my time at Bangor.

Professor Ian R. Gentle deserve thanks for allowing me the use of XPS facilities at the University of Queensland and Kym Ford for help during the collection of results. Thanks must also go to Rachel Tuffin at QinetiQ for providing the silicon nanogap devices so vital to many of my studies. It is also important to thank Professor Colin Lambert and his group at the University of Lancaster for performing theoretical calculations to corroborate my experimental work.

Finally, the greatest of thanks must go to Siân and my family for many years of love and support.

Abstract

Molecular electronics provides a route to extend silicon-based technology and, as shown here, self-assembly offers a simple, scalable, geometrically-independent method of creating molecular layers on gold and silicon substrates. Moreover, reaction of chemical components at the surface of the film provides a convenient method of building complex electroactive molecules and overcomes the solubility problem with long molecular wires. Using an *in-situ* stepwise synthetic approach, in this case by coupling components *via* imine groups, a monolayer can be extended to form complex structures. With careful selection of components, functionality can be introduced and electrical properties tuned.

Quartz crystal microbalance and X-ray photoelectron spectroscopy were used to verify the assembly of molecules onto gold-coated substrates and the subsequent presence of imino groups. The electrical characteristics of various wires were investigated, using scanning tunnelling spectroscopy alongside an additional method that has been developed, using an electromagnetic cantilever. A two-component two-part wire, containing electron-accepting and electron-donating moieties, demonstrated weak rectifying characteristics following the Aviram-Ratner scheme with a current ratio of 4 at ± 1 V. Other systems investigated, for example, by assembling up to seven component units, produce symmetrically conducting molecular wires. Current magnitudes through these wires are *ca.* 1 nA at ± 1 V using a scanning probe.

Significant to molecular electronics, this stepwise imino-coupling technique has been used to bridge electrode gaps. For the first time, using silicon structures, molecules have been covalently bonded to the top and bottom electrodes and then linked to form a molecular bridge. Empty devices, and those with electrodes coated using the aldehyde terminated 4-ethynlybenzaldehyde anchoring molecule exhibit leakage currents in the sub-picoampere range. Bridging occurred after the insertion of different amino-terminated molecules, creating wires that were either *ca.* 3 nm or 6 nm in length. Surface roughness was relied on to produce gaps to match the molecules. The devices exhibit symmetrical I-V curves with lower limiting currents of 12 nA and 10 nA respectively at ± 1 V, which probably correspond to a single bridge or a few connecting molecules. Gold nanogaps have been bridged previously, but this is the first time that a silicon nanogap has been bridged and the molecule covalently bonded to each silicon electrode.

Chapter 1

Introduction

Nanotechnology is a rapidly emerging field of research that holds great potential to influence vast areas of human life.[1–5] It is a broad field, concerned with the properties of materials and devices with one or more dimensions in the sub-100 nanometre regime. It is a modern discipline, with the majority of progress occurring since the early 1980s. However, as early as 1959, the emergence of the field was envisaged by Richard P. Feynman in his talk of December 29th, 'There's plenty of room at the bottom'.[6] During the lecture, he outlined his view that there was a vast area of untapped possibility in materials science. He claimed there was no fundamental physical reason preventing the manipulation of matter atom by atom. It should therefore be possible to inscribe not just a book onto a pin head, but an entire library. While it is debatable how much influence this talk, or its sequels, had on the development of nano-scale science,[7] it is a useful illustration of the exciting possibilities that nanotechnology offers. At the time, Feynman's challenge was merely an speculative dream, but we have now progressed to the point where such a venture is technologically feasible.[8]

While humans are only just beginning to master and control materials at the nano-scale directly, many of the processes on which life depends are essentially nanotechnology. Mechanisms such as protein folding,[9] and bacteria flagella motors[10] are all nano-scale systems. Indeed, it is interesting that deoxyribonucleic acid (DNA) is appearing in nano-science literature on an increasing basis, both as a structural building block and as a path to functionalizing nanotechnological devices.[11,12]

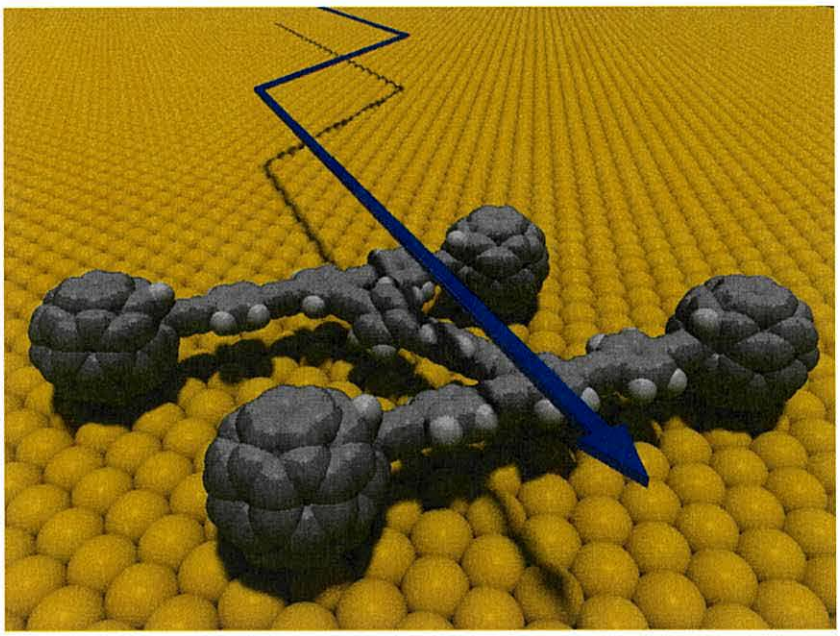

Figure 1.1: A Drexler inspired 'nano-car'. Others have been synthesised that have rudimentary motors or can pivot[13]

Broadly speaking, there are two approaches to nanotechnology. The first was outlined by K. Eric Drexler's in his influential 1986 work 'Engines of Creation: The Coming Era of Nanotechnology'[14] in which he laid out a startling vision of the future populated by miniature machines he called 'universal assemblers'. This view has its roots in the talks of Feynman and the idea of iteratively smaller factories he extolled.[6] These machines are generally constructed of a small number of carbon atoms arranged in strong, rigid, diamond-like latices to mimic macroscopic components such as struts, cogs and axles. They are fitted together in a similar way to their larger counterparts to create moving, actuating machines such as those shown in figure 1.1. Drexler proposed that these nano-bots could manipulate matter atom by atom to take virtually any specified form. In such a way, they could do anything from fight disease to build skyscrapers. However, this view is controversial; such a system would have to overcome the huge influence of certain effects that become dominant at the nanoscale but are largely irrelevant in the macroscopic world. Van de Waal's forces, Brownian motion and surface tension all make the world at the nanometre length-scale very different to the one with which humans are familiar. These factors make it appear as a very hostile environment

for the this rigid, deterministic, hard-nanotechnology stand-point.

The second view takes a different approach, using the nature of the nano-scale world to its advantage. In this soft-nanotechnology paradigm, the inspiration comes from biology and the manner in which life itself operates.[15] Probability plays a much more important role and the desired processes happen because they are made energetically favourable. Now, for example, rather than fighting against the random walk of a molecule, such a process is essential to allow the system to achieve the desirable total energy minimum.

1.1 Current Silicon Technology

One area in which both approaches can work together is that of computing. The impact of computers on modern human life cannot be over-stated. They are involved with almost every activity, from communications and commerce to science and entertainment. Silicon has been fundamental to the development of these computers. Abundant and cheap to obtain, it is unsurprising that it has become such an important material in such a mass-market industry. It is strong and stable and yet easily shaped with plasma or acid etching. Through doping, silicon can also be made into a p-type or n-type semiconductor or insulating as it readily forms silicon dioxide when exposed to oxygen. These possibilities make silicon such a capable material for electronic device fabrication and presents a formidable challenge for emerging technologies that might compete.

Advances in silicon technology have driven progress in computing at an incredible rate, one of the main characteristic trends used to measure this progress has been the ever increasing processing density on silicon chips. Computer processors become smaller even while the number of calculations they can perform per second increases. The most well known formalisation of this trend was by a co-founder of *Intel*, Gordon Moore, when he predicted the doubling of processing speed every two years. This exponential correspondence has remained relevant since its introduction in 1965 and has become known as 'Moore's first law'.[16] Figure 1.2 illustrates the trend graphically. Although it is not a law in any physical sense, it has become the guiding light for the industry, striving to keep up with its inexorable progression.

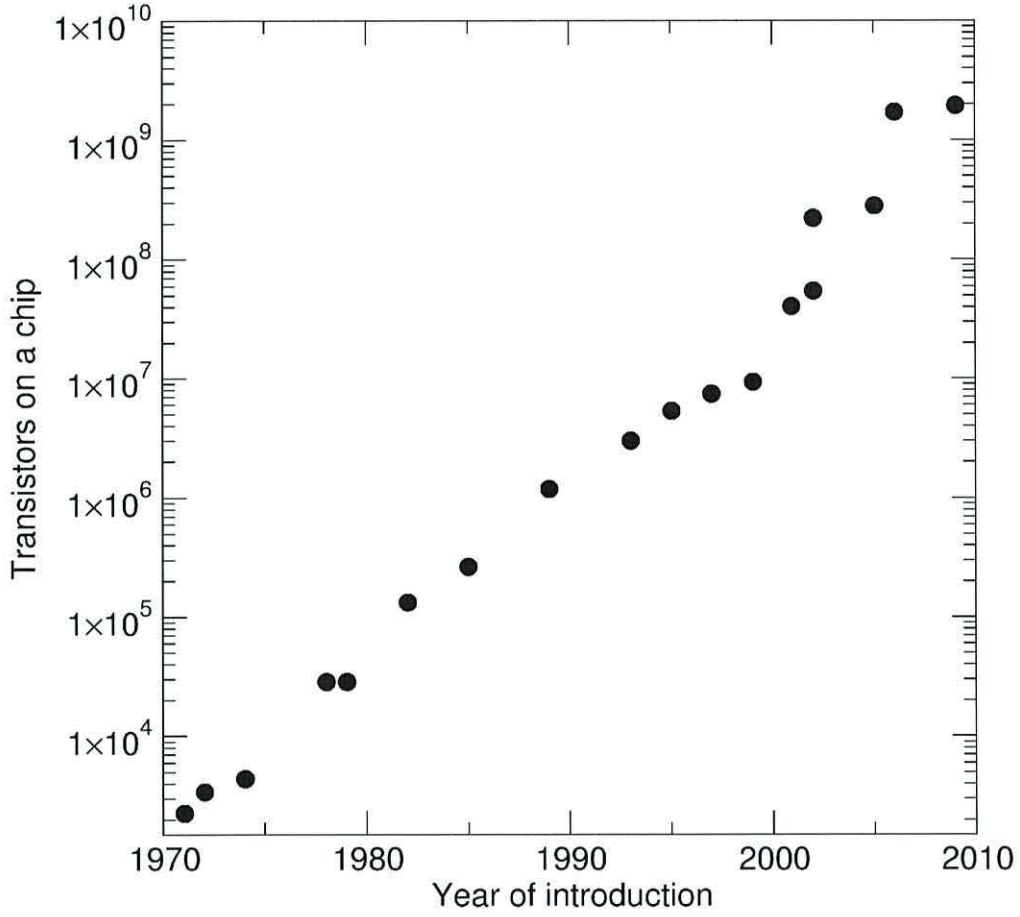

Figure 1.2: Moore's Law, showing the transistor count of a number of processors plotted against their date of introduction. There is a doubling of transistor count approximately every two years.

1.2 Technological Innovations

Unprecedented investment in silicon research has led to greatly improved techniques for processing, resulting in the production of single crystals or silicon of incredible purity and homogeneity. Using the Czochralski technique,[17] a seed crystal is used to draw a single ingot of 99.9999 % pure crystalline silicon from a molten poly-crystalline melt. The silicon is then cut into wafers, cleaned and polished. The quality of the silicon wafers used in making chips has been advanced about as far as it can, but other techniques used during the manufacturing process still present opportunities for improvement and innovation.

1.2.1 Photo-lithography

The integrated circuit was invented by Jack Kilby in 1958.[18] Wiring up the solid state transistors of the time, although a step forward from vacuum tubes, was a very time-consuming procedure that had to be performed by hand. However, Kilby realised that if all the components and their interconnecting wires were built out of the same block of material, device throughput could increase dramatically. Kilby's chip was made of germanium, but almost simultaneously, James Noyce was creating a silicon device that was very similar. This silicon chip solved many of the problems Kilby was having with his when it appeared just half a year later.[19] Silicon chips today still rely on photo-lithography, the same fundamental approach as those very first integrated circuits. This is a process that can involve many steps, but the basics are outlined in Figure 1.3.

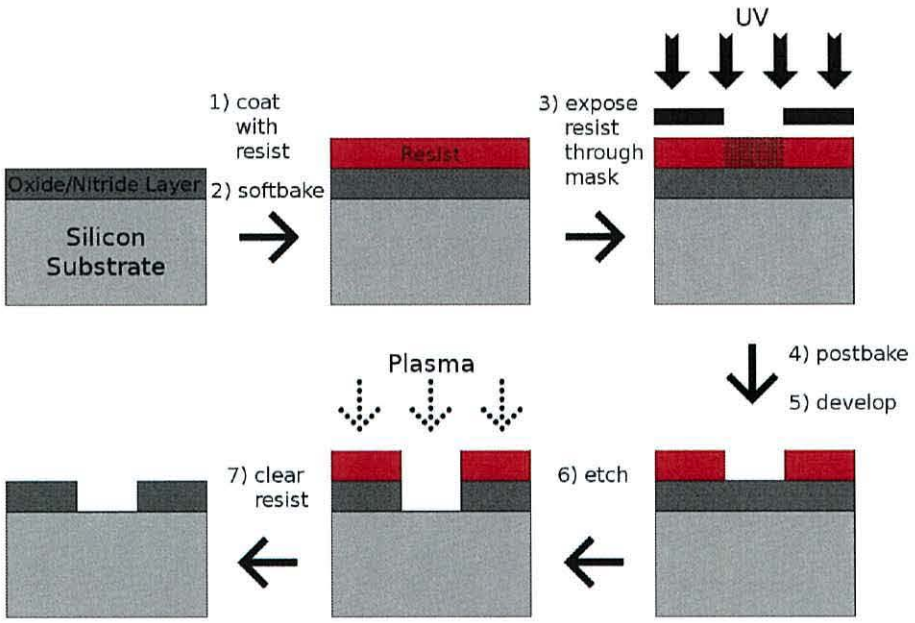

Figure 1.3: Overview of the basic photo-lithographic process

Firstly, a polymer resist is added to the surface of the silicon wafer, usually applied *via* spin-coating. Next, an image of the desired components is projected onto the polymer through a mask. The light selectively hardens parts of the polymer and therefore, when it is subsequently developed in a suitable solvent, the un-radiated polymer is washed away, leaving a mask. The silicon itself is then

etched, with an acid or plasma; the choice depends on if an undercut is required. A plasma etch erodes the material *via* bombardment and so is effective only in the direction of the plasma beam, usually normal to the surface. An acid, however, will react with any surface it comes into and so will open up an aperture in the plane of the surface as well as perpendicular to it. The two processes can be used in sequence to achieve a more complex etch. The polymer resist prevents the etch from occurring except where it is required. When the mask is washed away, the remaining wafer, when combined with doping, contains the correct arrangement of material to produce the components of the chip. Photo-lithography is a top-down technique, whereby a bulk block of material is machined down and material is removed to create the desired configuration. In the case of current processor chips, the silicon wafers that are used have diameters as large as 300 mm, driven by the need to increase throughput, but the ultimate feature size can be less than 100 nm.[20] A large aspect of recent innovation has been to push down this feature size limit, thus allowing more devices to fit onto a wafer. Increased density results in greater processing ability with reduced power consumption and thus is greatly desirable.

The smallest feature size, or critical dimension (CD) that can be produced from a projected image is related to the wavelength of the light λ, the numerical aperture (NA) and the quality factor of the process (κ) by equation 1.1:

$$CD = \frac{\kappa\lambda}{NA} \tag{1.1}$$

The constant of proportionality, κ, is a measure of the defects present in the apparatus. The smaller it is, however, the greater the sensitivity to variations in energy and focus during the exposure. Through continual improvement in manufacturing control, κ has decreased from 0.8 in the 1980s to $\simeq$ 0.3 today. However, it has a limiting value of 0.25 as the sensitivity makes it impossible to form an image below this value.[21]

1.2.1.1 Shortening the Wavelength

From equation 1.1, it is clear that $CD \propto \lambda$ and reducing the wavelength of the radiation producing the mask will reduce feature size. The current commercial

practice is to use a 193 nm ArF eximer laser. This wavelength emits in the far ultraviolet (UV) region of the electromagnetic spectrum. There has been considerable investment in attempting to reduce this wavelength to the vacuum ultraviolet range at 157 nm,[21] but this wavelength is absorbed by water, air, simple organics and even the fused silica traditionally used for lens material. These are considerable challenges to overcome, and the effort has been largely abandoned as infeasible. There is potential to go even smaller, to the extreme UV (EUV) at 11-14 nm[22,23]. This technology has yet to be proven,[24] however, and EUV is not expected to be a viable production tool until at least 2015.

1.2.1.2 Immersion Lithography

While the wavelength of light impacts the feature size of an image it projects, another important factor is that of refraction. As stated in equation 1.1, the critical dimension is inversely proportional to the numerical aperture. However, the numerical aperture relies directly on the refractive index of the medium between the lens and mask. Historically, the exposure of the mask was performed in air, but recently there has been a move to supplant this with a layer of ultra pure water. This technique is known as immersion lithography.[25] To prevent localised heating, the water is constantly cycled; this precaution ensures that the refractive index of the medium is homogeneous and there is no degradation due to distortion. In air, a refracting lens has an upper limit for the NA of 1.0. The higher refractive index of the water allows the NA to increase beyond this limit to $\simeq 1.35$. Ultimately, using higher index liquids such as saturated hydrocarbons and lenses made of high index materials, it should be possible to increase the NA to a value of 1.8.

1.2.1.3 Double Patterning Lithography

Another recent innovation that is helping drive down feature size is known as double patterning lithography (DPL), outlined in Figure 1.4. Two exposures combine to facilitate a critical dimension smaller than that available for each individual exposure.[26]

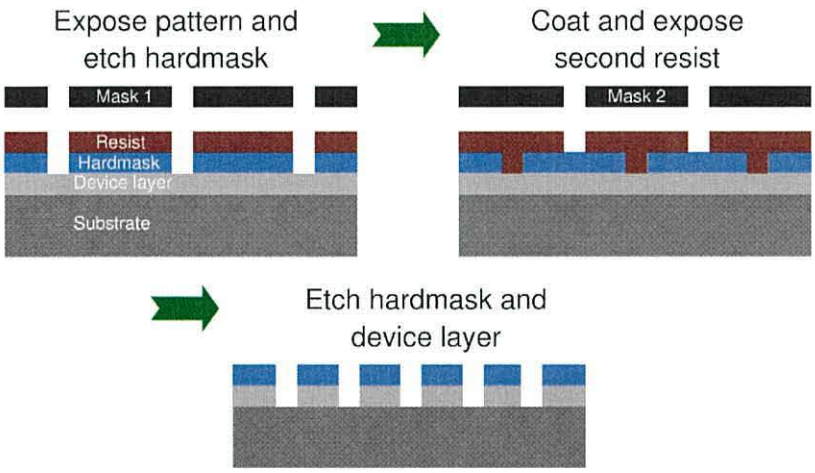

Figure 1.4: Schematic of double patterning process.[27]

Two exposures, both with 30 nm lines and 90 nm half-width can be used to pattern a regular grating of 30 nm with a 30 nm half-width. This procedure is not ideal from a commercial point of view. It requires twice the number of exposures and etch steps and double the amount of material for the resists. It also requires precision in the alignment of the masks of just a few nanometres. An adaptation of this general idea has also been proposed to create a related technique, known as double exposure lithography (DEL), shown in Figure 1.5.[27]

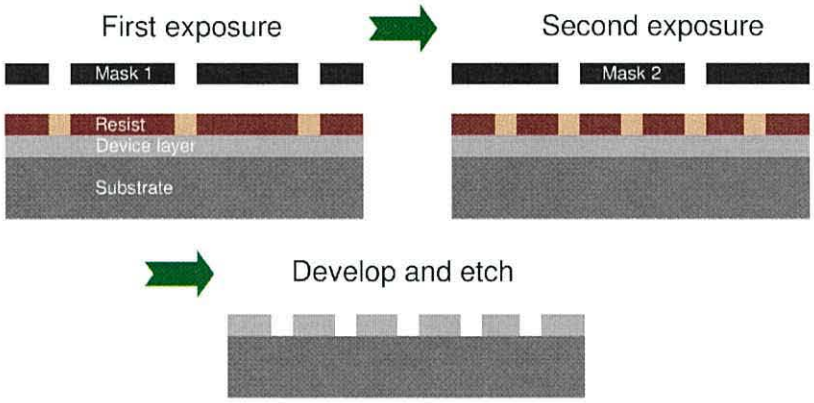

Figure 1.5: Schematic of double exposure process.[27]

If a resist material could be developed that is non-hysteretic for exposures below a certain threshold level, then it will be possible to greatly simplify the

technique and simply expose the same resist twice with two masks and only involve one develop and etch steps. This will have obvious throughput and cost benefits but as yet nothing has been identified that has proven its suitability.

1.2.2 New Materials

Ultimately, silicon can only be pushed so far and it is necessary to utilise alternative materials in certain key areas when the dimensions have shrunk below the operating boundaries of silicon. To combat the gate leakage as described in section 1.3.1 for example, it is possible to use materials with a higher dielectric constant, either a different semiconductor such as gallium-arsenide or a metal oxide such as Al_2O_3, ZrO_2, HfO_2, or Y_2O_3. These materials allow a thicker gate oxide layer to be used without altering the capacitance of the layer. Therefore, for a given channel width there is a reduction in the unbiased tunnelling probability while maintaining the operating currents.[28] In contrast, the interconnects between devices are becoming problematic due to the increased resistance and capacitance of thin channels and there is a move to use material with a lower dielectric constant for these areas. These include silsesquioxanes, doped silica and organic polymers.[29]

1.2.3 Three-Dimensional Advances

Another proposed solution has been to explore the possibilities offered by three-dimensional architecture.[30] Currently, chips are fabricated using lithography in a plane as previously described. By having sections of the transistor extended out of the plane, it is possible to constrain the electrons more effectively. Several potential structure configurations have been proposed and demonstrated. One that shows considerable promise is the finFET, as shown in Figure 1.6.

1.3 Limits and Problems

As mentioned previously, the semiconductor industry has kept pace with the ambitious prediction of Gordon Moore for almost half a century. Many times a problem has appeared impossible to overcome but new innovation and discovery has allowed progress to continue and reach the next stage of development.

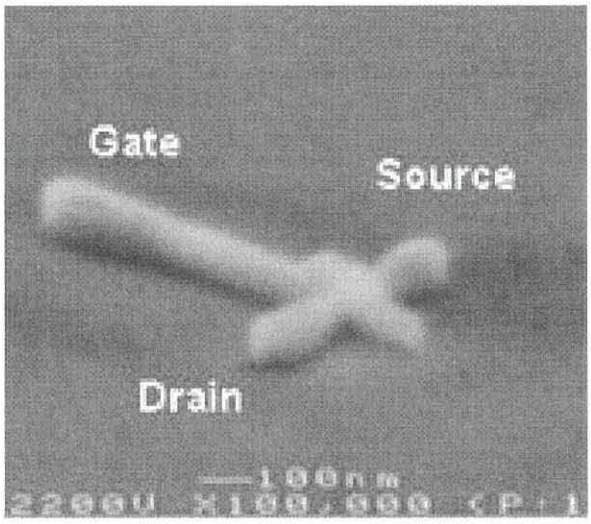

Figure 1.6: An SEM image of an example single channel finFET. Reprinted with permission. Copyright 2002 IEEE.[30]

Unfortunately, as the dimensions of devices shrink below the 32 nm level, silicon based technology is approaching a regime where the limiting factors are not because of technological inadequacies or knowledge gaps but because of well-known fundamental physical properties of matter. The 32 nm technology node is the current benchmark, with the 22 nm node expected to move from the development stage to production in late 2013. The novel techniques currently under investigation will have to mature quickly to allow silicon to be used beyond the current regime. Even if they succeed, the technology is now very close to its ultimate minimum feature size.

1.3.1 Gate Leakage

Classically, the charge-carrying electrons in doped silicon are free to move throughout the material but constrained by boundaries. However, when charge transport channels approach the nanometre regime in one or more dimensions, it is not satisfactory to describe electrons using the classical model. Quantum physics plays an ever more important role as bulk approximations are no longer applicable. Instead, their wave-like nature dominates behaviour. Of particular concern is the fact that the wave packet of an electron will not be contained by a channel

boundary that is of comparable width, but will spread beyond it. Therefore, when a separation layer becomes smaller than a few nanometers, electrons can tunnel across with significant probability. This behaviour has obvious implications for a device such as metal-oxide silicon field-effect transistor (MOSFET). A very common device in computers and other devices, a schematic diagram is shown in Figure 1.7. Without a bias on the gate electrode, there are two p-n junctions formed by the contacts and substrate channel. These act in opposing directions between the source and drain electrodes and stop any electrons from travelling through the device. However, with sufficient bias on the gate electrode, charge carriers accumulate at the channel-oxide interface, switching the doping of the channel in that region. This reversal of the channel eliminates both p-n diodes and allows a current to flow from source to drain.

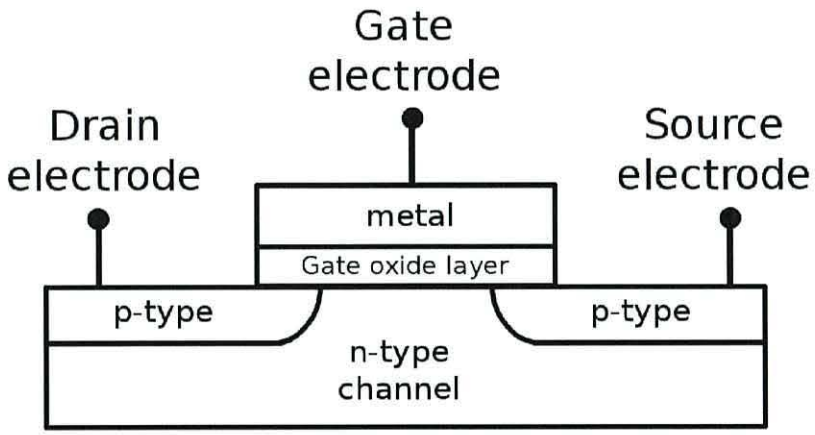

Figure 1.7: A metal-oxide silicon field-effect tranistor (MOSFET) device. It is equally valid to exchange the n-type and p-type regions, the operation is identical.

The gate oxide layer thickness necessarily scales with the channel length. As devices have become smaller, the oxide layer has reached a point where it is only 1.5 nm thick. This thickness equates to just 4 silicon atoms. With such a narrow gap between the gate electrode and channel, electrons are able to tunnel across without the applied bias, thus compromising device integrity.[31]

1.3.2 Heating Problems

All electrical devices experience thermal effects due to their operation. Three common causes of heating in CMOS architecture include Joule or Ohmic heating, thermal recombination and the Thomson effect.[32] As MOSFETs are formed on integrated circuits with ever increasing densities, the problem of localised areas experiencing thermal build-up becomes an ever greater threat to the integrity of the device. Large amounts of thermal energy can disrupt the operation of the circuit, causing cycles to run more slowly and compromising the structural integrity of the transistor. This damage can cause failures and reduce the useful lifetime of a chip. Heat-sinks are a crucial element in any chip design. They are required to be larger or more efficient to cope with increasing demand despite having less room due to the high density.

Excessive heating is particularly problematic in situations such as load switching, a function that MOSFETs are increasingly performing in place of electromechanical relays. Their on-state resistance is high relative to the mechanical relay and thus the Ohmic heating is much greater. Switching a capacitive load can present the device with ten times the steady-state load and has a proportionately higher chance of causing a burn-out.[33] Another example is poly-silicon gate meltdown[34] where stress induced leakage currents, resulting from hydrogen bridge defects cause Joule heating.[35] The melting filaments in the gate have a lower resistance than the rigid lattice and so even more current can flow. This situation can cause thermal runaway where the temperature rises quickly and uncontrollably, ultimately resulting in device failure.

1.3.3 Doping Issues

Another issue that appears as dimensions shrink relates to doping, a process essential for silicon functionality. Atoms with one additional or fewer outer-shell electrons are added to the silicon to create n-type or p-type semiconducting material respectively. This addition has usually been applied *via* a diffusion process. Generally, doping only reliably alters the properties of the silicon because the regions are large relative to a silicon lattice unit cell. Even if the implantation is not perfectly uniform, the average silicon to dopant atom ratio is still correct across

the larger volume. Homogeneity is increasingly important as the doped region shrinks, and eventually, the dimensions will become so small as to render directed doping impossible. For example, a region so small as to require a fractional number doping atoms to maintain the desired ratio is obviously prohibited. However, even before that regime is reached, the simple diffusion process does not offer sufficient control and manufacturers need to move to the costly, but more controlled ion implantation and annealing of the dopants. Therefore, it may become necessary to explore alternative architectures such as those with a double gate, as such a system is not as sensitive to doping level.[36]

1.3.4 Summary

Currently, the silicon chip industry is producing DRAM devices at the 32 nm node. The 22 nm, 16 nm and 11 nm nodes are predicted to be made available from 2016, 2019 and 2022 respectively.[37] The technology in development could be fine-tuned, but there will be no further leap along with Moore's Law using the same basic technology. With each new iteration of the photolithographic silicon process, the cost and difficulty in creating a chip increases dramatically. There needs to be a radical change of direction to prevent the progress of computing development waning.

1.4 Molecular Electronics

Ultimately, we will look to quantum computers to take computational power to its true limit, if indeed there is one. However, quantum computers are still a very long way from being a commercial reality and it will be necessary to look to alternative technologies to extend our current position to that eventual future. Organic molecules have great potential to make progress in this direction.

Molecular electronic components are already being developed that function as well as their rival solid state equivalents.[38,39] By integrating them into devices, not only will they offer an alternative route to pursue Moore's law, but will also provide a characterisation platform to study molecules on the nano-scale. Completely replacing the silicon semiconductor industry with one based on molecules is unrealistic, especially in the short term. However, there are many opportunities

for extending the usefulness of silicon, beyond existing capabilities. For example, a chip can be built of many layers with molecules forming the connections between layers. Three dimensional architecture could allow several times the processing power for the same chip footprint. Upper levels could obstruct those below during assembly and prevent wiring the parts together. However, wires dispersed in a solution would be able to enter between the layers and form the connections.

There is increasing interest in computers that can adapt themselves to broken components or even self-repair.[40] Organic electronics has great potential to fulfil a role in this type of system. Identical, flexible molecular components and the self-assembling process is ideally suited to a cross-linked three-dimensional architecture. This type of system has been referred to as chemically assembled electronic nanotechnology (CAEN).[41]

There are generally two situations in which molecules can be used for their electronic properties. The first takes advantage of bulk assemblies, whereby a complete layer of molecules is used for itself or to modify the properties of a surrounding device. Examples include conducting polymers for large-scale, flexible, 'plastic electronics'[42,43] and the 2 nm thick self-assembled monolayer (SAM) of alkyltrichlorosilanes used in place of a conventional oxide as the gate insulating layer in silicon FET devices,[44,45] which showed reduced leakage currents for equivalent insulator thickness.The second is where molecules act in relative isolation from each other, the ultimate aim of which is for devices to be based on the properties of single molecules. While the first is an undoubtedly important development, it is the second that is the main concern of this thesis.

1.4.1 Brief History of Organic Electronics

The earliest ideas that began the study of molecular conduction came from the pioneering work of Mulliken and Szent-Gyorgi in the 1940s.[46,47] Mulliken produced theories of molecular orbitals, essential to an understanding of molecular charge transport. He also worked on the donor-acceptor charge transfer complexes that would spawn a whole class of devices and inspire Aviram and Ratner's important work, described in section 1.4.3.1. Szent-Gyorgi, meanwhile, was the first to propose a complete theory that suggested proteins molecules might not necessarily act as insulators.[48]

The next important step came when the field was expanded to include electronic functionality to molecules. In 1974, Aviram and Ratner published the first prediction of a unimolecular rectifying device.[49] A decade later, Forrest Carter at the U.S. Naval Research Laboratories produced a series of designs for molecular wires, switches and logic elements.[50–52] These designs, if they were realised experimentally, promised to transform the limited possibilities of simple molecular conductivity into the more useful field of molecular electronics.

Test-bed platforms for analysing molecular components did not exist when the theoretical work was first being done. However, the development of scanning microscopy in the 1980s was a huge leap forward and there has since been an increasing level of interest in the field, both with scanning probe microscopes and other nanoscale experimental platforms. It is important to note that the conductive properties of a molecule have a large number of influences, including contact geometry, molecular chemistry and the electrostatics of the surrounding environment.[53] It is vital that any electrical characteristics are known to be molecular in origin and not from extraneous influences such as small interstitial atomic clusters at the contacts.[54] If a technology is going to be exploited on an industrial scale, it needs to be reliably repeatable. However, homogeneity is one of the great strengths of molecule-based electronics. Every molecule is absolutely identical. Therefore, if it is in identical conditions, each unit will behave in exactly the same way.

The rapid progress and scope of the discoveries in the 1980s and 1990s led to the journal *Science* awarding the field of Molecular Electronics their *'Breakthrough of the Year'* commendation in 2001. Specifically, the award was for:

> Scanning probe microscopes, technologies for producing carbon nanotubes and nanowires made of various materials, and new organic materials that lend themselves to conducting assemblies [and] for the extraordinary accomplishment of arranging them into circuits that can actually perform logical operations: amplify signals, invert current flows, and even perform simple computing tasks.

1.4.2 Organic Wires

The most basic molecular electronic device acts as a wire. It has the simple function of enabling the efficient transport of electrons from one location to another. A good candidate for a molecular wire will possess a number of characteristics. The most obvious is that it must have a good conductance to length ratio, thus facilitating a high degree of electron flow over a large distance. In addition, a wire will ideally consist of compact geometry in the directions perpendicular to that of the charge transfer for easier integration with devices. This will also minimise interference with any material that might be around it. Depending on the situation, a flexible or rigid wire may be preferable as the molecule may be required to manoeuvre into constricted gaps or support other structures. It is possible to inject charge onto a wire through a tunnelling barrier. However, a suitable terminating chemical group at either end will also be useful, both for bonding with contacts to anchor the molecule and for lowering the charge injection energy barrier.

1.4.2.1 Conducting Polymers

Early examples of organic, wire-like materials, are the conducting polymers discovered in the 1970s. For many years after the introduction of polymers, it was believed that they could only be insulating. It took a fortuitous error, when many orders of magnitude extra catalyst were added accidentally during the attempted synthesis of poly-acetylene, that a conducting polymer was realised.[55] In recognition of this break-through, Shirakawa, along with subsequent collaborators MacDiarmid and Heeger, were together awarded the 2000 Nobel prize for chemistry.[56–58] The conductivity of the silvery film created by Shirakawa, when exposed to iodine, was found to increase by up to seven orders of magnitude relative to the unaltered polymer. The halogen acted much like a conventional dopant in solid-state semiconductors. The polymer on its own has π-bonds that are de-localised along the molecule, but will have no net movement when in an applied field. The iodine oxidises the molecule, removing one electron and creating a positively charged polaron.

With one electron missing, the remaining charges can move, thus enabling a current to flow.

1.4.2.2 Saturated and Conjugated Wires

The ability of poly-acetylene to conduct current efficiently comes from its conjugated backbone. Alternating single and double bonds result in a de-localisation of π-electrons along the entire length of the molecule. However, saturated molecules can also be considered molecular wires. A group of molecules that has received considerable interest are the alkane di-thiols (ADTs). These molecules are unlikely to find significant application commercially; they consist of sp^3 hybridized atoms with no free π-electrons. Transport relies on tunnelling and so they are not efficient conductors. However, they are relatively simple systems that are ideal for testing theoretical predictions and experimental methods. ADT molecules contain only σ-bonding throughout and therefore the electrons must rely on tunnelling to get from one end to the other. This is known as superexchange and described in section 1.5.1.

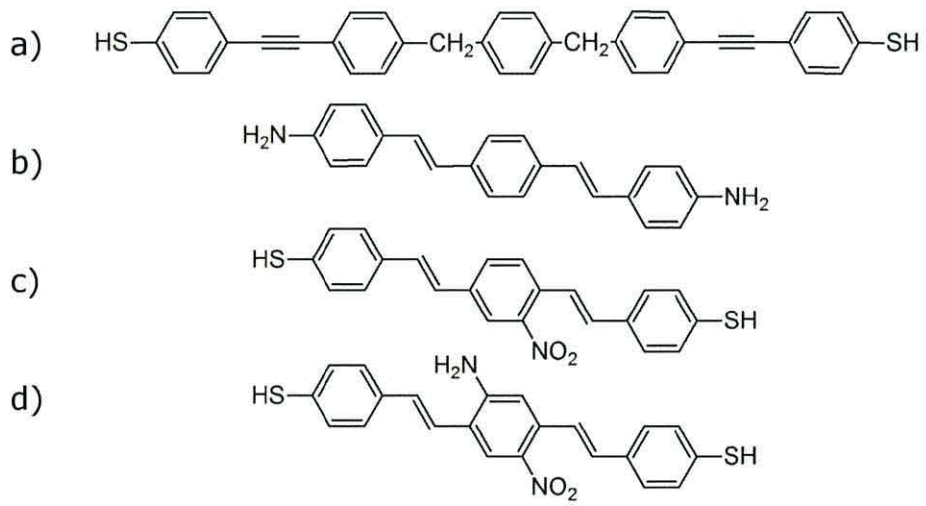

Figure 1.8: Examples of 'Tour wires' devices: an oligo(p-phenylene ethynylene) based resonant tunnelling diode (a) and an oligo(p-phenylene vinylene) based wire (b), rectifier (c) and rotationally controlled switch (d).

One set of molecules that has generated considerable interest are the conjugated oligo(*p*-phenylene ethynylene) (OPE) and oligo(*p*-phenylene vinylene) (OPV) molecules and their derivatives such as those in Figure 1.8. Capable of being modified to perform rectification, negative differential resistance (NDR), charge storage and switching operations, they have been collectively referred to as 'Tour Wires'.[59] Tour et al. also proposed a radical rethink of the way computing systems should operate in the molecular electronics paradigm. He suggested that emulating macroscopic systems directly was undesirable as this involved the movement of large quantities of electrons. Instead, by influencing charge densities, mere fractions of electrons would be needed to provide a signal and therefore perform logic operations. In this way several problems are removed simultaneously. These included energy consumption, dissipation and the resultant heating issues and the cause of impedance fall-off at high frequencies.[60]

The molecules proposed to form the basis of such a computational device are synthesised using a small set of components. These included the OPE and OPV backbones, methylene barrier units, multi-substituted benzenes as connecting hubs and acetyl-protected sulphur units to enable subsequent anchoring of the resultant molecule. Using these components, it was suggested that an array of devices could be assembled, including wires, wires with tunnelling barriers, resonant tunnelling diodes, three-terminal junctions, transistors and even four-terminal logic gates.

1.4.3 Molecular Diodes

After wires, the next simplest class of two-terminal devices is the diode or more precisely, half-wave rectifier. Such a device is a directionally dependent conductor. Ideally it possesses low resistance to charge moving in one direction but is insulating to charge moving in the other. The characteristic property of a diode is its rectification ratio (RR), defined as the ratio of current in the positive and negative quadrants at a particular voltage, usually ± 1 V. This dimensionless factor is formalised by equation 1.2 where the

denominator is arbitrarily chosen to be the smaller of the two values to produce a non-fractional ratio.

$$RR = \left| \frac{I(+1\,V)}{I(-1\,V)} \right| \tag{1.2}$$

An ideal diode will therefore have a $RR = \infty$ as the current will be zero in the insulating direction. In all practical devices, however, there will always be a small current in this reverse bias, even in the best devices due to back scattering and tunnelling. The benchmark, solid state device, that exists at present is the Schottky diode. The operation of this device depends on the Schottky barrier that forms at the interface between a metal and semiconductor with mismatched work-functions when they are brought into contact. The rectification ratio resulting from this junction is typically *ca.* 10^6. It is unlikely that any molecular system will be able to achieve as high a ratio, but it is an unfair comparison as a solid state diode is orders of magnitude larger in size than molecular dimensions. Much of the leakage current in the reverse direction, that acts against rectification, relies on quantum tunnelling. This phenomenon is exponentially more significant across the smaller molecular devices.

1.4.3.1 Aviram-Ratner

While the work on conducting organics was becoming established by the 1970s, it was the ground-breaking 1974 paper by Aviram and Ratner that brought serious consideration to the idea of building functionality into molecules.[49]

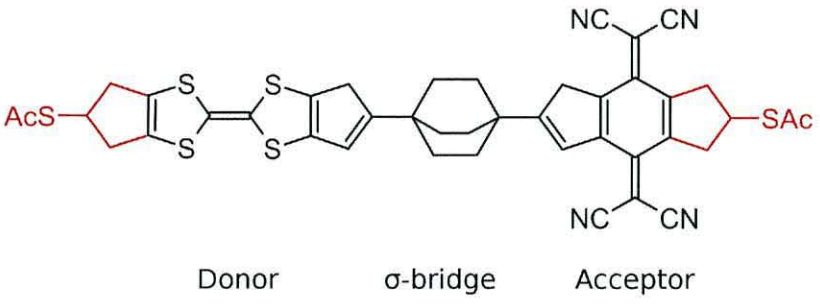

Figure 1.9: The unimolecular rectifier proposed by Aviram and Ratner (black). The additions in red present an option for anchoring the molecule to contacts for characterisation.[49]

The central concept in the paper was the idea that electron donor (D) and acceptor (A) moieties, separated by a σ-bridge, present an arrangement of energy levels that will result in unimolecular rectification. The D-σ-A molecule they proposed is shown in Figure 1.9.

In contrast to a p-n junction semiconductor diode, where the two materials must be adjacent, the electron accepting and donating moieties are kept separate. It is the interaction of these sections of the molecule with the contacts that creates rectification. An energy-level diagram for the molecule, in an unbiased state, is shown in Figure 1.10. There is no energetically favourable path through the molecule in either direction.

There was initially some controversy over the Aviram-Ratner model; it was counter-intuitive when trying to relate the molecular system to a p-n junction. According to the theory, current moving through a molecule, relies on three steps. During the first two steps, an electron tunnels from the cathode on to one end of the molecule, and an electron tunnels from the opposite end of the molecule on to the anode. The third step involves an internal rearrangement of the electrons and relaxes the molecule back to the ground state. The σ-bridge is of vital importance as it keeps the donor and acceptor ends coherent. Without the separation, an electron could pass from the donor to acceptor with the molecule unbiased, thereby neutralising the components. Under forward bias, electrons will be moving into the lowest

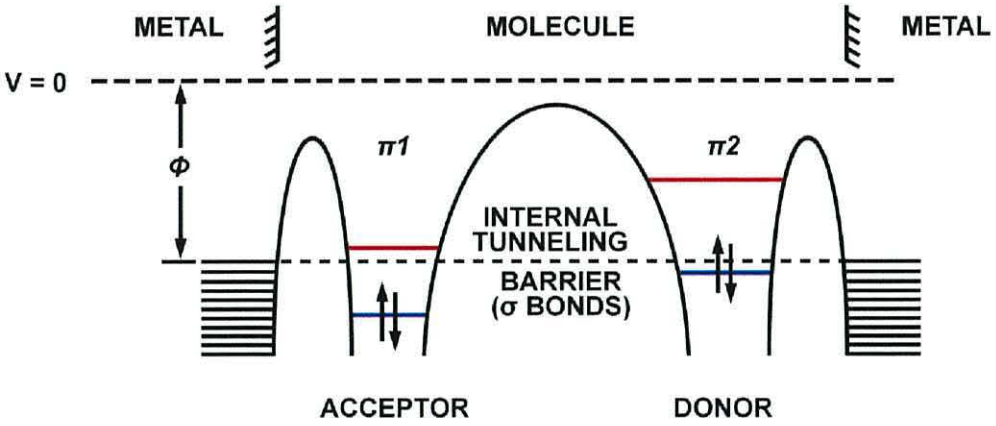

Figure 1.10: Energy level diagrams for a D-σ-A molecular rectifier under equilibrium conditions. ϕ is the workfunction of the metal.[49]

unoccupied molecular orbital (LUMO) of the acceptor and from the highest occupied molecular orbital (HOMO) of the donor moiety. As can be seen from Figure 1.11 (top), this happens readily as it only requires a small amount of energy. In reverse bias, Figure 1.11 (bottom), the opposite is true. Electrons must be forced to higher energy when they are injected onto the LUMO of a donor and taken from the HOMO of an acceptor. To overcome the energy barrier, this process requires a large bias across the electrodes. The disparity in voltages required to produce the same current flow in forward and reverse bias manifests itself in the external circuit as rectification.

Difficulties in synthesising the Aviram-Ratner molecule has meant that the electrical properties of the proposed rectifier have never been verified experimentally. Although many molecules have been trialled,[61] rectification ratios were generally small and not necessarily unambiguous due to contact geometry and other asymmetries of extra-molecular origin.[62] A major breakthrough occurred when Ashwell et al. found that donor-acceptor separation could be achieved with a twisted π-bridge.[63] With the orbitals of each system sterically locked in a non-planar orientation, there is little overlap between the π-orbitals either side of the bridge. The conjugation is effectively broken and so separation is maintained.[64] Rectification ratios

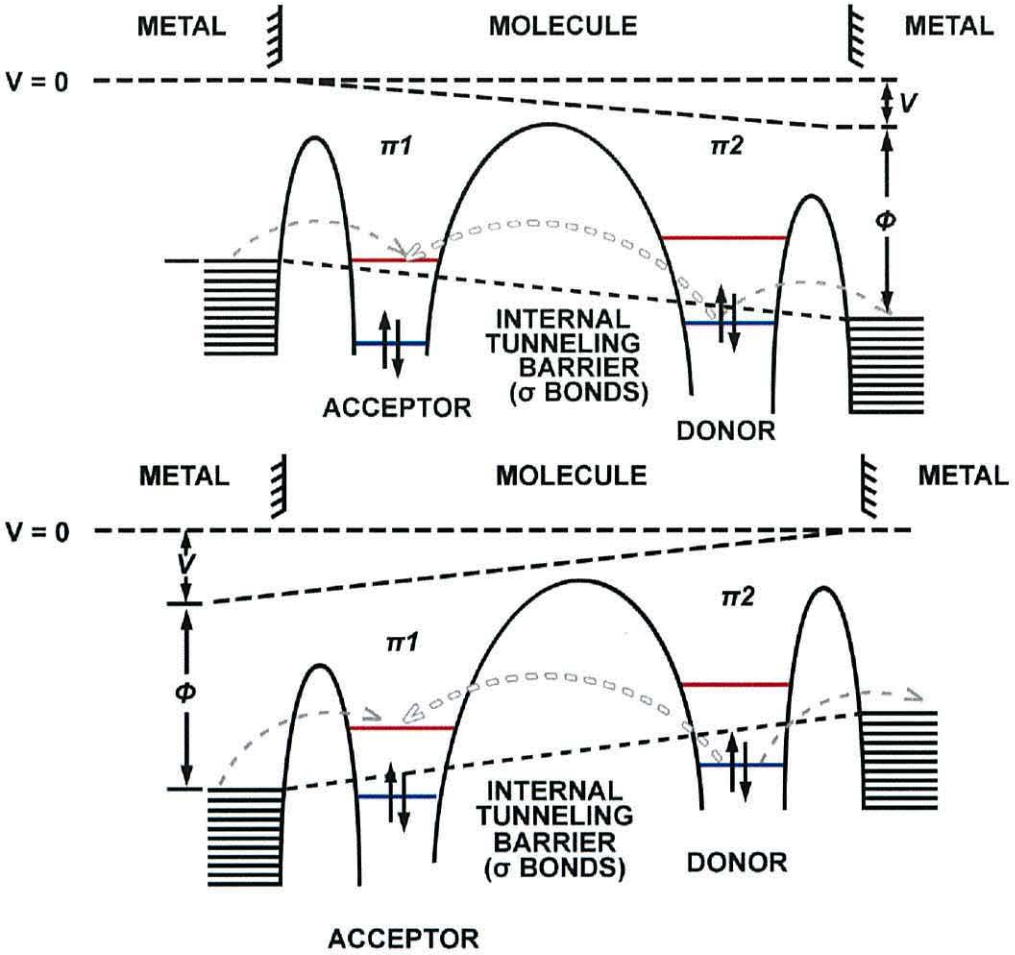

Figure 1.11: Energy level diagrams for a D-σ-A molecular rectifier under: forward bias (top) and reverse bias (bottom). ϕ is the workfunction of the metal, V is the bias.[49]

have gradually increased[65] culminating in an ionically coupled system with RR $\simeq$ 3000 at $\pm$1 V,[39] comparable to p-n junctions and Schottky diodes.

1.4.4 Other Molecular Devices

The wire and rectifier are important constructs, but there are others that need to be replicated using molecules if molecular electronics is going to have an impact on the micro-electronics industry. In particular, there is a need for switches and storage units for use as short and long-term memory.

1.4.4.1 Switches

Switches are one of the most fundamentally important electronic components for computing. They allow current flows to be controlled and directed. Facilitating the movement of information around a circuit and forming the basis of logic systems.

There are many processes that can form the basis of a bistable, two-terminal, switching device. Two that show promise are the catenane and rotaxane type molecules. For example, a [2]Catenane-based molecule was sandwiched between silicon and metal electrodes and addressed electronically.[66] The device demonstrated bistable I-V characteristics, opened at -2 V, closed at +2 V and read at *ca.* 0.1 V. The device was stable in ambient conditions for many cycles. A schematic is shown in Figure 1.12.

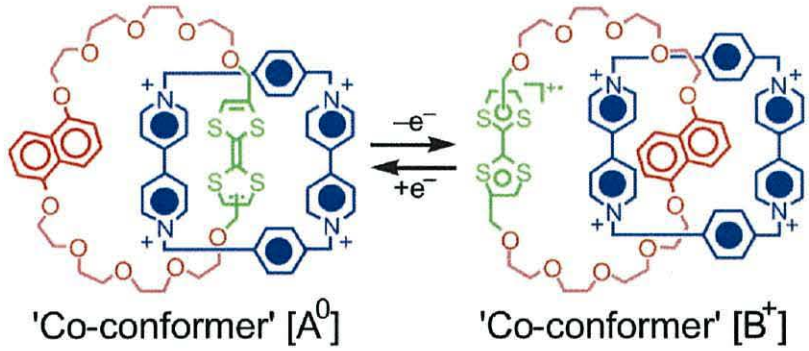

Figure 1.12: A bistable [2]catenane used as a switch. A voltage drives the circumrotation of co-conformer [A^0] to co-conformer [B^+] to create the '0' and '1' states of the device. Reprinted with permission from AAAS.[66]

A different rotation mechanism, using the central benzene ring of 2'-amino-4-ethynylphenyl-4'-ethynylphenyl-5'-nitro-1-benzene-thiol, can also be used for switching. Reed et al. found that the dipole formed by the donor-acceptor pairing of NH_2 and NO_2 can be driven by an external field.[67] Twisting the central moiety out of resonance with the rings on either side caused attenuation of the current flow. By varying the gate voltage, the molecule could be repeatedly switched from a conducting to non-conducting state. This effect was also confirmed by theoretical calculations.[68] Similarly,

a theoretical study by Cuniberti et al.[69] showed that cis-trans isomerism can be used for switching.

Electrochemical methods have also been used to drive a switch. Molecules containing redox centres can have their oxidation states reversibly altered. This in turn changes the electronic structure, enabling electrochemically controlled switching. Nichols et al. used a bipyridinium moiety, connected to a substrate and gold nanoparticle by thiol-terminated methylene chains. The system was immersed in an electrolyte with a counter electrode and the nanoparticle addressed with an scanning tunnelling probe tip. With the molecule in the oxidized $bipy^{2+}$ state, no current flows. Applying a sufficiently large bias between the counter-electrode and substrate injects an electron into the bipyridinium system, reducing it to $bipy^{\bullet+}$. In the reduced state, the molecule is highly conductive and a large current can flow between the probe tip and substrate.

Additionally, mechanical stress can alter the current carrying capacity of a molecule. Hiang et al. investigated the effect of compressing a system containing citrate capped gold nanoparticles.[70] They found that the conformational changes that occur to the molecule under stress alter the electron pathway. This transition could reduce the electrical conductivity up to a factor of 10 and was backed up by theoretical simulations.

1.4.4.2 Memory devices

Crucial to the creation of molecular devices suitable for memory applications is one of the major problems of molecular electronics; long-term stability. A potential solution, from Tsoukalas et al., combines gold nanoparticles and an organic insulating monolayer to create charge storage islands. The device, contained within a silicon structure, demonstrated non-volatile memory characteristics at low operating voltages. Importantly, the characteristics remained unchanged in normal ambient conditions for over 11 hours.[71] A similar technique, used a layer-by-layer method to build up the memory units to create a device with high density; up to 10^{13} cm^{-2} in four bilayers.[72]

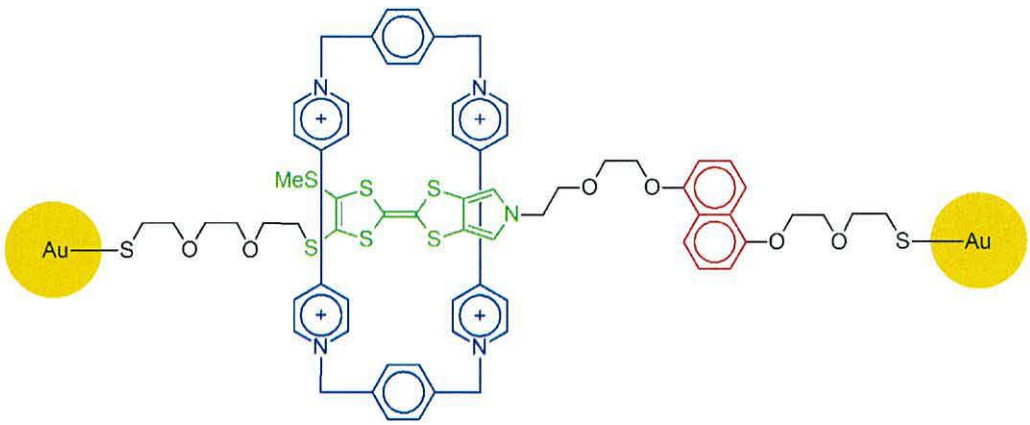

Figure 1.13: An example rotaxane-based memory device.[73] The moiety in blue is bistable between the green and red positions.

An alternative mechanism uses the high and low resistance of bistable rotaxanes, as shown in Figure 1.13, for the '1' and '0' bits of a memory cell.[74] A molecular monolayer of [2]rotaxanes was sandwiched between a crossbar structure of metal nanowires. This arrangement resulted in 8×8 memory devices contained within 1 μm^2. The switching mechanism of a rotaxane has already been described in section 1.4.4.1 and the redox states of the bipyridinium system is used in the same way as the switch, simply over a longer time-scale. Using each cross-point of the crossbar structure as a memory unit, a rewritable, non-volatile memory device is formed with a density of 6.4 Gbits cm^{-2}.[75]

Redox behaviour has also been exploited as a route to information storage. Bocian et al. studied porphyrin based molecules bound to Si(100).[76] The information, stored in the redox state of the molecules was stable for up to an hour, even at high temperatures of up to 400°C in an inert atmosphere. Also, the behaviour of the molecules did not degrade significantly after 10^{12} read-write cycles.

1.4.4.3 Three-Terminal Devices

It is very difficult to create a contact architecture with three point contacts meeting within nanometers, precisely spaced to accept a three-armed

molecule. Fortunately, there are other means of incorporating a third electrode into a molecular electronic system. Two that have been studied extensively are field-effect gating and electrochemical gating.[77,78]

The efficiency with which a molecule conducts depends on the level of parity between electrode Fermi level and energy levels within the molecule. Imposing an electric field on the molecule causes the levels to shift up and down. Tuning the field will bring certain levels into or out of resonance, thereby switching the molecule on and off.[79]

Similarly, the energy levels of a redox molecule are affected by its oxidation state. With electrochemical gating, the system is immersed in an electrolyte and a counter electrode is used to add or subtract electrons from the molecule and so alter its conductive properties.

1.5 Charge transport

Any description of the conductivity of a molecule is only valid in the context of the environment it is contained within.[80] The conductivity of a molecular electronic system is the combination of the efficiency with which charge can be injected into the molecule from the contacts and the transport properties of the molecule once an electron is travelling through it.

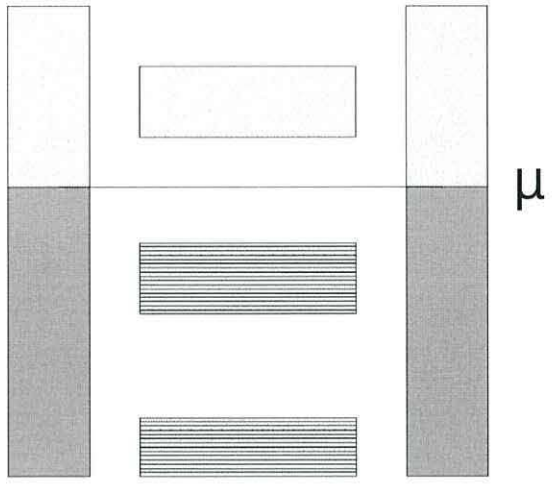

Figure 1.14: Energy levels of a simplified molecule between two unbiased contacts with chemical potential μ.

A molecular system between two contacts may be represented schematically by Figure 1.14. Both contacts have filled states up to their chemical potential, μ. The energy levels of the molecule will align so that the Fermi energy (E_f) lies between the LUMO and HOMO levels. If this is not the case, electrons will flow to satisfy the condition.[81] For current to pass efficiently between the electrodes, there must be energy levels close to the chemical potential. When a voltage is applied to the system, the potentials are shifted as shown in Figure 1.15. Now there exists a level below μ_1 but above μ_2. μ_1 requires all levels below it filled so adds electrons to the molecular level. However, μ_2 requires all levels above it empty so removes electrons from the molecular level. Therefore, electrons move from one contact to the other through the system. If the external voltage replenishes the contacts, current will continue to flow.

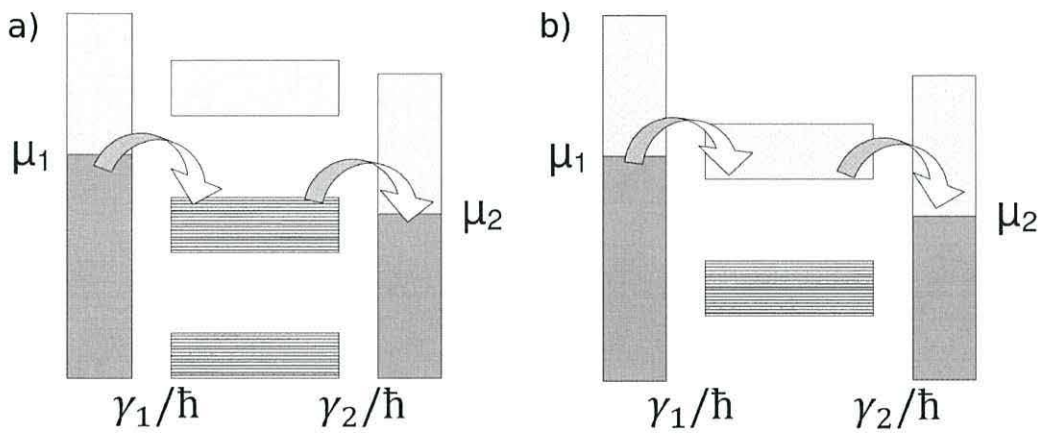

Figure 1.15: Energy levels of a molecule and two contacts under the influence of a potential: LUMO (p-type) transport and b) HOMO (n-type) transport.

Quantifying how well the contacts are coupled to the molecule, the escape time for an electron to be injected onto the molecule is defined as $\gamma_1/\hbar$. The equivalent quantity for the second contact is $\gamma_2/\hbar$. Each contact tries to achieve occupation according to the Fermi function (f_1 and f_2) in that contact. This results in a current flow of:

$$I = \frac{e}{\hbar}\frac{\gamma_1\gamma_2}{(\gamma_1+\gamma_2)}\left[f_1 - f_2\right] \tag{1.3}$$

where e is the charge on an electron and $\hbar$ is the modified Planck constant. The maximum current flow possible in this situation occurs when $f_1 - f_2 = 1$. This equation implies that any current can be driven through the system depending on the quality of the contacts and the energy levels in the system. However, when molecular levels are linked to the levels in the contacts, broadening occurs. This can be thought of as due to the uncertainty principle or coupling of the levels. Broadening causes the molecular levels to spread out so that some of it is above μ_1 and some is below μ_2. However, there is still only one electron allowed to occupy the level and the current takes the form:

$$I = \frac{e}{\hbar}\frac{\gamma_1\gamma_2}{(\gamma_1+\gamma_2)}\frac{qV}{(\gamma_1+\gamma_2)} \tag{1.4}$$

The maximum of equation 1.4 occurs when $\gamma_1 = \gamma_2$, at which point:

$$G_0 = \frac{I}{V} \sim \frac{2e^2}{h} \simeq (12.9k\Omega)^{-1} \tag{1.5}$$

where G_0 is the quantum of conductance, the maximum conductance of this simple system.

A molecule may be regarded as a very small quantum dot. One of the simplest possible quantum dots is two contacts bridged by a short chain of identical atoms, known as a quantum point contact (QPC).[82,83] The resistance of such a system is not dependant on the length of the chain but is quantised in multiples of G_0 as in equation 1.5. Length independence is due to the fact that all the resistance arises from the interface of the wire with the contacts rather than from scattering within the chain. This occurs when the mean free path of the electrons is greater than the distance between the electrodes; also known as ballistic transport.

The situation described in the QPC case is an idealised system. Inserting a molecule between the contacts will couple to incoming electrons, affecting the barrier shape and therefore the transport process across it. More generally, the current-voltage characteristic of a system is given by the Landauer formula. Taking the transmission function, T_i of each channel i, produces an expression for the conductance, G:

$$G = \frac{2e^2}{h} \sum_i T_i \tag{1.6}$$

The Landauer equation can be converted into the more useful form for finding I-V characteristics by making the transmission function continuous and integrating:

$$I(V) = \frac{2e}{h} \int_{E_F - \frac{1}{2}eV}^{E_F + \frac{1}{2}eV} T(E)\,\mathrm{d}E \tag{1.7}$$

1.5.1 Superexchange

Coherent quantum tunnelling is the most common mechanism by which electrons travel through a molecule. The HOMO-LUMO gap of an organic molecule is typically found at *ca.* 2 - 7 eV. The Fermi energy usually sits approximately in the middle of the gap, therefore the energy required to access an available level during transit is too great. However, the molecule is more than just a spacer, setting the width of a vacuum gap. The presence of electronic states coupled to the contacts can lower the tunnelling barrier, even if the electrons do not interact with the molecule as they traverse the gap. Strongly chemisorbed molecules lower the barrier more than when the interaction is weak. For this reason, dithiol alkanes show orders of magnitude higher conductance than mono-substituted molecules contacted in similar ways.[84,85] To distinguish the molecule mediated tunnelling process from tunnelling through a vacuum, it is known as superexchange. The conductance of a system under superexchange conditions with a molecule of length L can be described by:

$$G = \frac{2e^2}{h} \exp(-\beta L) \tag{1.8}$$

where β is a decay constant, taking values of *ca.* 0.5 - 1.0 $\mathring{A}^{-1}$ for saturated molecules and *ca.* 0.2 - 0.5 $\mathring{A}^{-1}$ for conjugated systems. The strong exponential dependence of saturated molecule conductance means that as the length increases beyond a few nanometres, the conductance attenuates rapidly. It should be noted that the limited interaction with the environment means that electron transfer under superexchange conditions do not dependent on temperature.[86]

1.5.2 Thermally Activated Hopping

Broadening of molecular levels means they have a finite lifetime. Therefore, this suggests that an electron traversing the molecule can be localised at a level for a small amount of time. If an electron interacts strongly with the environment it is tunnelling through, coherence can be lost. In this case,

alternative mechanisms of transport will dominate.[87–89] The interaction time (τ) of an electron as it traverses a molecule is given approximately by:

$$\tau \approx \frac{N\hbar}{\Delta E} \tag{1.9}$$

where N is the number of subunit sites contained in the molecule and ΔE is the energy gap between the electrode potential and the appropriate orbital energy.[90]

It is clear from equation 1.9 that a short, saturated molecule with a large HOMO-LUMO gap is likely to have a short interaction time. An electron will be unlikely to couple to any vibrational or orientational modes of the molecule. However, a long conjugated wire will have many subunits and a reduced energy gap. Combined, these variables can increase the interaction time considerably. As the electron traverses the molecule, it is much more likely to couple inelastically and so coherent tunnelling becomes less probably.[91] Instead, the electrons will travel *via* a series of short hops between charge traps along the molecule. This transport mechanism is thermally activated as in equation 1.10:

$$G \propto N^{-\eta} exp(-\frac{\Delta}{k_B T}) \tag{1.10}$$

where Δ is the characteristic potential barrier height, N is the number of trapping sites and η is a numerical factor ($1 \leq \eta \leq 2$) depending on the specific hopping type.[92] Importantly, the conductance in this equation is only weakly dependant on the length of the molecule, characterised by N. Therefore it is considered to be more conventionally 'wire-like'.

In most systems, both coherent tunnelling and incoherent hopping can occur to some degree simultaneously. The former dominating at low temperatures and short, wide gap molecules; the latter dominating at higher temperatures, with longer molecules and narrower HOMO-LUMO gaps.[93,94] Oligo(*p*-phenylene ethylene) based molecules, for example, show a distinct change after three phenyl units, or approximately 3 nm; as in Figure 1.16.

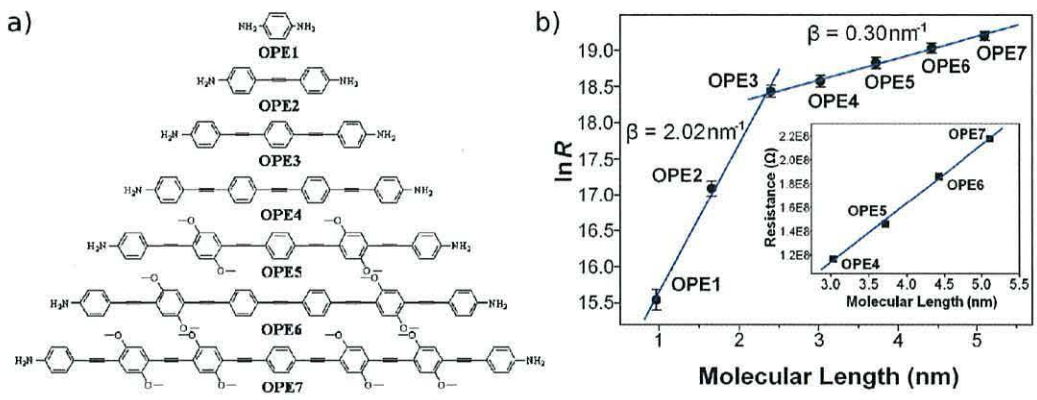

Figure 1.16: Example of the tunnelling to hopping transition: a) Scheme of seven amine terminated OPE based wires and b) Semilog plot of the resistance *vs.* length for the seven OPE wires. Fitting lines use an adapted equation 1.8. Inset is a linear resistance *vs.* length plot of the larger molecules to emphasise the reduced, linear, length dependence for the larger molecules. Reprinted with permission. Copyright 2009 American Chemical Society.[95]

1.5.3 Considerations for Electron Transport in Organic-Semiconductor Hybrids

Organic on silicon electronics is an attractive prospect. The bonding between molecules and a silicon surface is generally well understood.[96–98] Organics form strong bonds to silicon through carbon (Si-C bonds are *ca.* 4 eV and Si-O-C *ca.* 4.7 eV.) and the silicon surface itself is very stable. Combined, these factors produce an organic layer on silicon that can withstand high temperature and resist oxidation. For analysis purposes, the molecules will occupy well defined positions that are maintained for repeat measurements.[99] Also, the regular, stable surface can act as a template for incoming molecules. However, the lack of mobility at the surface acts to diminish post-bonding rearrangement and the chance of a well ordered system.

When investigating an organic molecule assembled onto semiconductor electrodes, the contact interaction is different than when dealing with metal contacts.[100] The requirement for semiconductor energy levels to vary smoothly results in a Schottky barrier forming at the interface.[101,102] Assuming most of the bias falls across the interfacial space-charge region,

the current density takes the form:

$$J = AT^2 exp\left(-\frac{E_a}{k_B T}\right) \cdot \left[exp\left(\frac{V}{k_B T}\right) - 1\right] \tag{1.11}$$

where A is the junction area, E_a is the activation energy.[103] This process is known as thermionic emission. It has also been found that there can be complex broadening of the molecular energy levels, which increases with bias.[104]

Chapter 2

Techniques for Molecular Electronics

During this section, the major techniques and tools available for the study of molecular electronics will be reviewed. In section 2.1, the formation of molecular monolayers will be examined. Next, in section 2.3, contacting techniques and methods used for electrical characterisation of molecules. Methods for investigating physical properties of monolayers will be discussed in section 2.4. Finally, in section 2.5, specific experimental details will be given for the methods used to prepare substrates for the studies given in the results section.

2.1 Methods of Monolayer Formation

Addressing a molecule, in order to investigate it electrically, requires immobilisation of that molecule and the formation of contacts to at least two points. This task is made simpler by first anchoring the system to a macroscopic solid substrate of suitable material.[105] With one connection made to a large, easily contactable structure, fine control is only required for the second contact. The ideal first layer, for the studies presented in this thesis, is only one molecule thick. This monolayer is much more likely to allow the study of a single molecule. Complex interactions and unknown

configurations give rise to uncertainty with a multi-layer system. Therefore, several techniques have been developed to create monolayers.

2.1.1 Langmuir-Blodgett

One method, developed by Irving Langmuir and Katharine Blodgett, uses an air-water interface to form a layer. Deposited occurs when a solid substrate is passed through that layer. The Langmuir-Blodgett (LB) technique of monolayer deposition can only be used with amphiphilic molecules. This constraint requires that they contain both hydrophilic and hydrophobic moieties. While this may appear restrictive, polar groups such as alcohols, carboxylic acids and amines are common in organics. Also, the addition of a long saturated carbon chain satisfies the hydrophobic requirement. Therefore, it is possible to modify a large number of molecules to become suitable for LB deposition. It is an important technique because it allows precise control over the thickness of a layer. In addition, with good experimental technique, the quality of the layer is very high as the molecules arrange themselves homogeneously over large domains.[106]

The formation of a monolayer comes from energy minimisation at the air-water interface. With no molecules present, the water molecules at the surface have unbound dangling hydrogen bonds; a high-energy system.

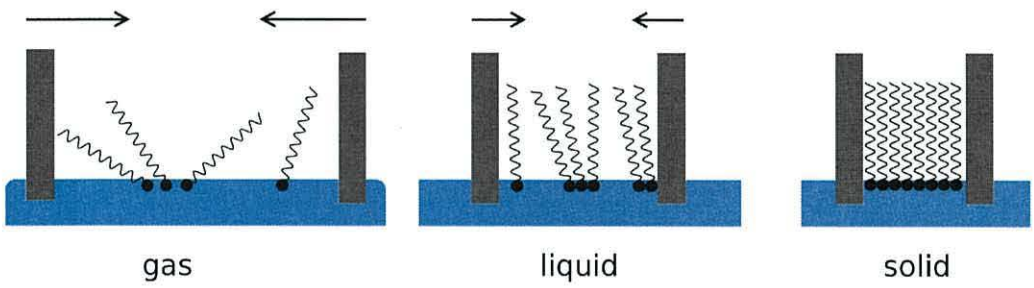

Figure 2.1: A Langmuir-Blodgett monolayer formed at the interface between air and water, showing the three phases as the barriers compress.

The addition of an amphiphilic surfactant to water reduces the surface energy, due to the nature of the molecules. The hydrophilic head group of the molecule interacts favourably with the water through hydrogen bonds so is

located just under the surface. However, the hydrophobic tails are repelled by the water and arrange themselves so that they project upwards into the air. This arrangement lowers the surface energy as it removes the higher energy air-water interaction and provides both media with a favourable interaction. When the surfactant is added in a dilute concentration, below that required for micelle formation, the molecules behave as a two dimensional gas constrained along the air-water interface. They are free to move and have little interaction with each other. As the concentration is increased by closing a barrier in an LB trough and reducing the surface area in which they are contained, the molecules are forced closer together and begin interacting. Domains form spontaneously to lower the energy of the system. These islands can be fairly ordered, again due to energy minimisation. As the barriers close, the domains merge together creating larger domains with more molecules closely interacting. The behaviour of the molecules at this pressure is more like a liquid. In this phase, the surface tension decreases in proportion to the surface area. These phase changes are shown in Figure 2.1.

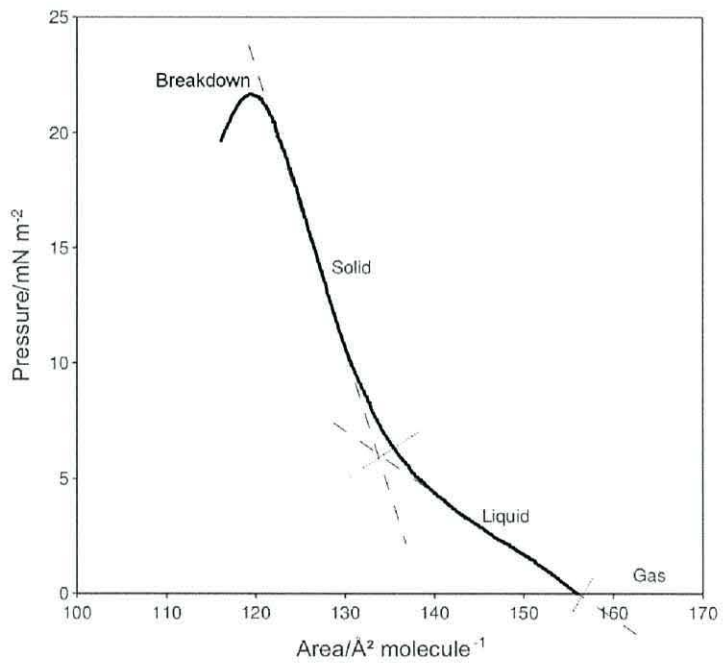

Figure 2.2: A Langmuir-Blodgett isotherm for a squaraine molecule showing the three phases and breakdown point at the turnover.

If the area is decreased further, a point is reached at which the surfactant layer becomes entirely closely interacting as all the domains join to cover the entire area of water within the barriers. The layer enters into its solid phase, characterised by a steeper gradient in a surface energy *vs.* surface area graph. Ultimately, if the area inside the barriers becomes too small, the molecular monolayer is compressed to a point where discontinuities appear and breakdown occurs. The monolayer ruptures, forming multi-layers and even soluble aggregates. This is indicated by a peak and then fall in the surface energy. A graph of surface energy against molecule area is known as an isotherm and is used to determine the area at which to deposit, usually taken as a midway point in the solid phase. An example isotherm is shown in Figure 2.2.

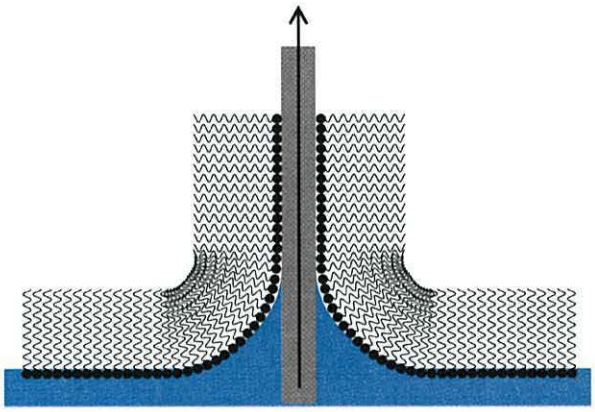

Figure 2.3: The Langmuir-Blodgett technique for transferring monolayers onto a solid substrate.

A monolayer at the air-water interface cannot be used to study the electrical conduction properties of the constituent molecules; it must first be transferred to a solid support. During a Langmuir-Blodgett deposition, the substrate is passed through the monolayer, perpendicular to the air-water interface, as shown in Figure 2.3. By controlling the speed of the dipping mechanism and altering the surface area using a feedback loop to maintain a constant surface energy, it is possible to transfer a homogeneous layer onto a solid support. The direction of the stroke, up or down, determines the orientation of the molecules relative to the support. With multiple sweeps,

it is possible to build up a number of different types of layering. These are designated X, Y and Z depositions, as shown in Figure 2.4.

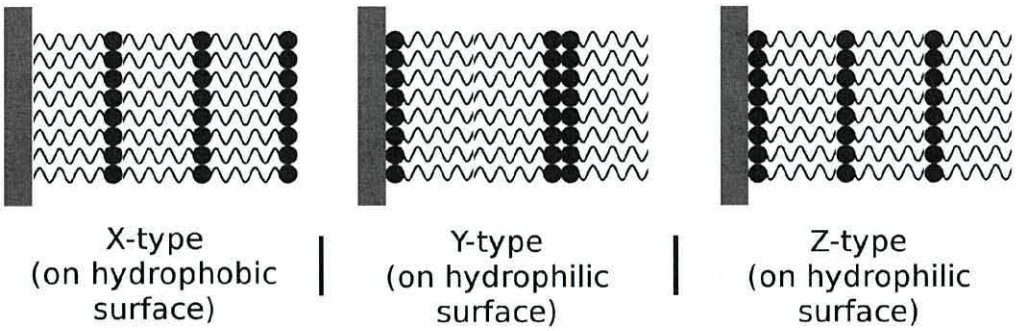

Figure 2.4: Several arrangements of building up monolayers with LB deposition.

The advantage of this technique is that the monolayer quality can be controlled very precisely and results in a highly homogeneous film. The layers are built up one at a time so the resultant thickness can be specified precisely. However, the molecules are only physisorbed to the substrate and therefore free to move under the influence of a high electric field. The sharp tip of an STM means that such a field is produced by the STS technique and so this instability makes some measurements difficult. Additionally, the nature of the deposition transfer relies on a flat or curved substrate which limits the range of situations in which the technique can be used.

2.1.2 Self-Assembly

While the Langmuir-Blodgett technique is still a relevant one, it is self-assembly that is becoming increasingly the focus of research.[107–111] It is, conceptually, a very simple method of forming a monolayer and offers several benefits over Langmuir-Blodgett deposition.

To begin, it is useful to define what is meant by molecular self-assembly. It is a process that requires three conditions:

1) The molecules to be assembled are free to move at random.

2) The substrate must contain suitable binding sites for the molecules to attach themselves.

3) Formation of the monolayer must result in energy minimisation for the system.

The process is undirected and happens spontaneously, requiring only a solution of molecules with a suitable head-group and a substrate that is compatible.

The foundation for self-assembly came with Zisman et al. and their pioneering work on the physisorption of surfactants on metal surfaces.[112] They found that oleophobic films of eicosyl alcohol, *n*-octadecyl amine and *n*-nonadecanoic acid formed onto glass and clean platinum, iron and chromium from dilute hexadecane solutions. However, the implications of this discovery only started to become clear when later work by Nuzzo and Allara showed that molecules containing a disulphide group self-assembled on gold.[113] There are many other examples of useful affinities that have been used to form self-assembled monolayers (SAMs) including sulphur and selenium to noble metals,[114–117] and organosilanes to semiconductors.[118,119] The simplicity of the mechanism involved has led to these end-groups being compared to, and occasionally known as 'crocodile-clips'.[120] The combination chosen for most studies of self-assembly during this thesis is sulphur and gold.

For assembly to occur, an approaching molecule must pass within range of a bonding site on the substrate surface. A thick oxide layer or other adventitious species can occupy these sites and prevent a molecule from binding.[121] Gold has only a thin oxide layer and does not readily attach to contaminating species. Therefore, there is little competition for binding sites and a thin oxide layer can be displaced by an incoming thiol. A heavily contaminated gold surface can be rendered clean by exposing it to a nitrogen plasma. Therefore, this technique does not require a ultra-high vacuum system or high specification clean-room facilities.

Figure 2.5 shows a self-assembled monolayer (SAM) forming onto one side of a substrate. An initially dilute, disordered layer becomes islands of tighter packing molecules with some disorder. These islands grow and join to each other until the surface is covered, assuming a supply of molecules is maintained throughout the time required for a full deposition.[122] Inter-

molecule interactions, such as π-π stacking, aid close packing to produce a dense monolayer.[123] It has been shown that this arrangement generally results in better conductive properties.[124]

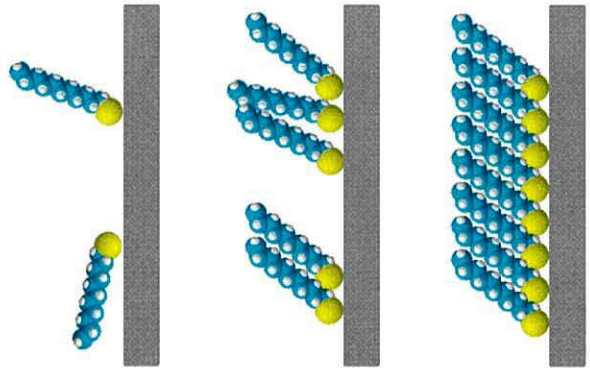

Figure 2.5: Process of self-assembly: A prepared substrate is immersed into solution; molecules spontaneously form a coating layer until all available sites are occupied and they are tightly packed.

A gold-sulphur bond is fairly strong and largely covalent, but has some ionic character due to the high electro-negativity of the sulphur, which causes slight polarity in the electron cloud at the bond. The energy required to break the bond, also known as the adsorption enthalpy, is generally greater than 120 kJ mol^{-1}[125] and the bond angle for gold-sulphur-carbon is typically 120° thus for a meta-substituted thiol benzene, the molecules can project perpendicularly away from the surface. The structure and packing of the molecules necessarily depend on the underlying structure of the gold. The annealed gold evaporated onto quartz typically used during this thesis has a (111) fcc structure. However, this is an energetically unfavourable arrangement and the surface will become disordered over time without re-annealing. There is still disagreement over the exact nature and configuration of the sulphur gold bond. The consensus of theoretical calculations suggests that a sulphur atom occupies a three-fold coordinated hollow site, interacting with all three of the nearest gold atoms. However, recent experimental work has provided evidence for alternative arrangements, with results that show the sulphur atop a single gold atom[126] or next to an atom that has been pulled

out of the surface.[127,128] As a self-assembled deposition proceeds, surface coverage generally follows the Langmuir absorption equation, as shown in equation 2.1. This equation was derived by considering the availability of bonding sites. In the resultant equation, θ, the fractional coverage of the surface, relies on P, the concentration and α, the Langmuir adsorption constant. α in turn depends on the relevant binding energy and temperature of the system.[129]

$$\theta = \frac{\alpha P}{1 + \alpha P} \tag{2.1}$$

The sulphur-containing molecules synthesised for assembly is often found in one of the three forms shown in Figure 2.6; a thiol, disulphide or protected sulphur such as thio-acetate.

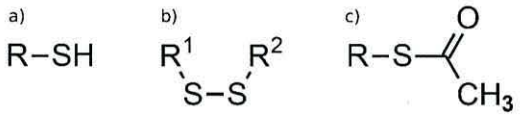

Figure 2.6: Self-assembling molecules with sulphur end-group examples: a) thiol, b) disulphide and c) thio-acetate

The bonding of a thiol to gold is considered to be a two step mechanism; oxidative addition, followed by reductive elimination of the hydrogen. The sulphur is believed to lose its accompanying element on bonding with the gold. Although this process is not well understood, it is believed that the hydrogen is lost either *via* molecular H_2 in the absence of oxygen or *via* H_2O and H_2O_2 if oxygen is present.[130]

The procedure used for depositing a SAM during this thesis was as follows:

i) A solution of the molecule is made up, usually with a concentration of 0.1 mg ml^{-1} although when attempting to decrease the coverage of deposition, weaker concentrations were used. The solvent used must dissolve the molecule completely, not interfere with the deposition mechanism and ideally be fairly volatile so it is removed from the layer easily. Otherwise, solvent molecules can become trapped within the lattice as the layer forms and affect its properties.

ii) The substrate is prepared as described in section 2.5 and immersed in the solution for a length of time.

iii) After deposition, the sample is washed in pure solvent. This action removes any material that is only physisorbed on the surface and not actually chemically bound.

iv$_a$) If the substrate is a quartz crystal, the layer is then dried thoroughly and its molecular coverage measured using a microbalance as described in section 2.4.1. The crystal is re-immersed, washed, dried and measured in a repeated cycle until a consistent limiting value is obtained, corresponding to a close packed monolayer.

iv$_b$) If the substrate is not a quartz crystal, then the sample is simply washed and re-immersed repeatedly, mimicking a previous known deposition pattern taken with a quartz crystal to ensure the layer is of equal quality.

2.1.3 Alternative Deposition Techniques

There are other techniques for creating a layer of material, two will be mentioned briefly here. Spin-casting can create a thin layer quickly and reliably from solution. A substrate, with a few drops of solution added to the surface, is revolved at very quickly; many thousand rpm. The layer thickness is determined by the speed of rotation and the viscosity of the solution. This technique is commonly used to create the photoresist layers for lithography. It has also found an application in creating organic light emitting diodes. However, the film that results from spin-casting is highly inhomogeneous as there is little control over the molecules as the layer forms. Therefore, it is best employed for bulk layers rather than films used for single molecule electronic studies.[131]

Thermal evaporation, or molecular beam epitaxy in its more refined form, deposits a layer using ablation from a solid block of material. Heating the solid forms a vapour which will expand away from the source. Imposing a cold substrate into the stream of vapour will cause the molecules to condense onto

the surface. This is generally a slow process as the coverage of the surface increases to form a complete layer. More commonly used as a method to deposit metals and inorganic crystalline materials, thermal evaporation has been used successfully with low weight organic molecules. As the vapour is required to traverse a chamber, the deposition must be performed at a low pressure to avoid scattering with the air molecules. Pressures below 1×10^{-4} mbar are typical.[132]

2.2 Stepwise Assembly

A monolayer deposited in one step is a useful construct, but has certain limitations. The constituent molecules must be synthesised in their entirety *ex-situ*, which presents certain constraints and complications to the process. An asymmetric molecule, essential for unimolecular rectification, is much more challenging to synthesise than a symmetric molecule. Longer molecules, required to fit into a large gap or for certain length dependant functionalities, present further hurdles for the synthetic chemist to overcome. However, it is possible to overcome these synthetic limitations with alternative methods.

With an initial monolayer formed on a substrate, it is possible to treat this layer as a new surface and absorb further layers on top. This is known as layer-by-layer or stepwise assembly. The coupling mechanism used to add the further layers can be either physisorption through electrostatic forces or chemisorption *via* a chemical bond formed through a reaction.

An early example of stepwise assembly came with the self-assembled polycation-polyanion multilayers of Decher[133]. Similar methods include using ionic coupling[134,135] and co-coordinating to a metal complex.[78,136] There are many reaction schemes that have been used to chemically join a second layer onto the first, including reaction of dianhydrides with diamines to form polyimides, reaction of di(acid chlorides) with diamines to form polyamides, and reaction of diisocyanates and diamines to form polyureas. However, the focus of this thesis is a common reaction, joining an amine with an aldehyde to form a imine group. While ionic coupling and forming metal complexes has produced some exciting results, there are some advantages to forming a

chemical bond. For example, Tang et al. showed that imine bridges, with their π-orbital overlaps exhibit a higher conductance than tetrahedral co-ordinated cobalt complexes, despite being 3.3 nm longer.[137] However, the metal complex is more easily switched *via* ethylenediaminetetraacetic acid (EDTA), for example, whereas the imine bridge is fixed.

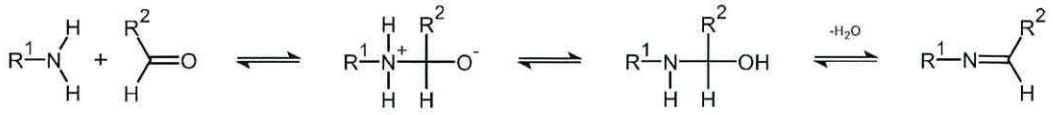

Figure 2.7: Mechanism for imino bridge reaction, showing the nucleophilic addition and water elimination steps necessary to form a chemical bond between an aldehyde and an amine group

The mechanism for imino-bridge formation is shown in Figure 2.7. It is a two step reaction; the first involves nucleophilic addition of the amine to the aldehyde. At this stage, the compound is highly unstable and so an extra proton transfers from the nitrogen to the oxygen to create a more stable carbinolamine intermediate. The second step is for water to be lost *via* an elimination reaction which results in the imino bridge between the two molecules.

The equilibrium of this mechanism is in favour of the separate compounds. However, it is possible to use a dehydrating agent such as a molecular sieve or an acid in order to alter the equilibrium towards forming the imine. The conditions required for this reaction are mild, and coupled with the ubiquity of the constituent end-groups, it is relatively easy to create a large library of diverse structures.[138]

It is possible to perform stepwise deposition in a vacuum *via* chemical vapour deposition (CVD) or in solution. However, a vacuum imposes certain limitations on the process. There are no solvent molecules to mediate proton transfer or stabilize intermediate molecules for example. Also, adding an acid catalyst is very difficult with the CVD technique and so altering the pH to alter equilibrium conditions is problematic.[139] For all these reasons, the technique used during this project has been reaction in solution.

2.3 Methods of Contacting a Monolayer for Electrical Characterisation

There are generally two ways to contact a two-terminal molecule; either anchor one side on a substrate as discussed in section 2.1 and subsequently connect to the other side, or insert a molecule into a size-matched gap, thereby contacting both ends simultaneously. The ideal contact architecture for investigating the conductive properties of a molecule in both cases is completely symmetrical; removing ambiguities due to non-identical coupling constants. Particularly when the initial substrate is a metal, one possibility for adding a second contact is to evaporate metal directly onto the monolayer. However, there are several disadvantages to this method. The incoming atoms and clusters can be energetic and therefore potentially destructive, particularly if the layer is thin. Molecules can be dislodged and the layer damaged as the contact forms. Additionally, if the layer is not perfectly close packed and without gaps, metal atoms can penetrate the molecular layer. These atoms can link together into tendrils that bridge the contacts, bypassing the molecules. These defects are known as pinholes and as they are likely to have a different conductive ability to that of the molecules, the current-voltage characteristics of the system can be significantly distorted and even dominated by the interstitial metal bridges.

An alternative, less destructive method uses a mercury drop to form a contact. At room temperature, mercury is a liquid but still highly conductive. By forcing out a small amount through a conductive capillary, surface tension will keep the droplet attached to the end of the thin tube. This drop can be lowered on to the surface of SAM and form a second contact as shown in Figure 2.8. Very small variance of the volume of the drop can be used to alter the gap between the contacts and probe transport properties.[140] The mercury is much less energetic than a thermally evaporated metal and therefore, if a monolayer is complete and compact, the top contact will not damage the underlying molecules and form pin-holes.[141,142]

Furthermore, molecules can be self-assembled on the surface of mercury, including the commonly investigated class with thiol end-groups. A layer of

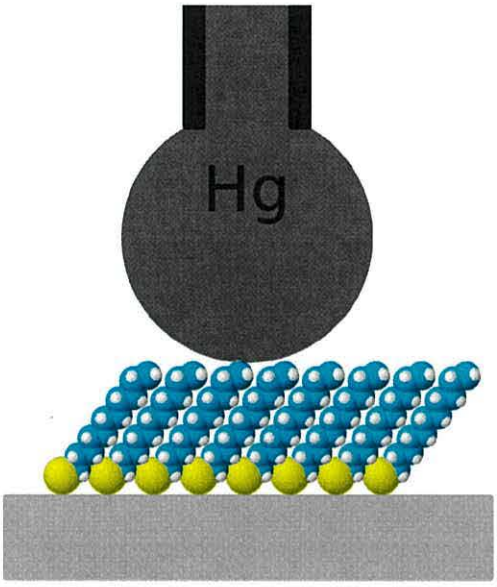

Figure 2.8: The mercury drop technique, showing a drop of mercury contacting a SAM on a solid substrate. Completing the circuit between the capillary and substrate allows the electrical character of the SAM molecules to be examined.

molecules can be assembled on both the bottom and top contacts and the two layers brought together simultaneously. Using this method, symmetrical and asymmetrical dual-layer systems can be investigated. However, although this technique has advantages over evaporation, it also has problems. The reliance on liquid mercury means that it is impossible to investigate systems below 234 K, its melting point. Working with mercury is also undesirable due to its toxicity, particularly dangerous due to its liquid state, and the fact that the surface atoms have high mobility. Repeat measurements of the same area, or selective alteration of particular areas is also not possible with such an unstable surface.

2.3.1 Scanning Tunnelling Microscopy

It is arguable that nothing has advanced the field of nanotechnology, and molecular electronics in particular, more than the invention of the scanning tunnelling microscope (STM).[8,143] Developed in 1981 by Gerd Binnig and

Heinrich Rohrer at IBM Zurich, it earned them half of the 1986 Nobel prize for physics. In contrast to the problems of the mercury drop technique, an STM is best used in an ultra-cold vacuum, is safe to operate and can offer very precise, repeatable measurements. Its precision operation relies on the piezoelectric effect. When a voltage is applied across a material with a dipole moment, the movement of charges under the influence of the field causes the bulk material to contract or expand, depending on the field polarity. The alteration in bulk dimension, produced by a small change in field, can be sub-nanometre. Therefore, three independently controlled piezoelectric crystals, arranged orthogonally, allow a small tip to positioned in three dimensions with atomic precision. The latest instruments are capable of imaging with a noise level of less than 0.3 Å, although at room temperature and pressure, Brownian motion and thermal noise can decrease the resolution. The tip itself can be made of any conducting material, but is usually platinum-iridium or a noble metal. Gold is a common choice, due to its thin oxide, high conductivity and affinity to many elements that are important to molecular electronics.

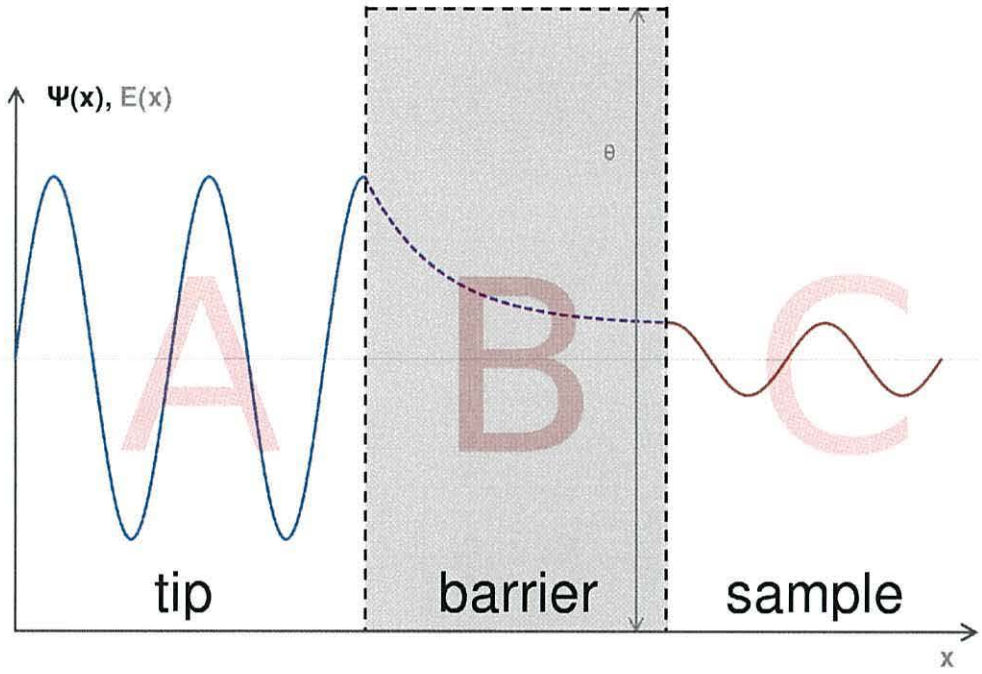

Figure 2.9: A quantum tunnelling barrier of height θ, showing an electron incident on the left and penetrating to the right.

The STM is a technique that does not make physical contact to the molecules under investigation. Instead, it relies on electrons penetrating a small tunnelling barrier between tip and sample. Classically, when a particle such as an electron encounters a barrier with higher energy than itself, it will always be reflected. However, a system on the scale at which the STM operates obeys quantum mechanical rules. These state that there is always a finite possibility that a particle will pass through a barrier; regardless of the relative kinetic and potential energies of the particle and barrier involved. This effect can be thought of as a natural result of the Heisenberg uncertainty principle, whereby an entity of one side of the barrier is not of fixed location but more a probability distribution, some of which can extend to the other side of the barrier. A schematic representation of the problem of tunnelling across a barrier is shown in Figure 2.9. Splitting the system up into three sections; the metal tip of the STM (A), the barrier due to the air gap (B) and the surface to be probed (C) simplifies the problem.

To calculate the transmission of a given electron through this simplified system, it is necessary to solve the time independent Schrödinger equation for one particle and dimension, using the parameters for each region.

$$-\frac{\hbar^2}{2m}\frac{d^2\Psi(x)}{dx^2} + V(x)\Psi(x) = E\Psi(x) \tag{2.2}$$

The equation, 2.2, consists of three terms, the first represents the kinetic energy of the particle, the second the potential energy of the barrier and the third is the total energy and can be re-written as equation 2.3:

$$\frac{d^2}{dx^2}\Psi(x) = \frac{2m}{\hbar}\left(V(x) - E\right)\Psi(x) \tag{2.3}$$

The simplified potential barrier takes the form of a sum of Heaviside step functions: $V(x) = V_0\left[\Theta(x) - \Theta(x-a)\right]$. There are solutions for all three regions of the problem, found by requiring that the wave-function, and its derivative, be continuous at the boundaries of the barrier. The solutions in zones A and C describe the wave-function of a free particle and it's reflection, and that of the transmitted particle respectively. However, it is zone B that is of greatest interest when examining the operation of the STM. Inside the barrier is where the behaviour deviates most dramatically from classical predictions.

The solution to equation 2.3 inside the potential barrier takes the form:

$$\Psi(x) = Ae^{+i\kappa x} + Be^{-i\kappa x} \tag{2.4}$$

$$\text{where } \kappa = \sqrt{2m(V_0 - E)/\hbar^2}$$

Examining the two terms from equation 2.4 as $x \to \infty$ implies that $Ae^{+i\kappa x} \to \infty$ whereas $Be^{-i\kappa x} \to 0$. The probability of finding the particle at a given position, x, is found through $|\Psi(x)|$, and so it is necessary to set the A coefficient to zero to avoid an infinite probability. Therefore, the solution takes the form:

$$\Psi(x) = Be^{-i\kappa x} \tag{2.5}$$

It is clear that the transmission of a particle is exponentially dependant on the width of the barrier. As the barrier grows wider than $1/\kappa$, the tunnelling probability is significantly reduced and little current passes. Once beyond the barrier, however, it is important to note that the solution to the Schrödinger equation is the oscillatory form of the incident wave. If an electron does pass through the barrier, it emerges with the same frequency, or energy, as it entered. Only the amplitude is suppressed.

An STM utilises the quantum tunnelling process to probe samples without making physical contact. With the fine control offered by the piezo actuators, the tip can be brought close enough for the tunnelling current to be sufficiently large to be measured. The tip is brought down to the surface based on two main parameters, tip bias and set-point. The bias is the potential applied between the tip and substrate; the set-point is the tunnelling current magnitude at which the tip stops advancing. Therefore, a lower bias or high set-point will result in a smaller air gap between tip and sample, but could cause the tip to crash.

There are two main modes of operation that the STM can employ for imaging a sample: constant height and constant current. In constant height mode, the STM scans across the surface without changing its position in the direction perpendicular to the substrate. As the tip rasters back and forth, the undulations of the sample under investigation cause variation in the tunnelling current. As the current has an exponential dependence on the barrier width, an effective map of the surface height can be inferred from the current. However, the constant height mode has a weakness in that it depends on the surface of the sample to be relatively flat. If there is a large variation, it is possible for the tip to collide with the substrate and cause damage to tip and sample. This problem is not an issue for the alternative, constant current, mode. Maintaining a constant tunnelling current, at a fixed set-point and bias, between the tip and surface requires a feedback loop. The tip is withdrawn or extended as the STM detects changes in the conductivity corresponding to changes in surface topology. This tip height map can then be used as a close approximation of the surface height. With both imaging modes, uncertainty can be introduced by any non-homogeneity in

the conductance of the surface. It is difficult to distinguish between changes in current induced by height changes and those due to the conductivity of the underlying material.

The STM measurements taken during this thesis were taken using a *Vecco* Nanoscope V Multimode system. A gold probe electrode is created by cutting a 0.25 mm 99.99+% pure gold wire at a shallow an angle as is possible in order to produce a very sharp tip. This tip is not sharp enough for good measurements from cleaving alone. However, due to gold atoms having a high surface mobility, when a bias is applied between the tip and substrate, electromigration will cause atoms to move towards the end. This effect produces the atomically sharp tip required for high resolution imaging.

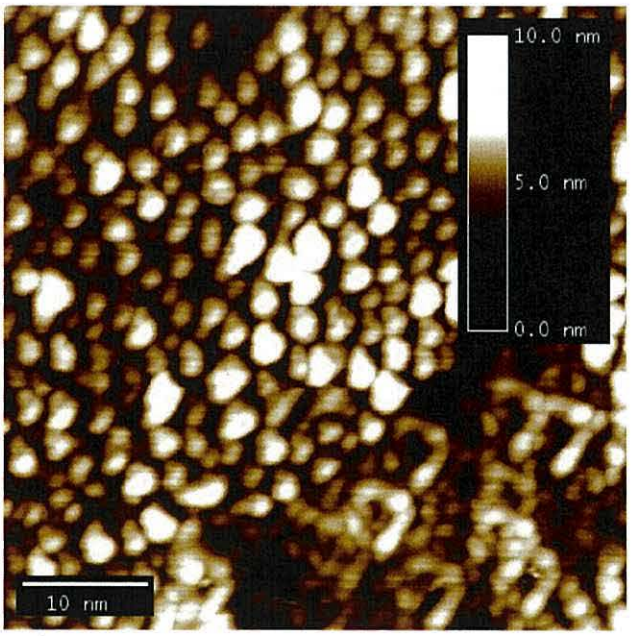

Figure 2.10: A 500 nm × 500 nm STM image of a gold coated quartz crystal, showing the gold clusters making up the surface. Inset are the length and height scales.

The nature of the STM means that a flat surface is more likely to produce consistent results as sharp changes in surface height cause more excessive feedback loop events which can disrupt a smooth scan. Therefore, all measurements begin with a large-scale, *ca.* 400 nm × 400 nm, image of the surface, which identifies the grain boundaries of the various gold clusters

as shown in Figure 2.10. Next, an area of consistent height is identified and the area of the scan reduced in several steps until it is confined to an area of approximately 25 nm × 25 nm. At this point, if the region has been chosen well, the scans should be relatively flat and noise free, indicating that measurements can begin.

2.3.1.1 Scanning Tunnelling Spectroscopy

The STM is also an invaluable tool for investigating the electrical characteristics of molecules. Known as scanning tunnelling spectroscopy (STS), this modes requires the tip to maintain a fixed position while the voltage is scanned and current measured. Electron energies are generally ≤ 3 eV[144] and so there is no damage to the molecules. This allows multiple scans for each reading to be obtained, and averaged, to reduce noise. While the STS method has been widely used, it does have a number of problems. Principally, the air gap between tip and molecule means that the contacts are not symmetrical. This difference can induce a small amount of asymmetry in an otherwise symmetric I-V characteristic, although studies suggest this is limited to RR ≤ 10. Also, the gap impedes charge injection and attenuates the overall transmission of current, providing an inaccurate measure of conductance. Additionally, as the tip is atomically sharp, it has the ability to probe a molecule at a point lower than its terminating group. In a very dense layer there is less chance of this occurring, but at defect site or sparsely occupied areas, it has an increased possibility. Long molecules, particularly those that tilt away from the surface normal or have a curved spine will also increase the chance of a mid-molecule connection. Overlapping the tip orbitals into the π-system of the molecule can still allow charge injection, but the unknown contact geometry limits the usefulness of such a result.

Another problem with STS is the uncertainty over the number of molecules being contacted. One method used to overcome this limitation is matrix isolation. A SAM of relatively insulating mono-substituted alkanethiols is interspersed with a small number of the bi-substituted thiol terminated molecules of interest. The insulating matrix separates the

relatively conductive molecules so that it is unlikely for an STM tip to be able to interact with more than one at a time. Therefore, single-molecule measurements are significantly more common. A further adaptation of this technique uses a nanoparticle as an intermediate electrode. Nanoparticles, typically made of gold, can be formed with a very high degree of uniformity in size and shape. The diameters are typically in the 10 nm to 30 nm range and therefore will form a contact to many more molecules than a tip on its own. However, if this method is combined with the matrix isolation technique, this problem can be reduced. The long-chain matrix molecules are chosen to have a similar length as the molecules under investigation. The resulting film then has a flat surface containing a dilute concentration of thiols. The gold nanoparticles will attach themselves to the thiol, while being supported by the surrounding layer, and provide a clear target for an incoming STM tip.

Extending the STS technique to more reliably characterise single molecules has been an important goal. For this reason, Haiss et al. developed a method that uses a drifting STM tip above a layer of molecules.[145–148] A standard STS measurement requires a feedback system to fix the tip in position above a molecular cluster during an entire voltage sweep. With the feedback disabled, the tip is free to drift about the surface. When a thiolated molecule is encountered by the tip, spontaneous attachment and detachment of the molecule is visible in the time domain as a jump in transmitted current. Therefore, this is known as the STS(t) or 'current jump' method. An example system is shown in Figure 2.11. This technique is particularly powerful as only the difference in current is used, between an empty and filled contact gap. This minimises the confusion resulting from different tunnelling barriers.

The technique is most effective at characterising dilute layers of flexible molecules that can re-orientate themselves upwards to make contact with a drifting tip.[12] To aid with the identification of the single molecule current, many measurements can be taken and a histogram created of current jump heights against counts. Ideally, the graph contains a low peak that corresponds to the tip contacting a single molecule. Then, at integer multiples of the current of this fundamental peak, secondary peaks appear

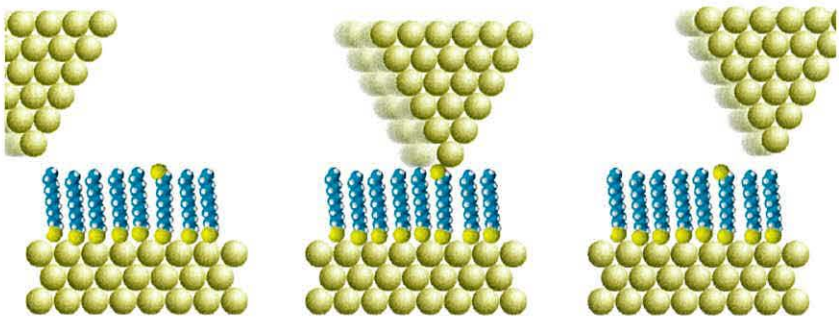

Figure 2.11: An example current jump event: The STM tip moves in from the left, encounters a thiolated molecule before disconnecting and continuing to the right.

that represent multiple contacts.

2.3.2 Electromagnetic Cantilever

The first iteration of this alternative contacting technique was developed by Kushmeric et al.[149] and used crossed-wires, brought together using the Lorentz force. The arrangement, as in Figure 2.12, shows two wires strung between conducting posts. One wire is coated with a SAM while the other is bought into contact and forms the top connection to the molecules. By positioning a magnet close to the wire and passing a current between posts 'B' and 'C', the deflection wire will be subject to a force orthogonal to the magnetic field. As the deflection current increases, the wires are brought gently into contact and the resultant junction allowed to relax. Then, by applying a voltage across posts 'A' and 'B', it will be possible to measure the electrical properties of the molecules sandwiched between the wires.

Unfortunately, the Lorentz effect applies equally to the current in the wires due to the measuring voltage. The act of electrically investigating the molecules will cause the wire to separate or compress, thereby affecting the measurement.

To solve this drift problem, the technique was developed further by Ashwell et al.,[150] in order to make the measurement process independent of the contacting process. The method by which the top connection is brought into contact with the molecules is still magnetic deflection. However,

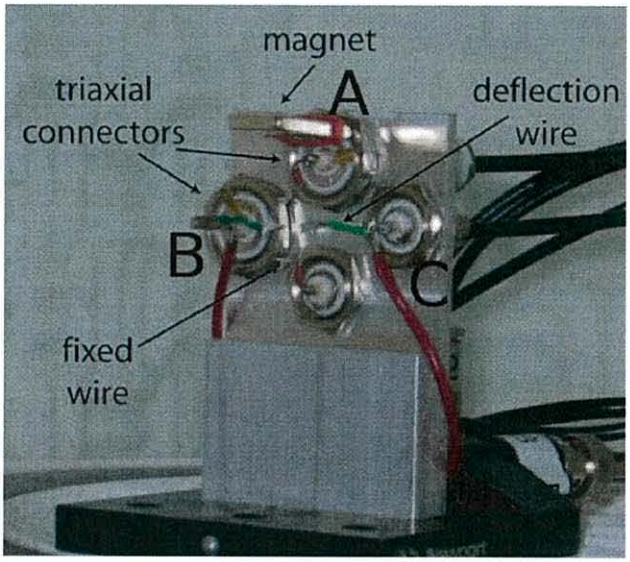

Figure 2.12: The original crossed-wire technique. Image copyright 2005, The National Academy of Sciences.[149]

rather than use the Lorentz force, a ferro-magnetic cantilever is bent by altering the voltage across an electromagnet positioned below it as in Figure 2.13. The contact wire is positioned away from the electromagnet at the tip of the cantilever, ensuring the measuring circuit is spatially separate and independent of the positioning circuit. This will be referred to as the Electro-Magnetic Cantilever technique (EMC).

There are several advantages and disadvantages to the EMC compared to the STM and so they are used throughout this thesis together as complementary methods. Principal amongst the differences is that the top contact makes physical contact to the molecules. This arrangement eliminates the asymmetry inherent in an STM, where the bottom contact has the molecules physisorbed or even chemisorbed onto a flat substrate whereas the top contact is separated by a tunnelling gap. There is always the potential for ambiguity and, particularly when investigating rectifying molecules, it is important to eliminate as much doubt as possible. For example, many early studies of molecular rectification were disputed because of contact asymmetry. Another advantage of EMC is that both contacts can easily be used as substrates for SAM layers. Two molecular layers can

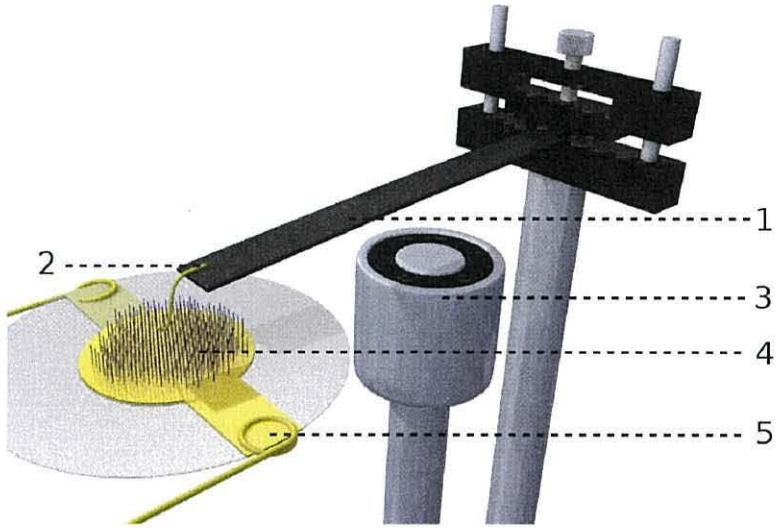

Figure 2.13: The experimental setup for the electromagnetic cantilever technique: 1) Ferromagnetic cantilever; 2) Top contact attached to end of cantilever; 3) Electromagnet; 4) SAM; 5) bottom contact

then be brought together and characterised electrically as one system. While not impossible with an STM, the delicate manipulation of the tip makes the operation difficult and the high electric field gradients experienced at the sharp tip adds an additional unknown factor. A further advantage is the ease and relative low cost of setting up and running the equipment required for an EMC.

Disadvantages to the EMC technique mainly result from the large contact area between the two electrodes. It is often assumed that the current through many molecules will approximate a simple scalar multiplication of a single molecule current.[151,152] However, inter-molecule interactions can mean that this is not necessarily the case, if only for the geometrical alteration.[123] Therefore, the STM's ability to examine fewer, or even single, molecules will produce clearer indications of how a molecule behaves. Also, an STM tip doesn't change its contact area after it is formed. Even with rearrangement, the current will always preferentially flow through the lowest atom. However, with the EMC, the contact area will change depending on how firmly it is pressed onto the lower contact and as the surface will not be perfectly flat any change in precisely where the two contacts meet will also result in a change

in area. These factors introduce ambiguity to the number of molecules being contacted. Therefore, the shape of an EMC result is of more interest than the magnitude.

2.3.2.1 The Bitwise Method

One method developed to compensate for the uncertainty in contact area, particularly in the cases where there is slight drift during a measuring run or noise due to vibration, is the bitwise method. A customised LabView virtual instrument is used to create feedback. Rather than only measuring the current at a series of incrementally changing voltages, the bitwise method also takes a measurement at a constant voltage, 0.5 V, after every voltage increment. When the feedback current rises or falls over time, it may be inferred than the contact area is increasing or decreasing respectively. The feedback current can therefore be used as a multiplier on each of the incremental currents and thus compensate for any drift, as in equation 2.6. In a perfect, stable system, the feedback measurements would produce a constant current and the multiplying factor would be unity:

$$I_{corrected}(V_n) = \frac{I_{raw}(V_n) \times I_{raw}(0.5V)}{I_{feedback}(0.5V)} \tag{2.6}$$

An example of this method in operation is shown in Figure 2.14. The raw data to the left shows a forward and reverse I-V curve that have drifted apart between runs. The corrected data to the right shows the drift corrected which results in the two runs being overlaid.

2.3.3 Break Junction

In the previous sections, the techniques discussed connected to each side of a molecule in turn. Alternatively, if a contact architecture is created that contains a gap that is precisely the length of the molecule being studied, both ends can bind simultaneously. However, the separation of the electrodes in such a system is typically nanometres or even angstroms. One method capable of this precision is the break-junction. There are two main

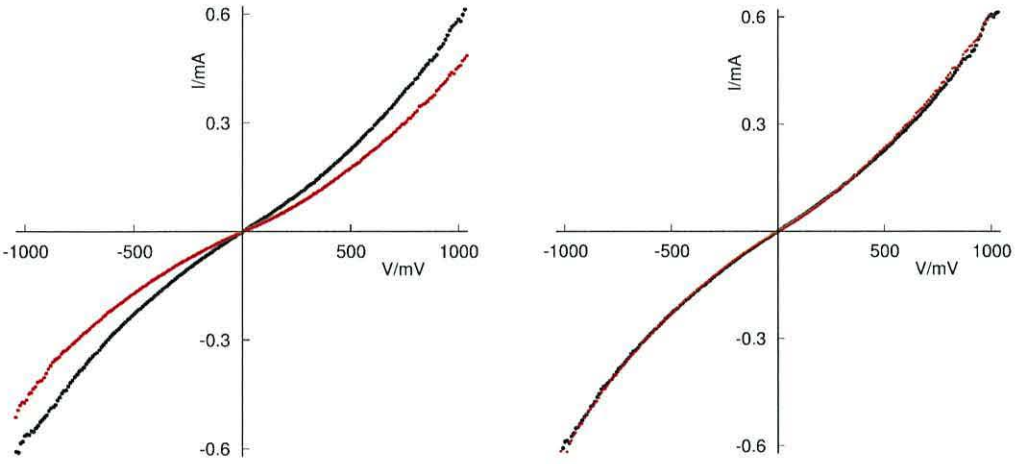

Figure 2.14: The bitwise method for capturing I-V characteristics using the EMC. The raw data on the left are modified by the information provided by the feedback current which produces a multiplying factor to correct for drift. The final data are shown on the right.

types of junction: mechanically controlled[153] (MCBJ) and electro-migration (EMBJ).[154,155] These will be described in turn, but the aim of both is to create contacts that are atomically sharp and whose separation is precisely controllable. A piezoelectric quartz crystal is one of the few technologies that can provide translational resolution at the molecular scale. This fine control can also be augmented by the experimental apparatus as shown in Figure 2.15. A thin strip of the electrode material is laid down on a flexible substrate. Lithographic methods are often used to make the initial wire as thin as possible, and a notch is made at the centre to nucleate the fracture. The wire is clamped at two points either side of the notch to concentrate the load. An actuator with very fine resolution then causes the substrate to bend upwards in the centre, straining the wire until fracture occurs. Then, by withdrawing the actuator, the two rough edges of the break can be brought back towards each other until the separation is reached to facilitate bridging.

As the wire approaches the moment of rupture, particularly when using a malleable material such as gold, the neck of the wire reduces until the strand becomes several atomic chains thick.[156–158] At this point, the current reduces as a series of steps as each channel breaks. The conduction reducing by the

value $G_0 = 2e^2/h$, the quantum of conductance.[83]

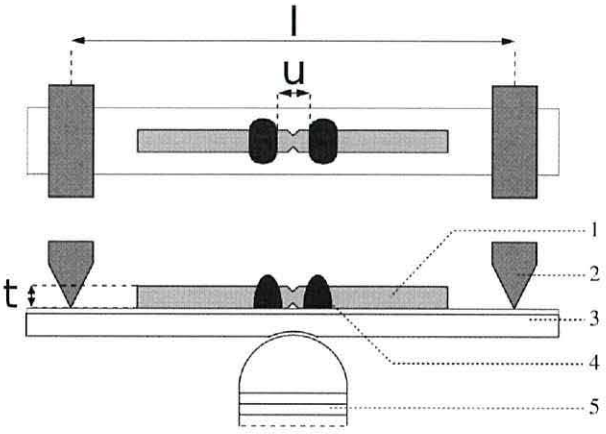

Figure 2.15: A schematic of the operation of a mechanically controlled break junction, including the: 1) wire used to form the junction 2) counter-balances 3) flexible substrate 4) clamps 5) piezoelectrically controlled actuator. Reproduced with kind permission of Springer Science+Business Media.[159]

The reduction ratio, r, that translates the movement of the piezo actuator to the separation of the junction is shown in equation 2.7:

$$r = \frac{\delta u}{\delta x} = \frac{6tu}{l^2} \tag{2.7}$$

where u, t and l correspond to the distances given in Figure 2.15. Much work has gone into reducing the size of parameter u in an effort to gain higher resolution control. To this end, break-junctions have been developed that use lithography to create a three-dimensional structure between a bridge, as shown in Figure 2.16.

This device has a separation between the supports of just 2 μm, which implies a reduction ratio of 10^{-4}, meaning sub-atomic precision is achievable.

Immersing the apparatus in a solution or gas of molecules that are bi-substituted with 'crocodile-clip' terminating units appropriate for the junction material causes bridging. A sudden increase in the monitoring the current between the contacts indicates the insertion of a molecule into the gap. Due the surface roughness, there will be a pair of nearest atoms that form the narrowest gap between the electrodes. Therefore, as the junction

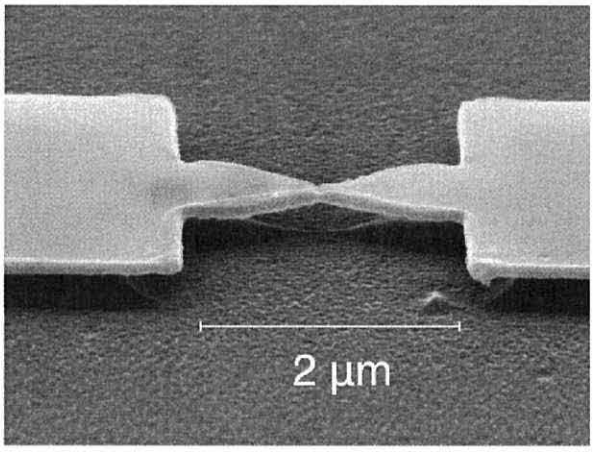

Figure 2.16: A transmission electron microscope image of a mechanically controlled break junction fabricated using lithography. Reproduced with kind permission of Springer Science+Business Media.[159]

is brought together, there is a good chance of forming a bridge with only a single molecule. An alternative technique is to coat the wire in a self-assembled layer of molecules before breakage. The molecules can move on the surface at the neck and bridge the gap spontaneously as the rupture occurs.

One of the great strengths of this technique is the fact that is is relatively straight-forward to cycle the separation of the junction; bringing the contacts towards and away from each other many times over. The molecules should remain intact as the gold-sulphur bond is likely to break first allowing the junction to be reused without significant degradation.[160] Rapid repeat measurements allow a histogram to be produced which can then be interpreted to infer a likely single molecule current, corresponding to the lowest peak, identified.

Pioneering work on break-junctions by Reed et al.[161] demonstrated the insertion of benzene-1,4-dithiol. A symmetrical IV plot was produced and was proposed to be from a single molecule. Subsequent work has helped to eliminate doubt over the origin of the conduction path. More complex molecules have been inserted, both symmetrical and asymmetrical. The resulting I-V curves were correspondingly symmetrical or asymmetrical,

depending on the molecule.[162] The agreement between the molecule and characteristic confirmed that the conduction is of molecular origin.

A different method of creating a break-junction utilises a phenomenon that is a major cause of faults in electronic systems: electromigration.[163–165] This technique takes a junction partially formed using the mechanical method and uses electromigration to complete the separation of the electrodes. Mechanically snapping a wire can result in uneven geometries and fractured contacts not ideal for electrical characterisation of single molecules. A more elegant technique for creating a break-junction is to use an electric current passing through the junction. This method is particularly effective when using a material with high atom mobility such as gold. The atoms migrate under the influence of force created by the electric field, particularly at defects, until a break is formed. The magnitude of the current can be controlled very precisely and dynamically as the junction forms to create the best surfaces for bonding. As the current is increased and the neck of the junction decreases, it moves into the same quantized conductance regime until the last nanowire breaks and the current falls to zero. This method is known as an actively broken junction. Unfortunately, even with this method it is possible to create nanoparticle fragments and clusters at the break that can bridge the gap. Moreover, these particles can behave in much the same way as a symmetrical single molecule thus introducing uncertainty into molecular measurements.[166] A further development of this technique is known as a self-broken junction. Instead of maintaining the field until fracture, the junction is taken to just before the point of breaking and then the field is removed, allowing the instability due to the natural mobility of the gold and the existing momentum within the system to complete the separation. This is a gentler process that has a greatly reduced probability of nanoparticles bridging the gap. Therefore, this results in a greater certainty that any Kondo effects or Coulomb Blockade phenomena are due to molecules rather than erroneous interstitial particles.[167]

2.3.3.1 Scanning Tunnelling Microscope Break Junction

A related technique uses an STM to create an architecture similar to a break junction.[168,169] A feedback loop is normally used to keep the STM tip at a constant distance from the substrate.

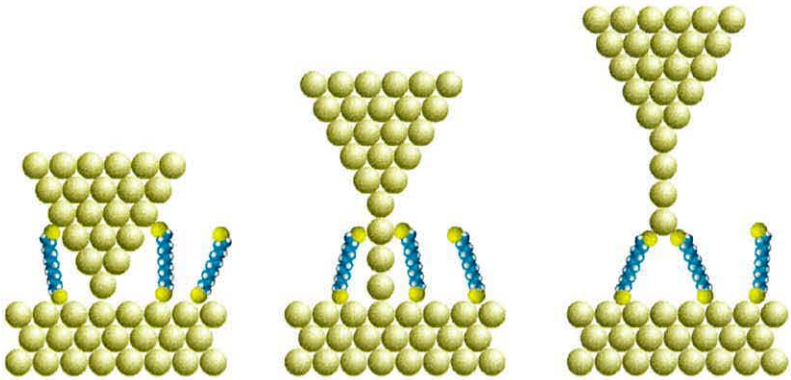

Figure 2.17: An STM break-junction showing a possible scenario as an STM tip is pulled out of a gold surface. An atomic chain is pulled out with the tip which forms an end contact to molecules attached to the surface.

By disabling this feature, the tip is allowed to drift into the layer of molecules and the underlying substrate itself. Reintroducing the feedback causes the STM to pull the tip away and break any contacts that may have formed, similar to a MCBJ. This process is shown in Figure 2.17. The cycle of connecting and breaking can be repeated many times to produce a statistical analysis of the molecules under investigation. This technique also provides information regarding the stretching of the molecules. The behaviour during the stretch reveals information about the bonding of the junction and its breakdown.[170]

2.3.4 Nano-sized Gap

There have been many other attempts to create architectures suitable for contacting molecules, adapting and extending lithographic methods. One technique that has been developed uses electrochemical methods to refine a larger gap to create nano-sized electrodes. Lithography can be used to

create a gap of sub-micrometre dimensions relatively easily. Electroplating, for example, can then be used to deposit atoms into the gap and grow the electrodes until a spacing of nanometre, or even atomic dimensions, is achieved. Etching can be used to reverse the growth, providing flexibility.

The difficulty in defining a nanometre sized gap is that few processes can be controlled with enough precision. An oxide growth thickness can be specified through the controlled addition of oxygen to a high-vacuum environment and can be made to have nanometre dimensions. By coating a platinum electrode in aluminium, for example, and exposing the structure to oxygen, an oxide will grow on the aluminium. This growth will then provide a mask for a subsequent platinum deposition to form a second electrode positioned an oxide depth away. Removing the aluminium along with its oxide results in a horizontal gap structure. Altering the oxide growth alters the gap width and so it is possible to obtain the required gap size.[137] Similar techniques have been used to form vertical nanogaps.[171]

Lithography and shadow deposition is normally limited by the size of the mask used to produce the structures. However, by suspending the mask above the substrate and altering the angle of deposition, the feature size can be reduced. If the incoming ions are oblique to the surface, the gap size depends on the angle and the position of the mask rather than the mask size itself. These factors can be controlled and thus electrodes with gap sizes of < 10 nm can be fabricated reproducibly. This process is illustrated in Figure 2.18.

Silicon and metals are not the only materials to be used for nanogap creation; carbon is also an excellent choice. In particular, graphene is increasingly the focus of nanoscale electronics research. One form of this material, as a carbon nanotube (CNT), has been used to create nano-spaced contacts.[77] CNTs are highly conductive, capable of carrying 10^6 times the current density of a noble metal. Also, they can form strong C-C bonds with incoming molecules so should be excellent as nanogap architecture.

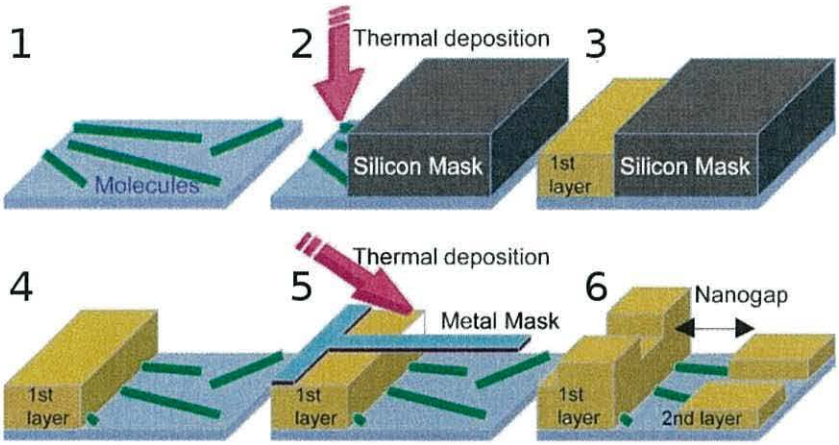

Figure 2.18: Fabrication procedure for the oblique angle shadow mask deposition technique. The metal mask shown in step 5 is significantly wider than the diagram suggests.[172]

2.3.4.1 Mushroom Devices

Another device fabricated to facilitate the insertion of molecules was used by Ashwell et al.[150] to measure the electrical properties of a stepwise molecule assembled on gold. Optical lithography is used to create an insulating core, sandwiched top and bottom by electrodes that are separated by a 3.5 nm gap. The various steps used to create the devices utilise a range of lithographic techniques to fabricate a mushroom-shaped core of SiO_2, thin Si_3N_4 layer with electroplated gold contacts above and below. A buffered hydrofluoric acid wash is then used to etch the Si_3N_4 dielectric in order to form an undercut and thus a nanogap between the top and bottom electrodes. Due to the geometry of the device, when molecules assemble between the contacts, they form a 'necklace' around the core. Macroscopic pads are linked to the electrodes during the fabrication process to allow for probing of the inserted molecules. A schematic of the device is shown in Figure 2.19.

A modular approach was used to create the molecules. First, a layer of aldehyde terminated anchor molecules was assembled onto both contacts and then a bi-substituted amino bridging unit was used to join the two sides *via* imino linkages. The current passing through the device increases by at least four orders of magnitude after the empty device is fully functionalised.

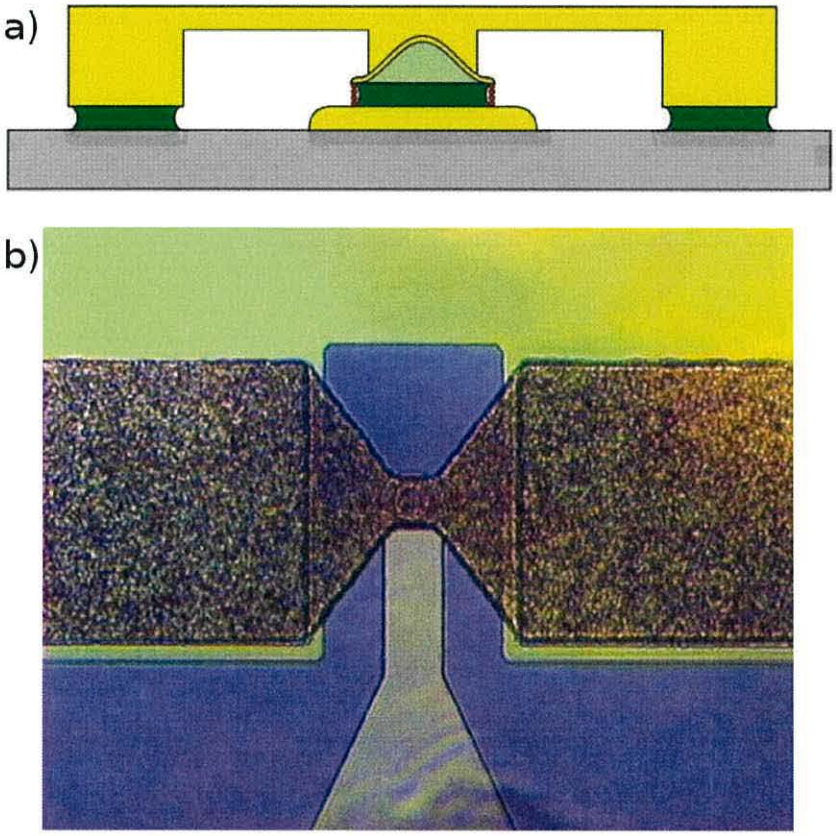

Figure 2.19: The gold mushroom device: a) schematic side-view: dark green corresponds to Si_3N_4, light green to a SiO_2 mushroom-shaped dome and yellow to gold contacts. The red beads represent the molecular wires that self-assemble as a ring around the core. b) top-view image.[150]

However, this device has too large an electrode surface area and is bridged too readily for the study of single molecules.

2.3.4.2 Silicon Nanogap Devices

A similarly fabricated device, although using silicon contacts rather than gold and with a differently configured architecture was used during parts of this study.[173,174] The silicon nanogap devices (SND) were fabricated by the industrial partner on this project, *QinetiQ* using similar techniques to those employed during the creation of complementary metal-oxide semiconductor devices. This method is ideal for the mass production of many identical

devices on one substrate chip. Two images of an example SND device are shown in Figure 2.20.

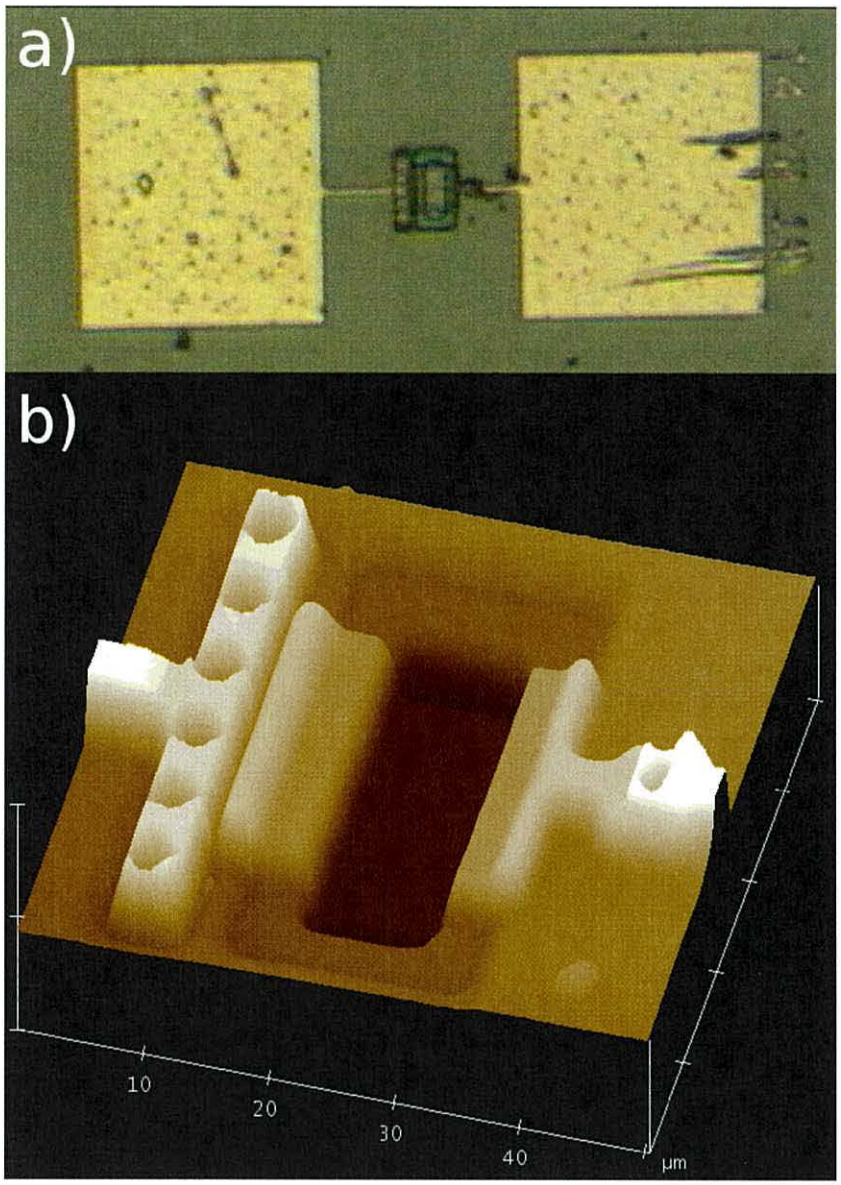

Figure 2.20: Images of a SND: a) taken with an optical microscope and b) taken using an AFM (Scan rate: 1.999 Hz, Vertical scale: 2000 nm div^{-1})

The steps used to fabricate an SND are outlined in Figure 2.21 resulting in a vertical $Si/SiO_2/Si$ architecture consisting of an upper electrode made of polycrystalline silicon and a lower electrode of Si(111). Both contacts

were highly n-type doped and the oxide layer separating the contacts is nominally 7 ± 1 nm thick. The undercut nanogap was exposed to NH_4F to reveal the silicon surface under the oxide layer and hydrogenate its surface. This step then facilitated the reaction of a diethylacetal derivative of 4-ethynylbenzaldehyde in a hexadecane solution at a concentration of 0.1 mg ml^{-1}. The reaction, carried out for two hours at 190°C was performed in an inert argon atmosphere to prevent further oxidation during the reaction. The molecules attached to the electrodes have two purposes. Firstly, they protect the surface from subsequent oxide formation, necessary as they had to be transported across the country between manufacture and subsequent use in experiments. Also, they provide the aldehyde linking group for reacting with amine bridging units. This terminating moiety is generated by rinsing with chloroform to remove physisorbed material and then with acidified solution to remove the protective acetal.

Although the geometry of the nanogap overhang makes it impossible to confirm the bonding of the anchoring molecule to the silicon surface, studies have been performed using planar substrates under the same conditions. Fourier transform infrared attenuated total reflection spectroscopy (FTIR-ATR) was one method used, which showed stretching vibrations that indicate the presence of the grafted molecules, for example ν_{CO} at 1703 cm^{-1}, in addition to showing evidence of SiO_x contamination.[176] Also, examining the grafted substrate using XPS produces spectra including a peak at 101.9 eV, corresponding to the Si_{2p} **Si**-C environment, from which it can be inferred that covalent grafting of the molecule has occurred.[177] However, the maximum of this peak is distorted by the presence of an oxide layer, manifesting as the nearby shoulder at *ca.* 103 eV, the binding energy of the oxide.[178] Both analytical techniques indicate that there is significant coverage of the molecule, covalently bonded to the surface, but also partial oxidation present. However, as the ultimate aim of the SND is to create a single molecule device, partial coverage will help limit the number of sites at which bridging can occur.

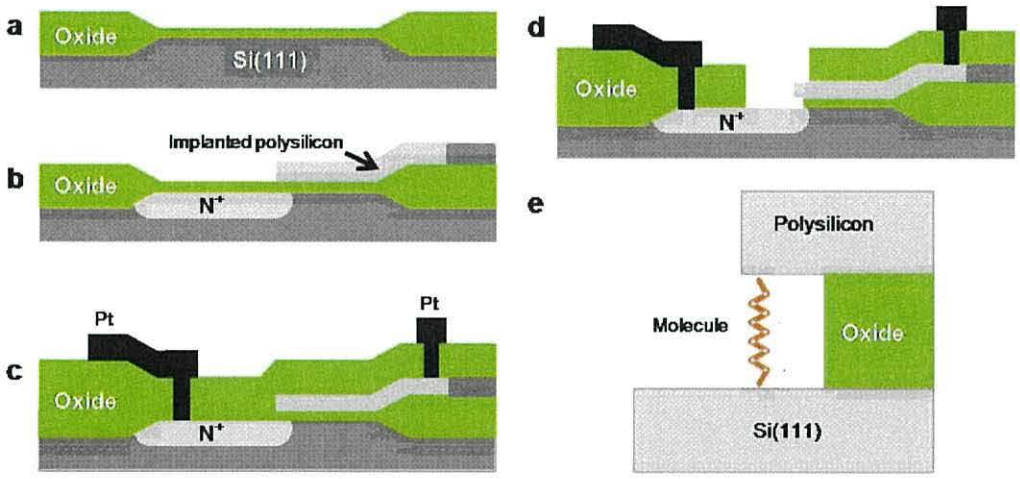

Figure 2.21: Microfabrication of a silicon nanogap structure: a) the gate oxide layer is grown on n-type Si(111), the thickness of this layer determines the height of the resultant nanogap, nominally 7 nm; b) arsenic is implanted in the Si(111) substrate to create a highly doped N^+ channel followed by the deposition of polycrystalline silicon on top of the oxide layer, which is patterned and similarly implanted with dopant ions; c) a low temperature oxide (LTO) is added, holes are formed and aluminium plugs inserted, which are etched to form electrical contacts to the doped silicon regions; d) the LTO is patterned and dry and wet etched to expose the nanogap structure and form the undercut; e) an enlarged view of the active area following etching with NH_4F solution, exposure to the anchoring molecules and stepwise reaction with a bridging molecule to connect the two electrodes.[175]

2.4 Physical Characterisation Techniques

In addition to the electrical characterisation of molecules, there are techniques used to reveal other information; to verify the composition of a layer, ascertain the quality of a monolayer or simply image the sample.

2.4.1 Quartz Crystal Microbalance

During this thesis, all depositions that can use gold and other metals as a substrate, at least one deposition is performed using a gold-coated quartz crystal, as this allows a microbalance to be used to determine the mass of molecules on the surface. This information can be combined with knowledge of the molecular structure to give an indication of how closely the layer is

packing. With many molecules, there is a favoured orientation for bonding to the surface. The packing is therefore simply an indication of the layer coverage and quality. However, some molecules can assemble in several different ways and, if the area each orientation occupies differs, it is possible to estimate the proportion of each orientation that has assembled.

When a mass is deposited onto a quartz crystal, its resonant frequency changes. The Sauerbrey equation, given in 2.8, is used to find the additional absorbed mass given a measured change in frequency:

$$\Delta m = -\Delta f \frac{A\sqrt{\rho_q \mu_q}}{2f_0^2} \tag{2.8}$$

where Δf = change in frequency due to deposition (Hz), f_0 = fundamental mode of oscillation of the clean quartz crystal (Hz), Δm = mass of material deposited (g), A = area of the electrode overlap (m^2), ρ_q = density of quartz (gm^{-1}) and μ_q = shear modulus of the quartz crystal ($gm^{-1}s^{-2}$)

From the change in mass, it is trivial to obtain the number of molecules present on the surface, using the relative molecular mass, M_r and Avagadro's number:

$$n = \frac{\Delta m N_A}{M_r} \tag{2.9}$$

A more useful value is the area per molecule,$A_{molecule}$, obtained by dividing the total area of the quartz crystal electrodes by the number of molecules that have been absorbed:

$$A_{molecule} = \frac{2AM_r}{\Delta m N_A} \tag{2.10}$$

By combining equations 2.10 and 2.8, the term for the area is eliminated. This area independence is important as it removes all ambiguity over the nature of the surface and allows different crystals to be compared directly. The final equation is shown in 2.11:

$$A_{molecule} = \frac{-2f_0^2}{\sqrt{\rho_q \mu_q}} \frac{M_r}{\Delta f} \propto \frac{M_r}{\Delta f} \tag{2.11}$$

To take a measurement using the QCM, the quartz crystal is set in a mount connected to an oscillator driven by a *Thurlby Thandar* stabilised current source-meter. A 9 V potential is applied between the electrodes on either side of the crystal and the voltage induces mechanical oscillations. These in turn causes an oscillating voltage due to the piezoelectric nature of the crystal. An *Agilent* Universal Counter measures the resonant frequency which is recorded by a computer. The system is allowed to stabilise for *ca.* five minutes to ensure a reliable reading. The resultant frequency, along with the molecular weight of the molecule being deposited can then be used by the equation given in 2.11 to provide an indication of the area per molecule.

Although it is a very accurate method of determining the mass of an adsorbate on the crystal, the QCM reveals nothing about the composition or arrangement of that mass. When using the Sauerbrey equation, there are several assumptions necessary. The matter is assumed to be only one layer thick and consist of only the molecules that have been intentionally deposited. Any unknown, adventitious, species will contribute to the mass but are unlikely to occupy an area homogeneously with the rest of the layer. Also, when the adsorbate forms multilayers, the mass to area relation is impossible to determine. Therefore, the QCM is an approximation only and must be used in conjunction with other techniques to increase the confidence in a result.

2.4.2 X-Ray Photoelectron Spectroscopy

Another technique, very useful for yielding information about the composition of a monolayer, is X-ray photoelectron spectroscopy (XPS). While there were some developments before WWII, it wasn't until the 1960s, when Kai Siegbahn advanced the technique to create a relevant analytical instrument. He was awarded the 1981 Nobel Prize in recognition of his work.

The foundation for this method was laid by Einstein in 1905 when he published his work on the photoelectric effect. He stated that when a photon impinges on a surface, it is possible for its energy to be absorbed by electrons within the material. If the energy of an incoming photon is below a certain

threshold then the light is simply re-emmitted. However, if the energy is above the threshold, then the absorbing electron can be ejected from the material. The kinetic energy of the emmitted electron is dependant only on the wavelength of the incoming radiation and the binding energy of the electron, not the intensity of the incident light. This relationship is shown in equation 2.12.

$$E_\kappa = h\nu - E_B \tag{2.12}$$

where E_κ is the kinetic energy of an ejected electron, h is Plank's constant, ν is the frequency of the incoming radiation and E_B is the binding energy, referenced to the vacuum level. The process of photoelectric emission is shown in Figure 2.22.

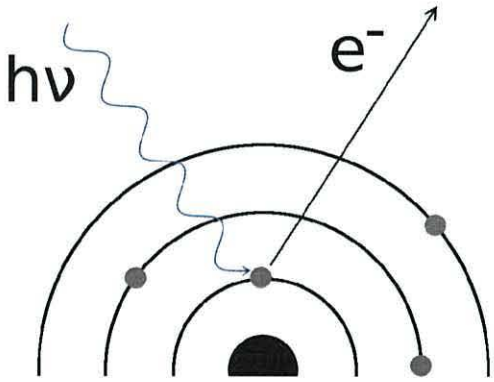

Figure 2.22: X-ray photoelectron spectroscopy, showing the photoelectric effect as an incident X-ray excites an electron which is ejected and can be captured by the detector.

Using a radiation source of constant energy that is incident on a material containing a mixture of atoms, the emitted electrons will have energies characteristic of those atoms. In a real system, the equation must be modified by correction factors. These take into account the sample work function (φ) and energy losses due to surface charging or structure relaxation for example (E_{loss}). The modified equation is given in 2.13 where the binding energy is referenced to the Fermi level of the sample.

$$E_B = h\nu - E_\kappa - \varphi - E_{loss} \tag{2.13}$$

Firing photons at a target and measuring the energies of the resultant ejected electrons creates a spectrum dependant on the elements within the sample. In a high resolution scan, the technique is sensitive enough to distinguish between several instances of the same element in different immediate environments. The different energies are the result of the type of bonding and the other elements involved in those bonds. As an ejected electron travels to the detector, there is a chance it may interact inelastically with other elements within the monolayer and the analysis chamber. This scattering process results in a small loss of energy and manifests as noise in the final scan. For this reason, an XPS chamber is held at a very high vacuum. Depending on the amount of a particular element and how strongly it interacts with the X-rays, the signal to noise ratio might be high enough to have confidence in fitting the peak cleanly. If the signal to noise ratio is low, multiple scans can be taken and then averaged in order to reduce the effect of random scattering.

XPS is a highly surface sensitive technique; while the X-rays can potentially penetrate up to the order of micrometers, it relies on excited electrons escaping the material after photo-emission. The mean free path of these electrons is generally of the order of nanometers, which results in a typical escape-depth of 1 - 10 nm, depending on material. This distance is ideal for most molecular monolayers, which are generally made of molecules that are a few nanometers long. XPS can be used to detect the elements present, and their relative abundances within the measurement depth. However, due to their low atomic masses, it is incapable of detecting the two lightest elements, hydrogen and helium.

An extension of the technique uses the angle at which the radiation arrives at the surface to make the technique more surface sensitive. By reducing the take-off angle, measured from the surface normal, the depth at which electrons can escape is decreased. The proportion of the layer that can be investigated reduces as the spectroscopy is performed at increasingly shallow grazing angles. From this technique, known as angle resolved XPS (AR-XPS), it is possible to estimate the thickness of thin films and the extent of contamination, implantation and variation across a layer.[179,180]

Commercial instruments generally use monochromated aluminium K_α or magnesium K_α X-rays, but it is also possible to use a synchrotron source to provide the source of photons. The high intensity of synchrotron radiation has enabled novel developments such as real-time measurements that reveal the changes that occur to a system as a reaction occurs.[181,182]

The results presented in this thesis were taken with the help of Kym Ford at the University of Queensland, Australia. The measurements were performed using an Axis Ultra spectrometer, from *Kratos Analytical Co.*, operating at a pressure of $< 9 \times 10^7$ Torr. The radiation impinged on a *ca.* 5 mm^2 area of the substrate, adjusted to find a location that maximised the signal and maintained throughout all measurements of that sample. Each monolayer was initially subjected to a wideband survey scan, taken in one sweep at a pass energy of 160 eV, a step size of 1 eV and a dwell time of 100 ms. With the constituent elements identified from the wide scan, high resolution scans of each element of interest were then taken. These involved typically two or more averaged sweeps, depending on signal to noise ratios. The setting used were pass energy of 40 eV, a step size of 50 meV and a dwell time of 500 ms all using monochromatic $Al_{K\alpha}$ radiation. The specimens were prepared by self-assembling molecules onto gold-coated highly ordered pyrolytic graphite (HOPG) as described in sections 2.1.2 and 2.5.3. HOPG was used in order to fit the sample holders available for the machine. A quartz crystal deposition scheme was replicated to increase the chance of a closed packed monolayer on the HOPG.

2.4.3 Atomic Force Microscopy

Developed in 1986 by Gerd Binnig, Calvin Quate and Christoph Gerber, the atomic force microscope (AFM) is a technique related to the STM. It uses the interaction of atoms in an atomically sharp tip and a surface to measure its properties, produce an image or manipulate matter. The microscope consists of a small, silicon or silicon nitride cantilever, with the tip at one end. As this tip is scanned over the sample, a laser is directed down onto the end of the cantilever. This photodiode registers the deflection of the cantilever by

monitoring the position of the reflected laser dot. This displacement can be used to measure the force that caused it using Hooke's law. Alternatively, by rastering the tip over the entire sample and relating the laser deflection to a tip deflection, a complete surface picture can be built up. The basic componants of an AFM system are shown in Figure 2.23.

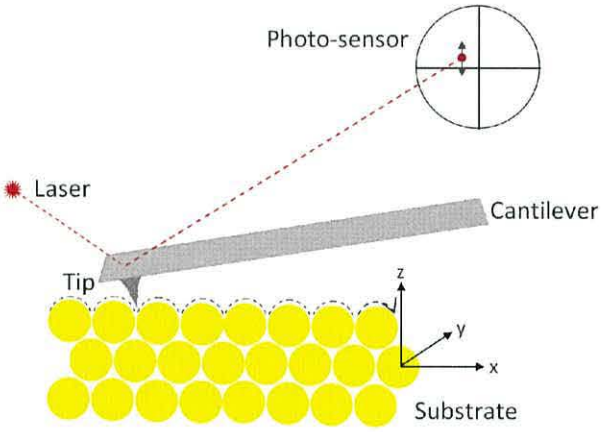

Figure 2.23: A schematic of the operation of an atomic force microscope.

There are three modes of operation when using an AFM. The standard operating mode is the most basic. The tip is pressed lightly on to the surface by the cantilever and is moved around the surface. The underlying structure physically deflects the tip up and down as it varies in height due to the Pauli exclusion principle preventing atoms in the tip and sample to overlap. An alternative approach is to invert the cantilever to pull the tip away from the surface. By allowing the tip to be close enough for van der Waals interactions to have an effect, the tip can still be deflected by the surface undulations and produce an image. This second method is a gentler approach with less chance of damaging a delicate surface, but has a reduced resolution due to the range of the van der Waals force. The third technique is known as tapping mode. As its name suggests, the tip is repeatedly raised and lowered over the surface as it is rastered across. This technique is slower than the standard, but it has a reduced chance of causing damage as the tip always approaches the surface from directly above. Unlike the inverted method, however, there is no compromise to the resolution. There is also less chance of 'shadowing'

in this mode, due to tip coming over a ridge and continuing a lateral scan before it follows the side of the ridge all the way to its base.

A further development of the AFM technique is the conducting probe AFM (CP-AFM).[183] This tool operates in much the same way as the standard method except the tip must be made of, or coated with, a conductive material and connected to an electrometer. This technique has a significant advantage over an STM as it removes ambiguity due to the air gap between tip and sample. An STS I-V curve is produced by a complex convolution of functions. Conversely, an AFM has no air gap and so treats all areas equally. The CP-AFM can still be used as a conventional AFM thus the sample can be reliably imaged before and after characterisation. This not only provides additional information on the sample, but allows the probe tip to be positioned with great accuracy.[184]

2.5 Preparation of Substrates

It was usually necessary to prepare the substrates used in this thesis, in order for them to receive molecules and bind to them appropriately. The surface must be free of any existing organics that might obstruct binding sites and minimise any extraneous, undesirable, oxide layer, that could hinder the formation of a bond.

2.5.1 Quartz Crystal

The type of substrate that has proved of greatest use during this project was a gold patterned quartz crystal from *International Crystal Manufacturing Co.* as shown in Figure 2.24. Not only is it a good substrate, but its properties allow a QCM to provide information about a deposition. It consists of a thin disk of cleaved mica, coated on either side with an evaporated 1 cm^2 circle and interconnect pattern. First a 10 nm layer of chromium is laid down to aid adhesion and then 100 nm of gold is added. The gold is annealed and forms a (111) crystal structure when new, although the lattice becomes disordered over time. This degradation is not of any great concern as long range order

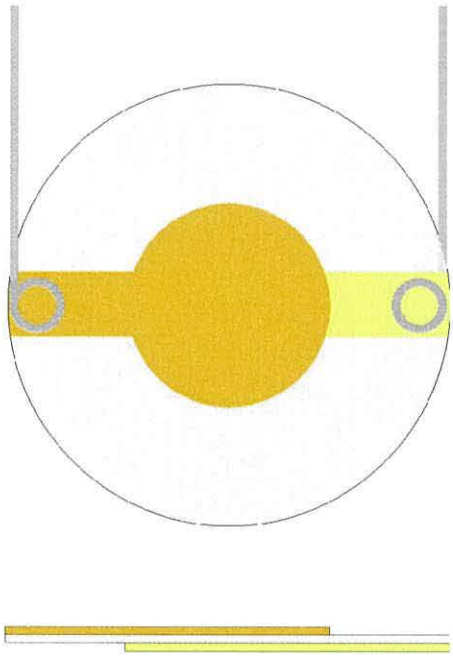

Figure 2.24: Representative diagram of a quartz crystal, showing the cleaved mica disk with two evaporated gold contacts deposited either side. Top and front elevations.

is not a requirement for deposition to occur. Only a small area is ever under examination during electrical characterisation so large scale surface structure becomes irrelevant. Preparation of the surface follows a three step process as follows:

i) The crystal is placed inside the chamber of a *Gala Instrumente, Plasma Prep II* (see Figure 2.25). This is evacuated with a vacuum pump for three minutes. The chamber is then flooded with a stream of nitrogen for a further three minutes to ensure that as much oxygen as possible is removed.

ii) A radio frequency emitter is then turned on which excites the gas atoms into ions and free electrons, thus forming a high energy plasma. The radiation is left on for a further three minutes to allow the plasma to

clean the surface of any remaining organic materials and reduce the oxide layer.

iii) The final preparatory step is to wash the crystal with pure solvent to remove any stray gold clusters that have been displaced by the plasma but have remained, settled on the surface. This latter step is performed in tandem with a microbalance to monitor the effects of washing. When the frequency readings from the balance are consistent before and after a wash, then it is clear all material has been removed and deposition can begin immediately.

Figure 2.25: The *Gala Instrumente Plasma Prep II* in operation, showing the glowing nitrogen plasma inside the chamber.

2.5.2 Gold Wire

Gold wire was used both as a deposition substrate and as a probe tip. Wire could be used as either electrode for the EMC technique and as a tip in the STM, all with or without a coating of molecules. The material, of several diameters from 0.25 mm to 0.025 mm, was supplied by *Goodfellow Ltd.* and nominally of 99.99+ % purity. For all applications, it was prepared in the same way as the quartz crystal *via* plasma cleaning. As with the quartz crystal, some oxide reforms practically instantaneously, but it is thin enough to be displaced by incoming molecules.

2.5.3 Highly Ordered Pyrolytic Graphite

For certain applications it is often simpler and cheaper to use gold coated highly ordered pyrolytic graphite (HOPG) as a substrate rather than the gold-coated mica. The HOPG sample cannot be used to determine surface coverage on a microbalance as with a quartz crystal, but if the layer is already well characterised, previous results can be used as a guide to produce a similar quality monolayer at significantly less cost. The graphite is cleaved with adhesive tape to remove the uppermost layer fragments until a complete top layer is removed, this reveals a clean, complete layer underneath which is rinsed in solvent and coated with gold ready for deposition.

Figure 2.26: A *Polaron E5000* sputter-coating

The coating was performed using a *Polaron E5000* sputterer, as shown in Figure 2.26, set at 1.2 kV and 10 mA for 42 minutes to produce a gold layer approximately 100 nm thick. If the sample is used immediately, straight from the sputterer, it requires no additional procedures; however, if it remains unused for longer than a few minutes, as was most often the case, it was cleaned in the same way the gold coated quartz crystals are prepared to remove any contamination (see section 2.5.1).

2.5.4 Silicon Nanogap Device

The SND devices, from *QinetiQ*, arrived with the organic coating already in place (unless requested otherwise), and could be used for depositions without further modification. The linker molecule was terminated with an acetyl protecting unit; the method used for de-protecting is as follows:

i) The chip was immersed in a 1:3 by volume solution of formic acid and hexanol for half an hour.

ii) Next, the wafer was sonicated in dimethylchloride for half an hour to dislodge any physisorbed material.

iii) Finally, the sample was washed in the solvent to be used for the deposition and dried to ensure no interference from cleaning.

However, as the molecule that is to be reacted with the aldehyde linker group should be able to displace the protecting group without de-protection, and complete coverage is unnecessary. In many of these investigations, especially during attempts to form single-molecule bridges, low coverage is desired and so de-protecting the chips was not performed during later experiments. The thorough procedure only occurred in the early experiments, when it was important to prove that the reaction was occurring. Evidence of bridging without de-protecting validated this approach.

Chapter 3

Results and Discussion

The molecules used during the following studies are presented below in table 3.1 for reference. **M1** was synthesised by Dr. Piotr Wierzchowiec, a colleague within the Nanomaterials group while at Cranfield University. **M3** and **M4** were synthesised by Dr. Mustafa Tavasli at The University of Durham. **M2** and all other components were purchased from *Sigma-Aldrich Chemical Co.* All solvents used for creation of solutions were HPLC grade and from *Fisher Scientific* and were used without further purification.

Key	Name	Structure
M1	4-[(3-mercaptophenylimino) methyl]benzaldehyde	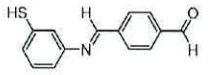
M2	2,6-diaminoanthra-9,10-quinone	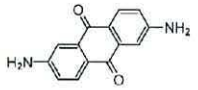
M3		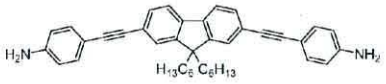
M4		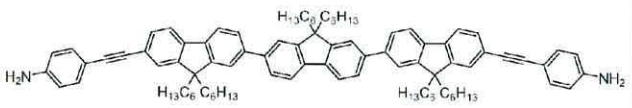

Table 3.1: A key for the molecules used during this study.

For brevity, when describing the wires assembled onto substrates, the codes outlined in table 3.2 are used rather than full descriptions of the wires. They are presented here for future reference. Also, while these wires will be described as being built up using layers, it should be noted that this identifies initial component parts only. When each sub-unit reacts with the wire already assembled on the surface, it is elongating that molecule and will result in a single unit, not identifiable layers.

Key	Structure	Length
W1	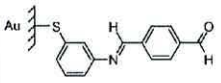	1.3 nm
W2	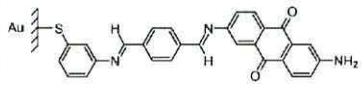	2.4 nm
W3	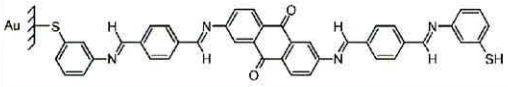	3.7 nm
W4	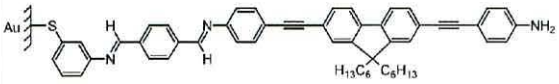	3.6 nm
W5	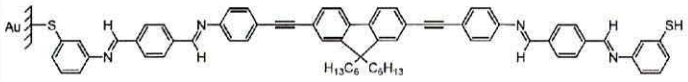	4.9 nm
W6	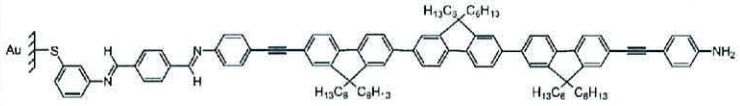	5.3 nm
W7	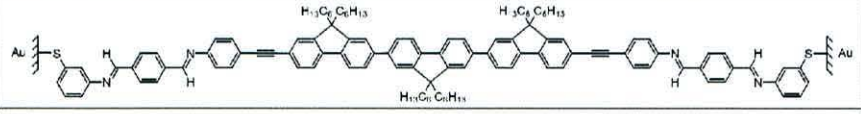	6.6 nm
W8	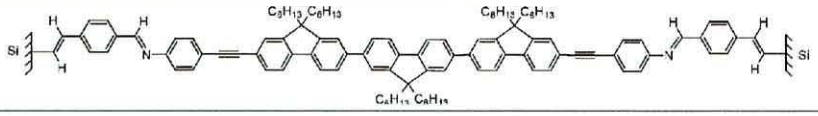	5.9 nm

Table 3.2: A key for the wires used during this study.

In the quest for single-molecule electronic devices, there are many challenges to overcome. Foremost, a reliable method of connecting the molecule between a pair of contacts must be developed. While there are plenty of examples of methods to connect to one end reliably, a robust method for contacting both ends of a molecule, suitable for mass production in commercial devices, is elusive. Another challenge is that of building adaptability and useful functionality into the molecules. Also, the devices must be robust enough to survive the everyday demands of today's technology hungry world.

The approach taken in this thesis to tackling these problems will be split into several sections. The first (3.1 and 3.2) focuses on the creation of molecular layers on solid substrates. Both the anchoring of a monolayer and the subsequent stepwise extension using synthesis at a surface will be examined. Second, in section 3.3, the electronic properties of the various wires will be investigated. Finally, in section 3.5, the first two strands will be brought together with using the silicon nano-gap devices. Quasi single-molecule electronic devices are created and tested, highlighting the possibilities of hybrid devices incorporating molecular electronics into silicon architecture.

3.1 Studies on Quartz Crystal Microbalance

The essential first step in examining a molecular electronic system is to attach the molecule to a solid support. Once synthesised, the molecules are usually found in a powdered crystalline form. When combined with a compatible solvent, a solution is made from which the molecule, providing it contains a suitable moiety, can undergo self-assembly. The process is described in detail in section 2.1.2, and will not be repeated here.

It was important to verify that the initial anchoring layer was assembling properly and to monitor the quality of the final monolayer. A QCM plot uses the mass of the deposited material and the relative molecular mass to indicate the average area each molecule occupies and how that changes over time with each immersion. The final limiting value of area per molecule is of

greatest interest. When combined with knowledge of the size of the molecules and an assumption of homogeneity, it is possible to infer the packing and to give an indication of any dual-layer character.

The information gathered in this section can then be combined with that taken during XPS measurements, shown in section 3.2, to give a thorough description of the physical nature of the layers as they assemble on the substrate.

3.1.1 Forming an Anchoring Layer on Gold

The majority of the molecular wire depositions studied during this thesis used the thiolated 4-[(3-mercaptophenylimino)methyl]benzaldehyde, **M1** in table 3.1, for anchoring the layer to gold. The compound was dissolved in acetone to form a 0.1 mg ml^{-1} solution. This molecule is an ideal candidate for the first layer of a multi-part system as the meta-substituted thiol results in the most likely arrangement of molecules being perpendicular to the surface. This is preferable for limiting the possibility of addressing the molecule part way along its length, rather than its end, when contacting with a probe tip, for example. Smaller molecules are generally found to assemble in less ordered layers, not conducive to forming the close-packed layers desired. **M1**, while still small, is long enough to induce energy minimising intermolecular interactions that encourage long-range order and close-packing. Importantly, **M1** is still small enough to dissolve easily in many solvents such as acetone and THF, enabling deposition from solution, without requiring the addition of disruptive alkane chain moieties. Finally, it is terminated by an aldehyde group. While either an aldehyde or an amine terminated molecule are suitable possibilities for the imine formation stepwise synthesis intended to be used to extend the wires. However, it has been shown that the nitrogen has a high affinity for gold, and the amine group may be the preferred anchoring group, over a thiol, in as high as 70 % of a layer, thus preventing *in-situ* synthesis.[185]

The gold electrode substrates, used to deposit the first layer, was used in two forms; a pure metal wire, or a thin layer coated onto a small HOPG

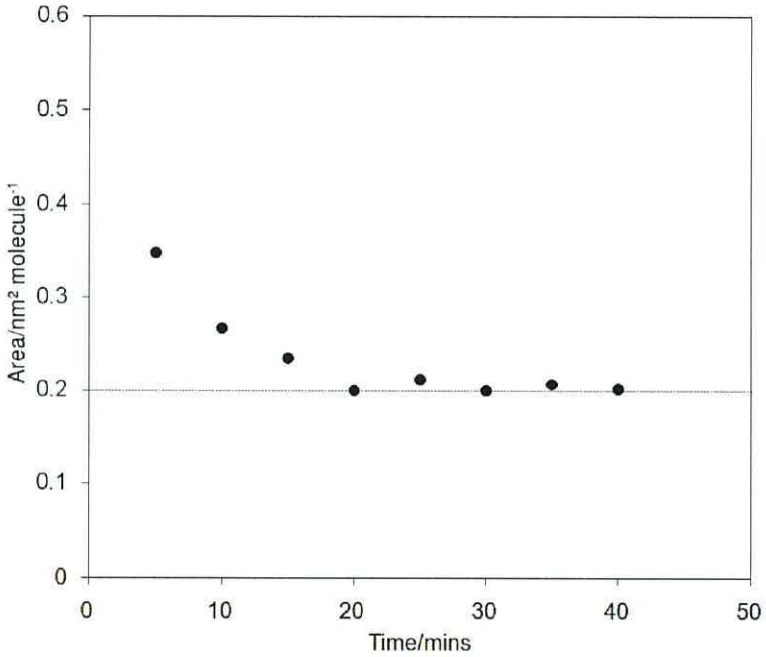

Figure 3.1: QCM of layer 1 - **M1**

block or a quartz crystal. To measure the progress of layer formation, the initial deposition was performed using a 10 MHz quartz crystal and the frequency change due to the assembly monitored using a microbalance. The deposition was found to proceed most efficiently as a series of short, five minute, immersions. Each immersion was followed by washing in copious quantities of pure solvent to remove any physisorbed material and time spent drying in a fume cupboard. The resonant frequency of the crystal was then measured using the microbalance and, when a stable reading was obtained, recorded. If the frequency continued to change while on the balance or changed with repeat readings without further immersion, extra drying time was allowed. The assumption being that solvent remained trapped in the lattice and was evaporating gradually during the measurements. Additionally, an anomalously large drop in frequency was most likely the result of adventitious material in the layer. This necessitated an additional washing and drying cycle, to make sure all physisorbed material is removed and avoids obscuring the rate at which the molecules of interest are bonding

to the surface.

Figure 3.1 shows a typical deposition for the thiolated **M1** as a first layer. The frequency quickly decreases until it reaches a stable value after around 20 minutes. A Sauerbrey analysis of the data yields a probable area per molecule of typically between 0.20 and 0.25 nm^2. The cross-sectional area of a benzene ring is *ca.* 0.25 nm^2 and therefore a tightly packed monolayer is consistent with this analysis. A smaller area suggests additional material and is most likely the result of a small amount of physisorbed multi-layering, trapped solvent within the lattice or other adventitious species not removed by washing. The spontaneous nature of self-assembly, coupled with the uncertainties discussed above, results in deposition isotherms that were not identical. However, the fact that more than 20 repeats of this deposition all produced very similar final areas increases confidence in the repeatability of the final layer. The equipment is capable of measuring a *ca.* 10MHz frequency to many decimal places, but the variability of the repeat depositions shows that the calculated areas are not known to similar precision.

3.1.2 Adding an Anthraquinone Extension

The first multi-step wire to be investigated had already been the subject of study by the Ashwell et al.[150] The second step is also a fairly small molecule, at approximately 1 nm in length, and is believed to assemble linearly as shown in Figure 3.2. Therefore, this wire was an ideal test subject with which to develop the EMC technique and provide a baseline for extending the work. The method for building up a monolayer *via* stepwise follows that of the first layer:

i) The molecular solution is made up in the same way, with concentrations similarly around 0.1 mg ml^{-1}. The solvent requirements are much the same as before. However, it is usually necessary to add trace amounts of glacial acetic acid to catalyse the reaction.

ii) The substrate with the previous layer(s) attached is immersed in solution for *ca.* 60 mins.

iii) After deposition, the sample is washed in pure solvent, any pinholes in the previous layers can allow a molecule to physisorb to the surface or, as is more likely, molecules can become lodged in-between the strands of the layer and held there with van der Waals interactions. This washing step is especially important after a layer of molecules containing side arms. These side chains increase the area per molecule and present a larger gap for subsequent molecules to enter.

iv$_a$) If the substrate is a quartz crystal, the layer is then dried thoroughly and its molecular coverage measured using a microbalance as described in section 2.4.1. The crystal is re-immersed, washed, dried and measured in a repeated cycle until a consistent limiting value is obtained, corresponding to a close packed monolayer.

iv$_b$) If the substrate is not a quartz crystal, then the sample is simply washed and re-immersed repeatedly, following a previous known deposition pattern taken with a quartz crystal in order to increase the likelihood of producing a layer of similar, known, quality.

For the second layer, the 2,6-diaminoanthra-9,10-quinone, **M2**, was dissolved in acetone to form a 0.1 mg ml^{-1} solution with *ca.* 0.05 ml glacial acetic acid per 25 ml. Then, the substrate with the first layer SAM already formed was subjected to similar immersion, wash, dry and measure cycles in the new solution to allow the imino-formation reaction to occur and produce a tightly packed layer. A longer immersion time was found to be necessary for **M2**, due to the slightly larger bulk and longer time required by the imino-formation reaction.

The graph in Figure 3.3 shows a typical deposition for this second layer. The frequency deceases steadily until it reaches a stable value after around 600 minutes. A Sauerbrey analysis of the data yields a probable area per molecule of typically between 0.20 and 0.25 nm^2. The minimum cross-sectional area of the second layer is similar to the final area of the first layer. However, the anthra-9,10-quinone unit is slightly bulkier than just a benzene ring and therefore the limiting area is smaller than expected

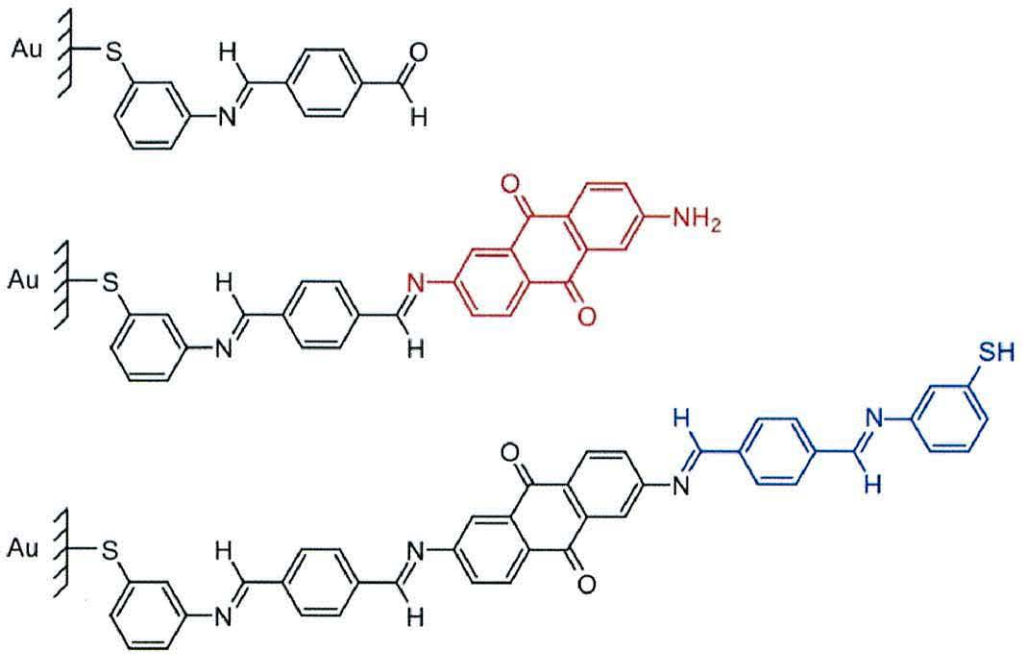

Figure 3.2: Formation of **W3**, showing each stage of stepwise synthesis

from close-packing. It is likely there are contributions from a small amount of multi-layering, trapped solvent or other adventitious species. However, a large proportion should contain good coverage of the **W2** SAM. Again, the confidence in the saturation point comes from several repeat readings. Despite varying deposition routes, the end point is consistent within ± 0.025 nm^2.

3.1.3 Adding a 2.3 nm Single Fluorene Extension

With the previous study of stepwise assembly using a short diamino molecule showing evidence of successful synthesis-at-a-surface, the next challenge was to extend this method to other molecules. In particular, two molecules were chosen that had been synthesised by Dr. Mustafa Tavasli, of Prof. Martin Bryce's group at the University of Durham. The first of these molecules, **M3**, contains one fluorene moiety, bounded by benzene rings *via* ethynyl linkages and terminated at either end by amines.

The fluorene unit is a common element in many light emitting diode

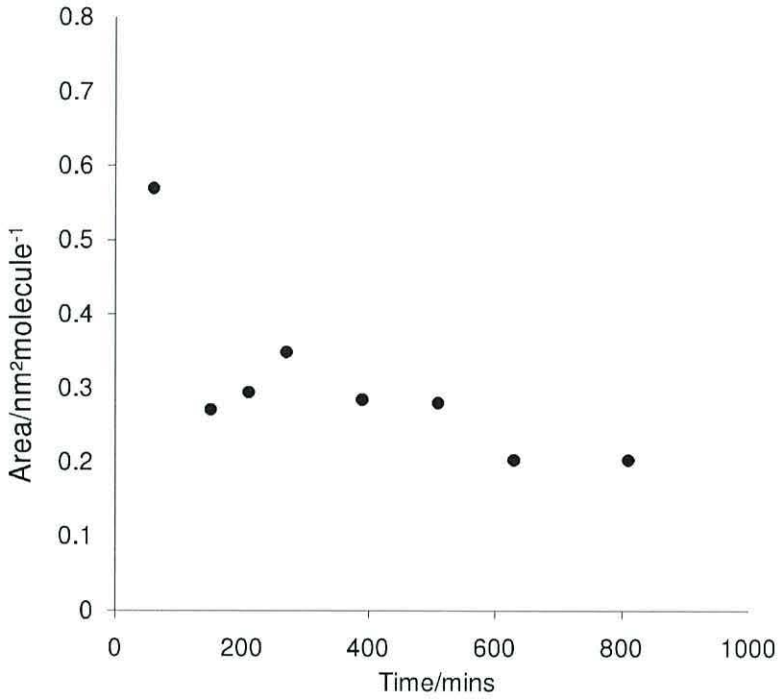

Figure 3.3: QCM of layer 2 - **M2**

(LED) systems.[186–189] It has excellent hole transport properties, polyfluorene having a hole mobility an order of magnitude greater than poly(*p*-phenylenevinylene), for example.[190] Electron mobility is lower than for holes, but the conjugation and small HOMO-LUMO gap still should still produce good electron transport. A polyfluorene molecule was found to have a decay constant, β, of 0.38 ± 0.09 Å^{-1}, better than most saturated molecules.[191] The molecule contains two ethynyl carbon triple-bonds. This type of bonding involves one σ-bond and two π-bonds and therefore continues the conjugation of the molecule. However, it has been suggested that the short bond length may disrupt the conjugation more than vinylene-based molecules and the rotational barrier for ethynyl moieties is lower than for vinylene compounds. This could lead to some freedom of rotation for the phenyl groups with respect to the fluorene at room temperature.[192] The overlap between the orbitals of two ring structures has a $cos^2\theta$ dependence where θ is the angle between them, and it is important for the conjugation to maintain overlap.[64]

There did not appear to be any reason why this molecule would not assemble in a similar way to the small diamino linker, **M2**. However, it was found that due to the electron density distribution being less favourable to the imino-formation reaction or simply the physical bulk of the molecule, deposition took considerably longer. Consequently, immersion durations were increased to keep total deposition times manageable; several hours being common, or even overnight.

To form a deposition, **M3** was dissolved in chloroform to produce a 0.1 mg ml^{-1} solution. The catalyst, *ca.* 0.05 ml glacial acetic acid per 25 ml, was added and the immerse, wash, dry, measure cycle using a quartz crystal could begin. The same initial layer of the **M1** molecule was used to provide an aldehyde terminated, tightly packed, SAM ready to react with the amines *via* imino formation.

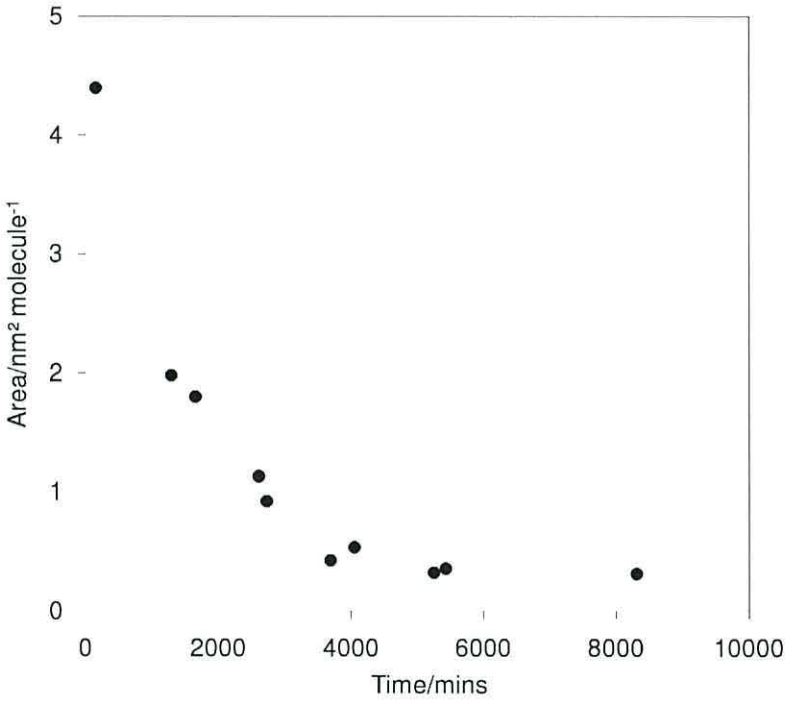

Figure 3.4: QCM for layer 2 - **M3**

The deposition shown in Figure 3.4, demonstrates the extra time taken for the bulkier layer. The SAM forms in *ca.* 60 hours, levelling out at an

area per molecule of *ca.* 0.4 nm^2. Although the molecules of the second layer assembled with approximately half the density of the first, the higher area is consistent with the extra bulk of the C_6H_{13} chains, in addition to the potential for disorder due to the slight curve introduced by the fluorene unit. The discontinuity between the two areas means that approximately half the first layer remains un-reacted.

3.1.4 Adding a 4.0 nm Triple Fluorene Extension

The second molecule of interest synthesised by the Bryce group, was similar to the first, but extended by an additional two fluorene units at its centre. It is shown in table 3.1 as **M4**. Chosen as the key linking unit to bridge the silicon nano-gap devices in section 3.5, this molecule was expected to behave in a similar way to the single fluorene linker, being identical but for the bulkier central moieties.

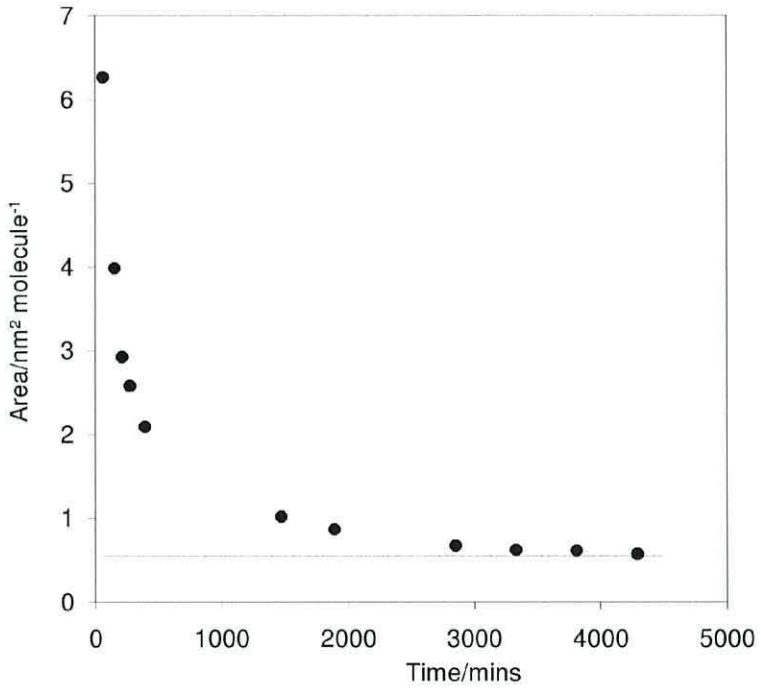

Figure 3.5: QCM for layer 2 - **M4**

The molecule is of particular interest because the side-groups attached to fluorene can lead to Fano resonances close to the Fermi energy.[193] Modification of this side-group or altering the conformation of the side-group can have a significant effect on the electrical transport properties. This can be exploited to produce a sensor, for example, that detects an analyte close to the side-groups. This presence is revealed due to the change in conductance across the molecule. This response could open up the possibility of a single-molecule sensor; able to detect the lowest possible concentration of a substance. The more common Breit-Wigner resonances, from conduction through broadened HOMO or LUMO orbitals cannot be used in the same way.

For this deposition, **M4** was dissolved in chloroform to typically form a 0.1 mg ml^{-1} solution with the addition of *ca.* 0.05 ml glacial acetic acid per 25 ml as catalyst. As can be seen from the deposition in Figure 3.5, the formation of the monolayer was typically very similar to the single fluorene diamino linker, forming in *ca.* 60 hours. The final area of the layer was *ca.* 0.5 nm^2 $molecule^{-1}$, forming on top of a **M1** initial layer with molecular area 0.2 to 0.25 nm^2. This approximately 1:2 registration with the layer below demonstrates again the side chains restricting the packing of the molecule and is consistent with expectation due to the cross-sectional area of the **M4** molecule.

3.1.5 Completing a Symmetrical Three-step Wire

The diamino bridging units, when in the nano-gaps, were required to react with aldehyde units at both ends concurrently. While this situation is impossible to recreate exactly in a planar test-bed structure, it was possible to extend the wires to three steps with an extra **M1** unit. This served two purposes; to examine how well the imino formation reaction occurs as a third step, and allowed electrical probing of the three-step molecule to provide an idea of the expected current flow in the system.

In all three diamino cases mentioned previously, the method for the third layer follows that of the second. A 0.1 mg ml^{-1} THF solution of **M1** was

made up, to which *ca.* 0.05 ml glacial acetic acid per 25 ml was added. The solvent for **M1** was changed from acetone as it can disrupt imino formation. Then, the substrate with the first two layers already assembled was subjected to immersion, wash, dry and measure cycles until a limiting value is obtained, corresponding to a tightly packed third layer.

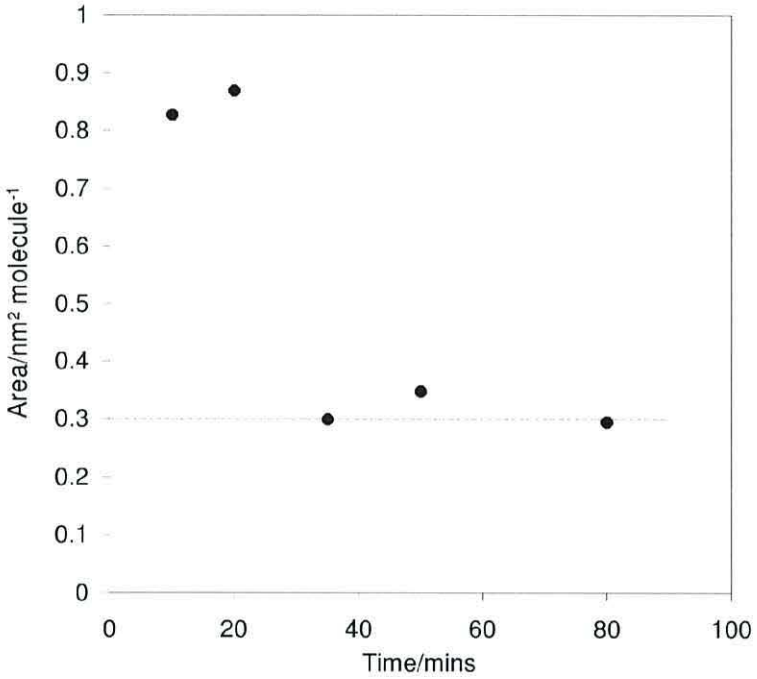

Figure 3.6: QCM of layer 3 - **M1**

The graph in Figure 3.6 shows a deposition for the third layer. Extending a **W6** unit consisting of the **M1** anchor layer and the larger three fluorene diamine, **M4**, to create a **W7** wire. The frequency quickly reaches a stable value after around 40 minutes. A Sauerbrey analysis of the data yields a probable area per molecule of *ca.* 0.3 nm^2. This is larger than that for the first layer, but smaller than a typical second layer. This suggests that while the availability of bonding sites should force the third layer molecules to pack more loosely than their cross-sectional area would otherwise dictate, the gaps between the second layer molecules allows a number to penetrate and become entangled. Copious washes in pure solvent failed to bring the area back up

to the size expected in an idealised system. However, this situation could not arise when the two anchor molecules are deposited first, nor would it interfere excessively in the electrical studies of the system. The adventitious molecules that become entangled will be below the surface and so too far away to be probed by a tip, and the influence on the conductance is expected to be minimal. The energy levels of the the conjugated backbone extend to the contacts and should dominate over any adjacent electron densities. It is possible that π-π stacking could occur and modify the transport, but this situation is unlikely to be common and so with repeat readings will not be significant.

3.1.6 Investigation of Many-Step Wires

Further studies were carried out, extending a molecule by many more steps. Theoretically, a molecule can be extended indefinitely using the stepwise method, but ultimately, in a practical system, disorder and adventitious physisorption will eventually corrupt an extended monolayer into a continuum mix of the various component molecules.

A useful molecule in the toolbox for the further reaction of molecules discussed previously is terephthaldehyde. The aldehyde moieties allow it to bind together the amines while the phenyl ring maintains conjugation. A typical deposition is shown in Figure 3.7, resulting from immersion of a substrate in a 0.1 mg ml^{-1} THF solution of terephthalaldehyde with 0.05 ml glacial acetic acid per 25 ml. Being a small molecule, the reaction proceeded relatively rapidly, and a short immersion, wash, dry and measure cycle quickly resulted in a limiting value for the minimum area per molecule.

The plot in Figure 3.7 represents reaction of terephthalaldehyde with an initial layer of **W5**, which has the single fluorene diamine as its second layer. The limiting area of *ca.* 0.16 nm^2 is much smaller than the area per molecule of the diamine, with its long side-chains. It is clear that a significant amount of physisorption occurred between the molecular strands, below the surface of the layer. The size of the molecule easily allows it to fall between the widely spaced second layer.

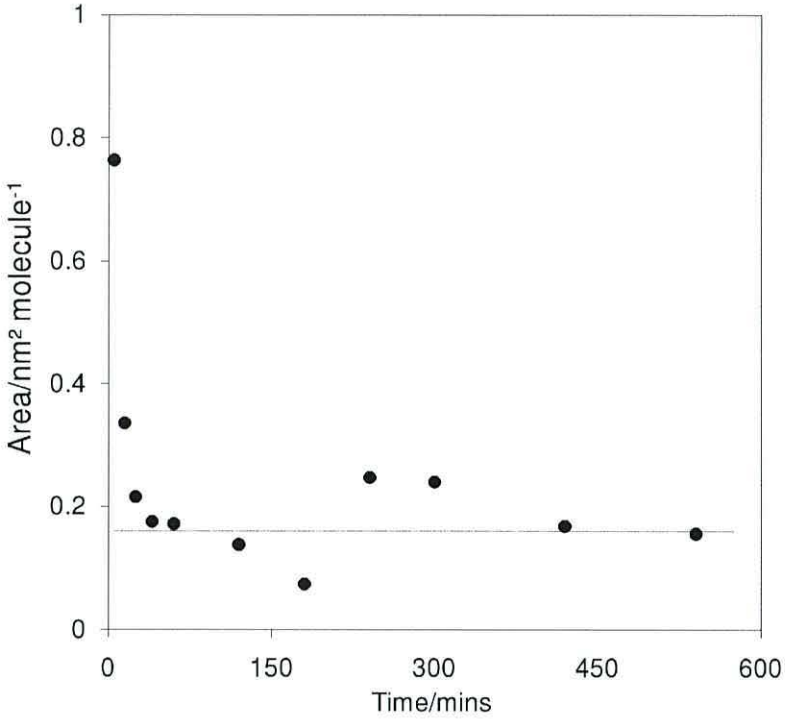

Figure 3.7: QCM of terephthalaldehyde as a 3rd Layer

The plot in Figure 3.8 shows a summary of a large multi-step elongated wire consisting of seven steps. A self-assembled **M1**, followed by three single fluorene diamine units, joined with two small terephthalaldehyde units and terminated by another **M1** unit. The points fall fairly linearly. However, the gradient of the **M3** sections are generally shallower due to the reduced coverage of side arms. Conversely, the terephthalaldehyde sections have a slightly steeper gradient, corresponding to the extra physisorption that occurs during those stages. This result demonstrates the power of the self-assembly technique, synthesising an incredibly long, complicated, asymmetric molecule in a matter of weeks.

3.1.7 Summary

It has been shown that by assembling molecular wires using a multi-step, modular approach, it is possible to build up very long wires consisting of

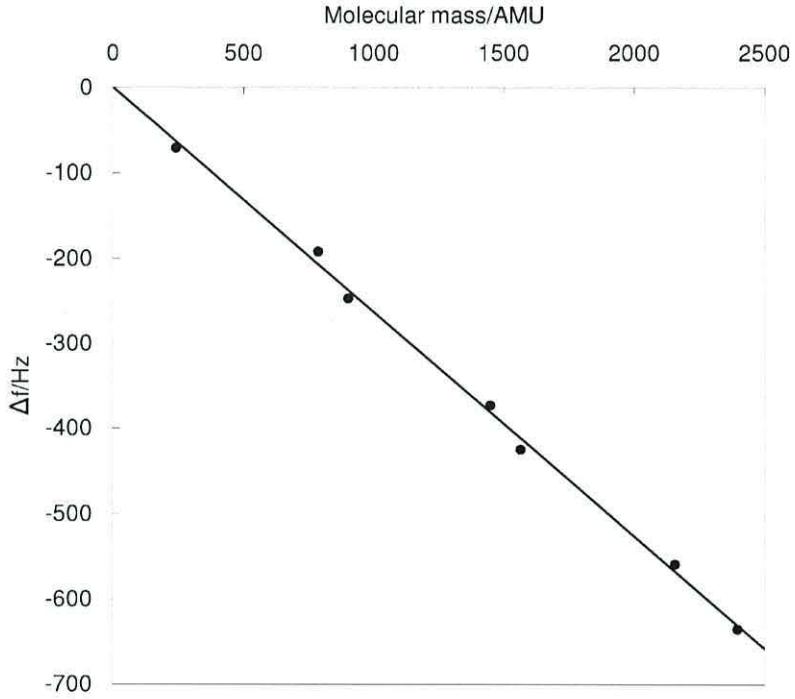

Figure 3.8: Multi-step QCM summary of **M1** - **M3** - (terephthalaldehyde - **M3**)$_2$ - **M1** system

many parts. The mass of the additional material from assembly on, or reactions at, a gold-coated quartz surface can be monitored from the resonant frequency change of the 10 MHz quartz crystal. A Sauerbrey analysis of the data yields limiting areas per molecule that closely match the molecular cross-section and therefore suggests the formation of generally close-packed, upright, homogeneous layers. Any variation from expectation tends towards an excess, due to a proportion of interstitial impurities and physisorbed material, particularly with the larger, more widely spaced molecules.

3.2 Studies with X-ray Photoelectron Spectroscopy

QCM studies of self-assembled monolayers are useful in determining the progress of a deposition and its likely packing, but is limited in the information it can provide about a layer's composition. XPS analyses were performed to complement that of the QCM data and provide further information regarding the binding of the molecule to the substrate and the quality of the layer.

The results were analysed using the Casa XPS software and corrected for surface charge error by introducing an offset. For monolayers, the gold 4f peak was taken as the reference point and calibrated to 84.0 eV. The background was taken to be of a Shirley type and subtracted from the data. Each total element peak was then deconvolved into constituent environment peaks, each fitted using a relevant function, typically a Gaussian-Lorentzian. These peaks used free parameters except for the case of the sulphur doublets where the known 2:1 area ratio and 1.2 eV gap between mid-points constraints were applied. In all cases, the analyses took account of the relative sensitivities of all elements by dividing throughout by their atomic relative sensitivity factors, from table 3.3. With the various elements directly comparable, it was possible to determine the relative amounts of each element present in the sample by comparing the area of each peak.

Element	Relative Sensitivity Factor
C1s	0.278
N1s	0.477
S2p	0.668
O1s	0.780
Au4f	6.250

Table 3.3: Normalisation factors to correct for the disparity in sensitivity to XPS radiation for various elements.

It was already known from the literature that there would be a significant presence from carbon and oxygen contamination on the gold; primarily in

the form of carbon monoxide absorbed *via* the carbon.[194–196] It is likely that these contributions will form broader peaks than those from elements within the molecules. This is due to the varied nature of impurity environments, compared to the homogeneous molecular environment. Therefore, it is difficult to be certain regarding the amount of oxygen and carbon present within the layers under investigation. The most useful information will be contained in the elements nitrogen and sulphur, more specifically identifiable as being of molecular origin.

All the peaks shown throughout this section have been corrected for charging drift, caused by the photoelectric effect when the X-ray beam impinges on the metal surface, using the Au 4f peak at 84.0 eV as a reference point.

3.2.1 Study of the Anchoring Layer on Gold

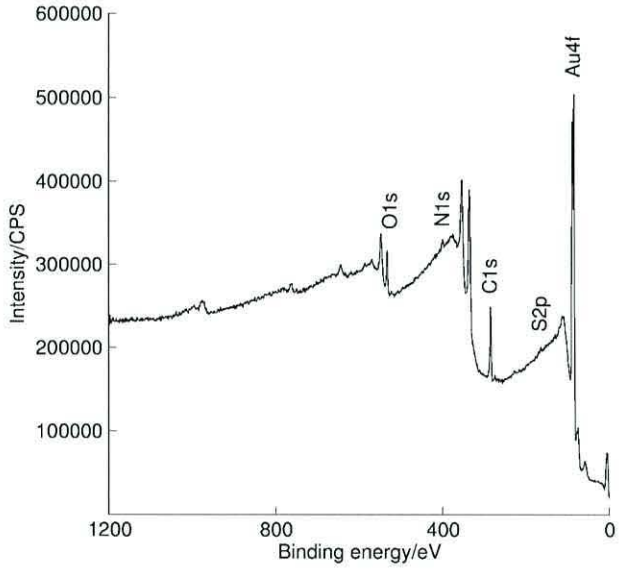

Figure 3.9: Low resolution, wide XPS scan of **W1** on gold-coated HOPG

A sample of gold-coated HOPG, on which a layer of **M1** had been deposited was analysed using XPS. The wide survey scan, shown in Figure 3.9, indicated the presence of all four elements expected in the layer in addition

to a strong gold peak and higher resolution scans of the areas relevant to each element are included below.

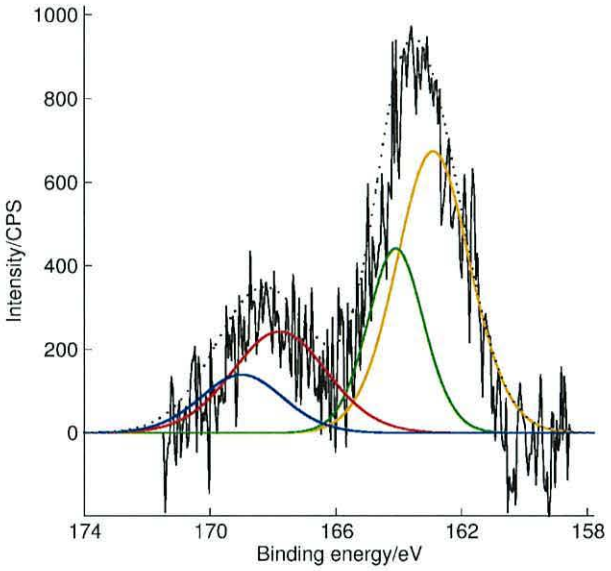

Figure 3.10: S2p region of XPS spectra for **W1**

There are two sets of sulphur doublets in Figure 3.10. The peaks with S $2p_{3/2}$ at 163.25 eV and S $2p_{1/2}$ at 164.45 eV are characteristic of the Au-**S** link indicating a significant amount of chemisorption occurring throughout the layer. The other set of peaks with S $2p_{3/2}$ at 167.91 eV and S $2p_{1/2}$ at 169.11 eV are likely to be due to oxidised sulphur species, which may or may not be bound to the gold.[197] The relative intensities of the peaks in table 3.4 implies a *ca.* 3:1 ratio between the sulphur bound to gold and unbound sulphur, indicating a highly chemisorbed layer.

The nitrogen 1s peak, found at 399.35 eV as shown in Figure 3.11, is characteristic of the C–**N**=C imine element. There is only one nitrogen species present in this molecule so it is as expected to find only one peak. The relative intensities of sulphur to nitrogen in table 3.4 show that there was 1.3:1 nitrogen to sulphur ratio rather than the 1:1 correspondence expected from the molecular formula. However, given that sulphur is buried closer to the surface than the nitrogen, it is possibly due to the attenuating effects of the layer between them. The escape depth of electrons ejected *via* XPS is

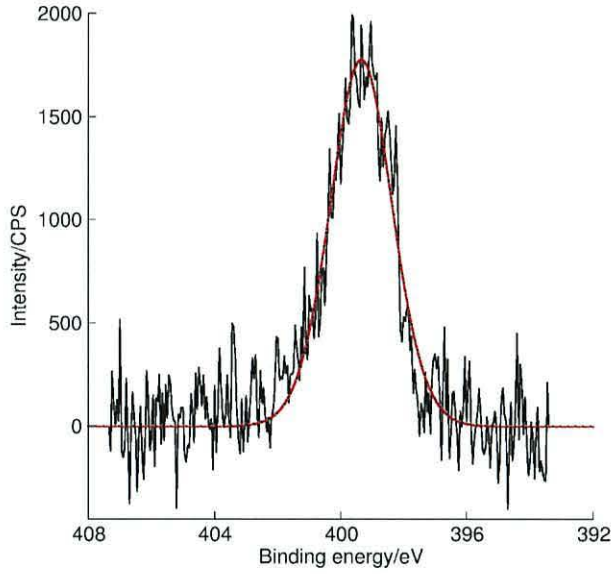

Figure 3.11: N1s region of XPS spectra for **W1**

only *ca.* 5 nm. Therefore, species located closer to the surface of a layer will produce a more intense signal. The molecules in this instance do not approach the thickness to absorb significantly and the effect should be minimal, but will always be present to some degree.[198] Note that for brevity, only the S $2p_{3/2}$ position is shown in table 3.4, and all subsequent XPS tables. However, the normalised intensity takes account of both the S $2p_{3/2}$ and S $2p_{1/2}$ peaks together. There is a constant 1.2 eV difference between the doublet peaks and so specifying one specifies both.

Element	BE/eV	Proportion of element	Normalised intensity
S $2p_{3/2}$	163.25 167.91	72% 28%	1.0
N 1s	399.35		1.3
C 1s	284.71 286.15 287.80	81.9% 9.0% 9.1%	17.3
O 1s	531.72		3.4

Table 3.4: RSF-corrected signal intensities for the elements in **W1**, normalised to the sulphur 2p intensity.

Also, included below in figures 3.12a and 3.12b are the carbon and oxygen regions respectively.

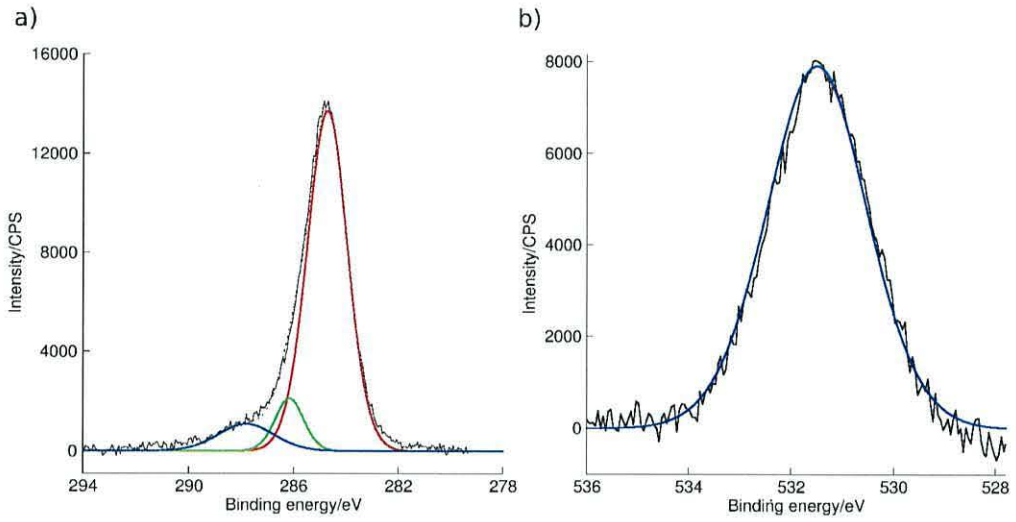

Figure 3.12: High resolution XPS spectra for **W1**: a) C1s region and b) O1s region

The constituent peaks for carbon indicate the presence of **C**–C/**C**–H at 284.71 eV, **C**–N at 286.15 eV and **C**=O at 287.80 eV. All these elements are expected, and in approximately the correct ratios, but with unknown impurities concentrations it is impossible to be more accurate. Similarly with the oxygen spectrum, the single peak is placed at the energy expected for C=**O**, but the normalised signal is over three times the intensity expected from the molecule alone. Part of this disparity could be due to the sulphur signal attenuation, but it is very likely that the signal is being skewed by additional contaminant oxygen species in the system. This could be from the small amount of oxide remaining on the gold surface, or adsorbed H_2O, CO or CO_2 species.

3.2.2 Study of stepwise assembly

It was important to corroborate QCM data suggesting imino formation, to prove that the stepwise process produces chemisorbed layers and not merely independent layers, held together by electrostatics or other physical effects.

3.2.2.1 Diaminoanthraquinone

It has been suggested previously in, section 3.1.2, that **M2** reacts with **W1** to form **W2**. Saubrey analysis of the QCM data of this two layer system indicated an approximate 1:1 correspondence between the layers.

Element	BE/eV	Proportion of element	Normalised intensity
S $2p_{3/2}$	162.48 168.41	55.1 % 44.9 %	1.0
N 1s	398.85 400.10	63.7 % 36.3 %	2.2
C 1s	284.94 286.84 288.41	88.6 % 5.0 % 6.4 %	35.2
O 1s	531.91		9.1

Table 3.5: RSF-corrected signal intensities for the elements in **W2**, normalised to the sulphur 2p intensity.

The main region of interest in this study is that in Figure 3.13 showing the nitrogen peaks with the second layer deposited. There are two peaks, at 398.85 eV and 400.10 eV, corresponding to C–**N**=C and –$\mathbf{N}H_2$ respectively. Comparing the areas of the two peaks, as shown in table 3.5, the imine species accounts for 63.7 % of the total nitrogen presence compared to 36.3 % for the amine. The ratio between the two environments is *ca.* 1.8:1 and so close to the expected 2:1 predicted by the molecular formula. The discrepancy implies a smaller relative signal for the buried species due to the absorption of electrons throughout the layer. However, this is strong evidence that the imino-bridge stepwise synthesis method is occurring as predicted.

The ratio of sulphur to nitrogen, shown in table 3.5 is 1:2.2, less than the 1:3 of a completely bonded homogeneous two-layer system, and this time the error is the opposite to that explained by absorption between the element and detector. Instead, the discrepancy may be explained by an incomplete second layer which results in a reduced nitrogen signal.

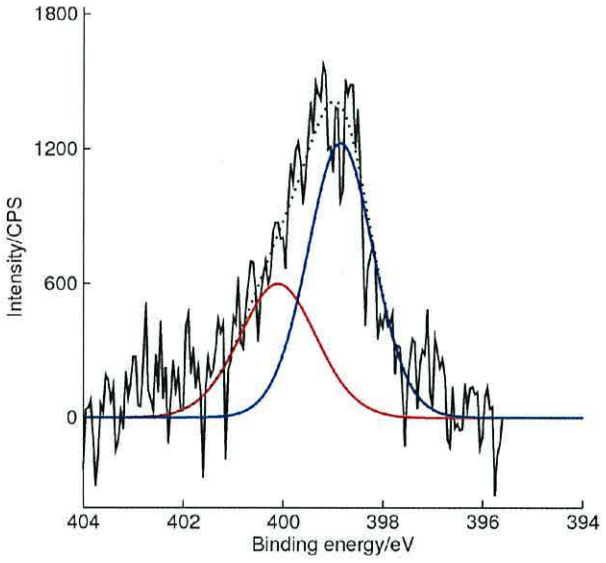

Figure 3.13: N1s region of XPS spectra for **W2**

3.2.2.2 4.6 nm Long Single Fluorene

The shorter, single fluorene diamine, **M3** was shown to react with the thiol-aldehyde **M1** to create **W4**. A Sauerbrey analysis of the deposition on a gold-coated quartz crystal indicated that the second layer was bonding only with 1 in 2 of the first layer molecules, assuming complete chemisorption, due to the 1:2 area ratio. The wide-scan XPS spectrum is shown in Figure 3.14.

The spectra in Figure 3.15 shows the two peaks produced by a high resolution scan of the nitrogen region.

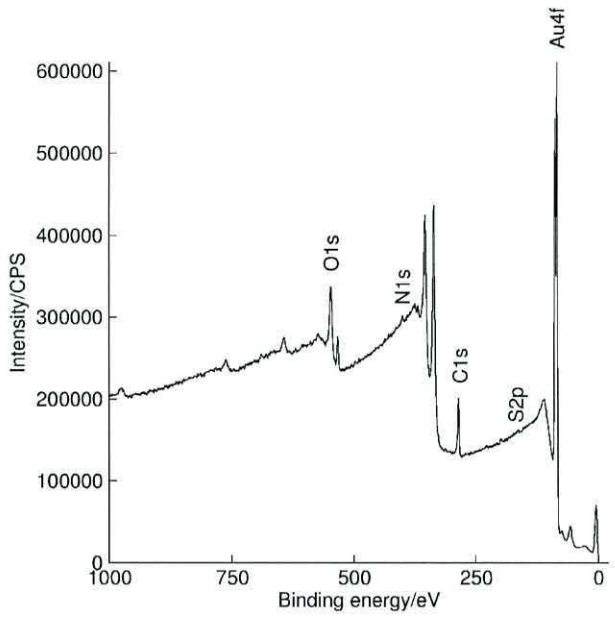

Figure 3.14: Low resolution, wide XPS scan of **W4** on gold-coated HOPG

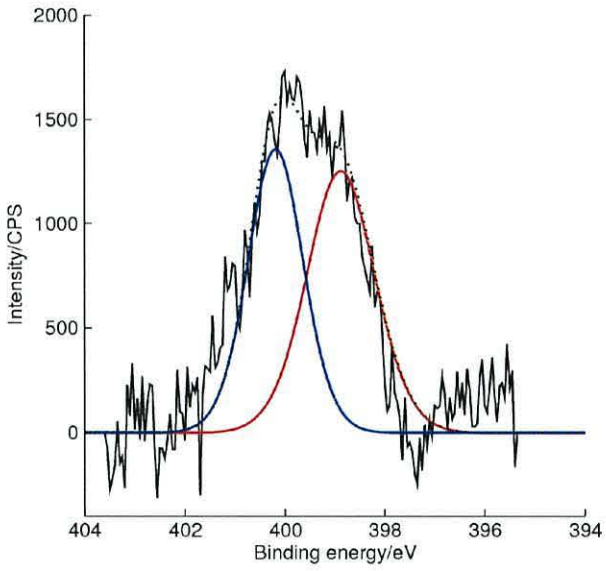

Figure 3.15: N1s region of XPS spectra for **W4**

The peaks at 398.87 eV and 400.18 eV are characteristic of the imine and amine respectively. The relative areas of 53.25 % to 46.75 % are closer to parity than the 2:1 expected from the two-layer molecular formula. If

the partial second layer coverage is taken into account, the expected ratio of imine to amine moves further away to 3:1 on average. This indicates that there is probably a degree of physisorption occurring with the second layer. However, it is important to note that the imine environments are both buried under a significant molecular layer while the amine is located at the tip furthest away from the substrate. Therefore, the intensities are biased in favour of the amine. The attenuation is of particular significance as this molecule is long and densely packed. In spite of the low ratio, when the large size of the molecule has been taken into account, this result still adds weight to the key result that imino linkages are being formed during the stepwise reaction.

Element	**BE/eV**	**Proportion of element**	**Normalised intensity**
S $2p_{3/2}$	162.08 163.73	45.5 % 54.5 %	1.0
N 1s	398.87 400.18	53.25 % 46.75 %	3.1
C 1s	284.74 285.87 288.59 290.94	64.8 % 23.7 % 6.9 % 4.6 %	42.0
O 1s	531.89 533.43	86.9 % 13.1 %	7.7

Table 3.6: RSF-corrected signal intensities for the elements in **W4**, normalised to the sulphur 2p intensity.

The relative intensities normalised to sulphur, as shown in table 3.6, indicate a closer parity between the layers than the QCM suggests as the 3.1:1 N:S ratio is very close to the 3:1 in a complete homogeneous two-layer system. This is further evidence for the attenuating effect that the long molecules have on the signal intensity from the sulphur or, evidence of additional diamine physisorption.

The sulphur peaks are shown in Figure 3.16. The high proportion of unbound thiol at S $2p_{3/2} = 163.73$ eV suggesting that the second layer could be pulling some of the first layer molecules out of the substrate. Alternatively,

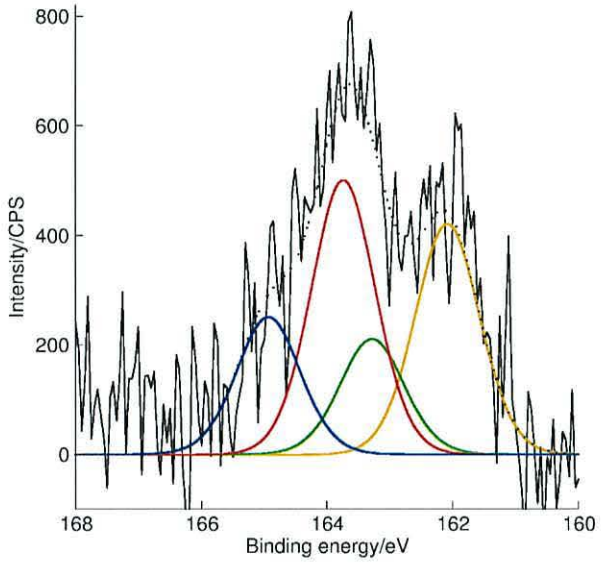

Figure 3.16: S2p region of XPS spectra for **W4**

the anchoring layer used for this study could have been of lower quality with a greater proportion of physisorbed molecules.

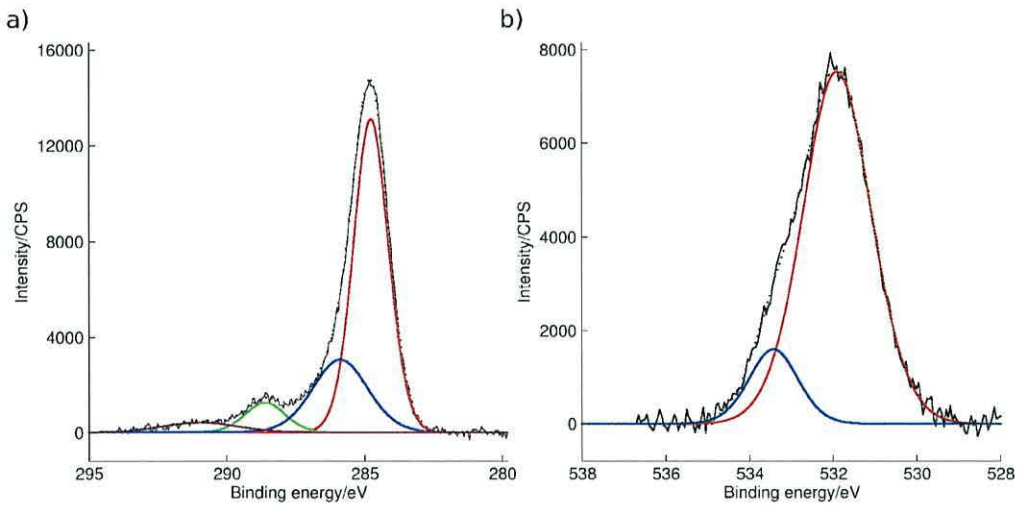

Figure 3.17: High resolution XPS spectra for **W4**: a) C1s and b) O1s regions

The remaining spectra for the carbon and oxygen regions are shown in figures 3.17a and 3.17b respectively. Carbon is present as **C**-H / **C**-C peak at

284.74 eV, **C**-N at 285.87 eV and a contaminant **C**=O peak at 288.59 eV. As there should be no oxygen present, the signal must come from adventitious species. This is mainly in the form of C=**O** at 531.89 eV and C-**O**-H at 533.43 eV, probably due to carbon monoxide and water at the surface.

3.2.2.3 7.5 nm Long Triple Fluorene Three-step Wire

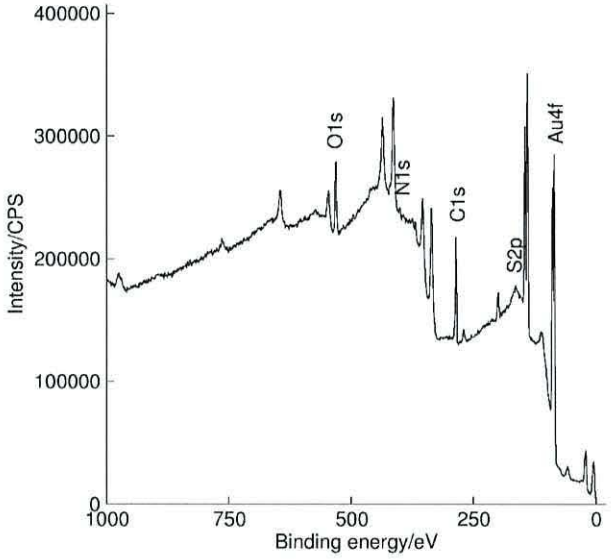

Figure 3.18: Low resolution, wide XPS scan of **W6** on gold-coated HOPG

The thiol-aldehyde anchor molecule, **M1** with the triple fluorene diamine, **M4** as a second layer was also examined for confirmation of chemisorption. A Sauerbrey analysis of this deposition, forming **W6**, suggested there was an approximate 1:2 bonding ratio from final area comparisons. The wide-scan XPS spectrum is shown in Figure 3.18.

The nitrogen signal of the **W6** system had an low intensity and the ratio of nitrogen to sulphur was only 1.4:1, see table 3.7. The **W6** molecule itself has a ratio of 3:1, but with 50 % coverage of the second layer, a ratio of 2:1 should be expected. This suggests that the sample being analysed had less than half of the first layer molecules bonded with a second. Figure 3.19 shows the two peaks produced by the XPS analysis. The peaks at 399.14 eV and 400.50 eV are characteristic of the imine and amine respectively, with

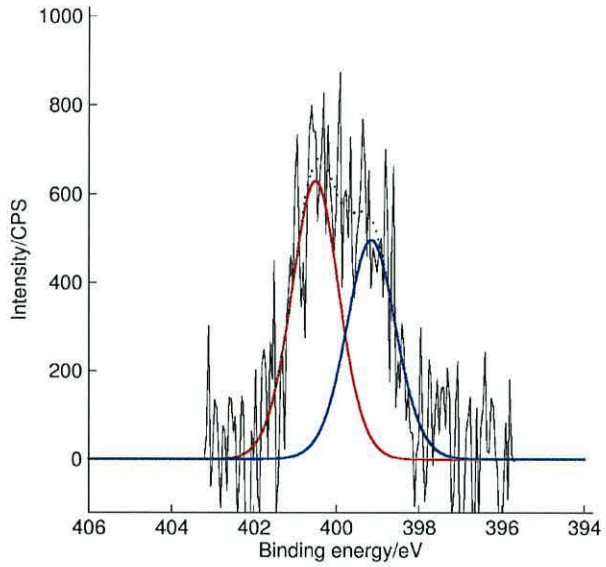

Figure 3.19: High resolution N1s region of XPS spectra for **W6**

proportional areas of 44.8 % and 55.2 %. In this instance, there is a slightly higher proportion of nitrogen in the amine environment than the imine.

Element	BE/eV	Proportion of element	Normalised intensity
S $2p_{3/2}$	162.09 163.72	66.2% 33.8%	1.0
N 1s	400.50 399.14	55.2% 44.8%	1.4
C 1s	284.91 285.60 288.69	66.0% 21.3% 10.9%	52.1
O 1s	531.42 529.50 533.07	79.2% 11.9% 8.9%	13.1

Table 3.7: RSF-corrected signal intensities for the elements in **W6**, normalised to the sulphur 2p intensity.

Therefore, it has to be surmised that either there is significant amount of physisorbed **M4** present in the system, or the attenuating effects are even greater with such a long molecule and only the nitrogen environment on the

outermost tip is producing a strong signal. Given the low overall nitrogen signal intensity, it is likely that this latter scenario is a valid one. The incredible length of the **M4** molecule is obscuring a significant part of the imino signal, but the fact that the two environments are visible in almost equal ratios is strong evidence that the stepwise reaction is occurring.

The spectra for sulphur is shown in Figure 3.20, which contains evidence for both bound and unbound sulphur peaks. Bonded sulphur appears at S $2p_{3/2}$ = 162.09 eV while the unbonded thiol is at S $2p_{3/2}$ = 163.72 eV. The relative intensities of 66.2 % and 33.8 % respectively from table 3.7 are indicative of good coverage, although less that the original **M1** SAM. However, as this is from a different sample, it could be due to be experimental variation. This is a more likely reason than the second layer dislodging the first, although the latter scenario is still a possibility.

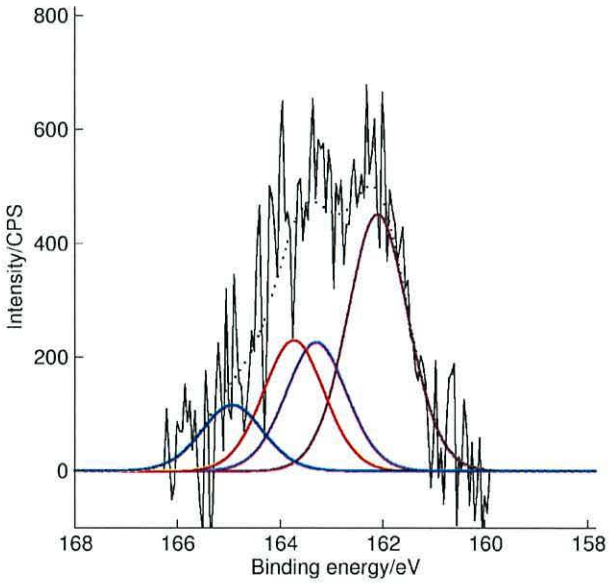

Figure 3.20: High resolution S2p region of XPS spectra for **W6**

The remaining spectra for the carbon and oxygen regions are shown in figures 3.21a and 3.21b respectively. Several carbon species are present including the main **C**-H / **C**-C peak at 284.91 eV, **C**-N at 285.60 eV and a contaminant **C**=O peak at 288.69 eV. All the oxygen peak comes from contaminants, and is mainly present in the form of C=**O** at 529.5 eV and

C-**O**-H at 531.42 eV; this suggests carbon monoxide and water.

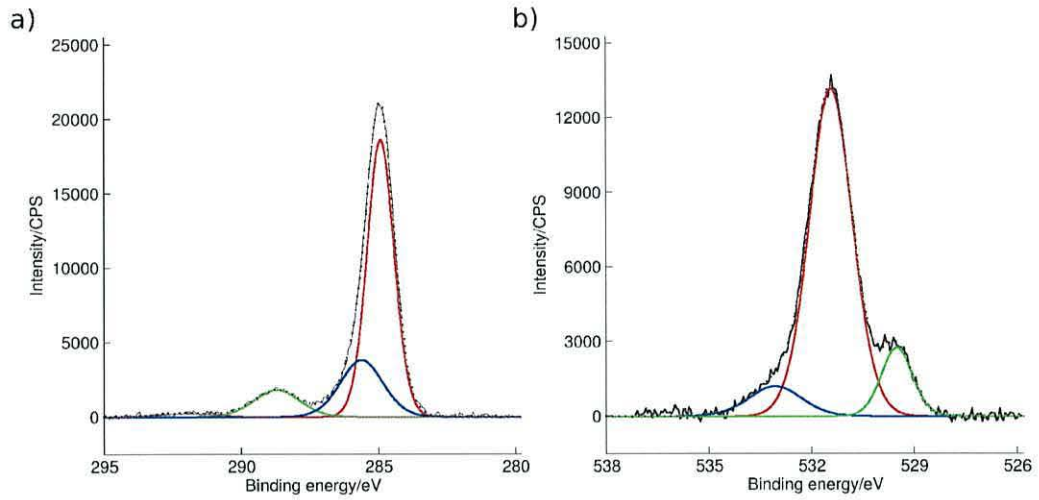

Figure 3.21: High resolution spectra for **W6**: a) C1s region and b) O1s region

3.2.3 Summary

The XPS data have confirmed the presence of the the various components in the stepwise wire systems by providing information on the elements and their environments, particularly nitrogen and sulphur, that match the molecular formula of the constituent compounds. The high percentage of sulphur present, at an energy indicating bonding to gold, provides strong evidence of self-assembled monolayers with good chemisorbed coverage. Additionally, the nitrogen regions of the spectra have verified that imino formation is occurring in a significant proportion of cases. From this evidence, it can be inferred that imino-linkage is the mechanism by which the wire is extended during stepwise synthesises. However, the nitrogen environment ratios suggest that some non-bonded physisorption is also involved, particularly with the larger molecules.

3.3 Electronic Properties of Molecular Wires

Previously, in sections 3.1 and 3.2, work has focussed on establishing self-assembly and stepwise assembly as a viable option for producing multi-step molecules. In the following section, the wires that have been synthesised using this modular approach will be electrically investigated to assess their suitability as components within a molecular electronic system. The behaviour must be established as due to the molecule itself; not obscured by the nature of the contacts or environment of the junction.

Reliably forming two contacts to a molecule remains a major focus for the field of molecular electronics. An STM tip is still the tool of choice for finding electrical characteristics by probing a molecule bound to a planar substrate. An alternative, the EMC method, will be compared to STM data in order to assess its suitability as a investigative platform. The study will examine the promise of the stepwise modular chemistry approach to synthesise both functional and large molecules; two important factors for creating useful molecular electronic components.

3.3.1 Study of the Anthraquinone Three-step Wire

The smallest wire was investigated first, having previously been the subject of a paper by the group.[150] Comprising three layers, initially 4-[(3-mercaptophenylimino)methyl]benzaldehyde self assembled as **W1**; adding 2,6-diaminoanthra-9,10-quinone to form **W2** and finally reacting with 4-[(3-mercapto-phenylimino)methyl]benzaldehyde again to form **W3**. The first layer has very weak donating character due to the sulphur but should produce an approximately symmetrical I-V curve. The anthraquinone moiety, conversely, is a strong acceptor and forms a weak molecular diode as described in section 1.4.3.1. The final layer restores symmetry to the system and should produce a completely symmetrical plot.

The plots in Figure 3.22, collected by a colleague, Dr. Piotr Wierzchowiec, are provided as a comparison. They were taken using the STS technique as described in section 2.3.1.1. The first and the last plots, for **W1** and **W3** respectively, are almost symmetrical. The first displaying very slight

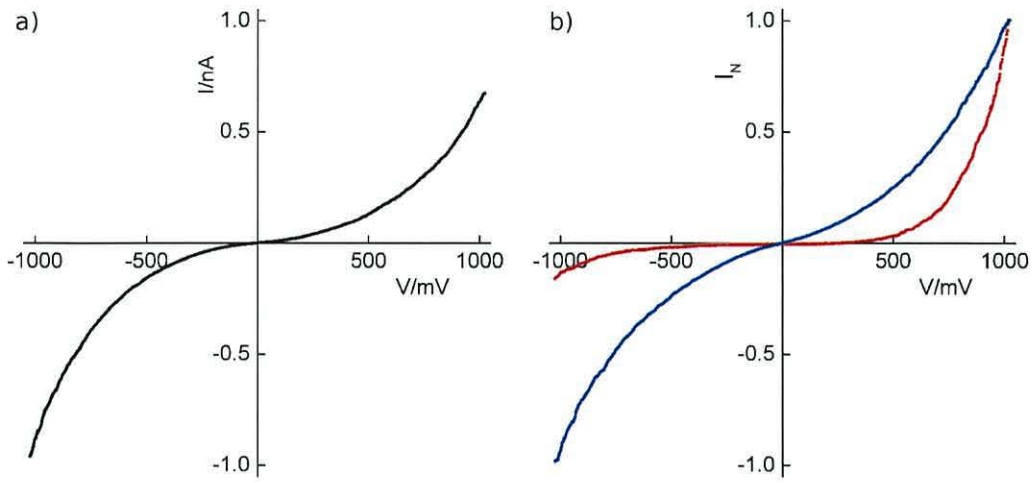

Figure 3.22: IV curves for a) **W1** in isolation and b) after reaction with **M2** to form **W2** (red) and after further reaction with **M1** to form **W3** (blue); the curves normalised for better comparison by the 1000 mV values. The sign corresponds to the substrate electrode and data were collected *via* STS.[199]

asymmetry induced by the weakly donating sulphur. However, after the second step, **W2**, is slightly rectifying in the negative quadrant and has a ratio of *ca.* 6 at ±1000 mV.

3.3.1.1 Study Using the Electromagnetic Cantelever

The same system was examined using the EMC technique outlined in section 2.3.2. A *Thurlby Thandar* stabilised current source was used to control the electromagnet and a *Keithley 6430* sub-femtoamp source-meter used for taking I-V measurements. The entire apparatus was vibrationally isolated using heavy marble slabs and rubber pads.

The technique produced similar results to the STM, the first and second layers symmetrical and the second showing slight asymmetry with the rectification in the negative quadrant. This is due to the arrangement of acceptor and donor moieties in the structure and follows the Aviram and Ratner scheme outlined in section 1.4.3.1. At forward bias, the electrons travel from the cantilever probe tip to the substrate. Electrons tunnel from the cathode to the anthraquinone (**M2**) acceptor and from the weakly donating thiolate-connected (**M1**) end of the molecule, to the anode.

The direction of forward flow confirms that the surface-based 2,6-diaminoanthra-9,10-quinone moiety is electron-accepting and it suggests that the NH_2 substituent is either resonantly coupled to the acceptor's ring structure or the electron-donating character of the substituent is otherwise effectively neutralised by adsorption to the contacting gold probe.

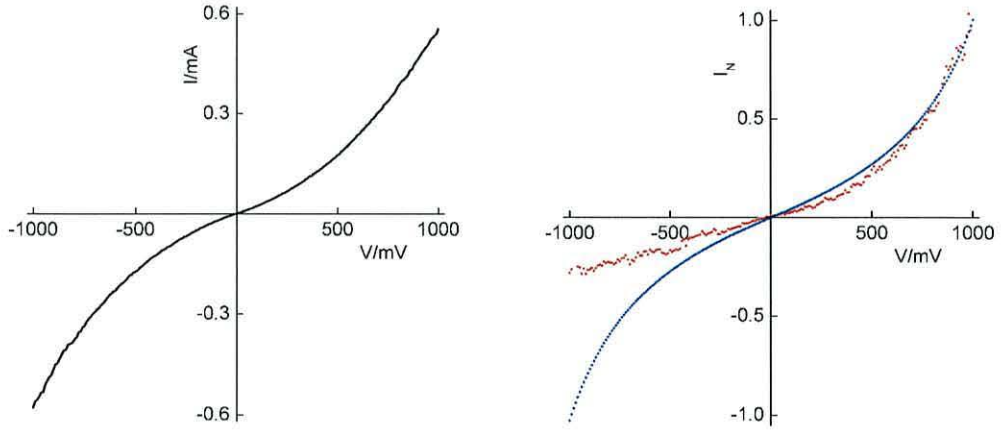

Figure 3.23: a) I-V curve for **W1** (black) and b) Normalised I-V curves for **W2** (red) and **W3** (blue) taken with the EMC

The current measured in Figure 3.23a is approximately 600,000 times that of the equivalent **W1** plot in Figure 3.22. This reflects the much greater area over which the EMC technique contacts the molecules, although the character of the plot is much the same. The rectification ratio of the second layer is *ca.* 4 at ± 1000 mV, shown in 3.23b. This is slightly lower than that of the STS measurement and is evidence of some disorder within the system. The STM tip probes only a small number of molecules at a time and favours those furthest from the substrate, which are most likely to be the complete system. The EMC measures many thousands of molecules at a time. Therefore, the top contact is likely to encounter a mixture of molecules; some with only the first layer present and some that are complete bi-layer systems. The resultant current is an average of the various configurations, where only a complete two-step molecule produces strong rectification, and thus the average ratio is diminished. For this reason, a good quality, tightly-packed layer is even more important with the EMC technique.

While the result might not be as strong as the STM, it does eliminate the uncertainty due to the air gap. An EMC rectification ratio represents a lower bound on the value, which should increase in accuracy with layer quality. Whereas, an STM may produce rectification when none should be present.

3.3.2 Study of the 2.3 nm Long Single Fluorene Molecule

The electrical characteristics of the **M1** anchoring thiol molecule was also studied after reacting it with the single fluorene diamino **M3** molecule to form wire **W4**. **M3** is a long, conjugated molecule containing two triple bonds, three fluorene units and two phenyl rings. When it attaches to **M1** *via* the condensation reaction to form an imino, there is good conjugation throughout the entire wire.

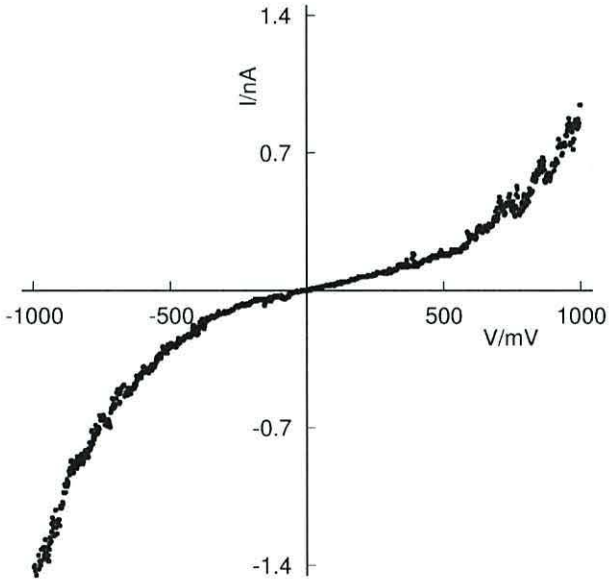

Figure 3.24: I-V curve for **W4** taken using STS with set point 400 pA and bias 60 mV, averaging 5 scans

Both ends of the wire have weak donating character, but from the slight asymmetry in Figure 3.24, it can be inferred that the amine is marginally stronger, or the sulphur substituent is partially neutralised by adsorption

to the substrate or coupling with the rest of the molecule. Electrons travel from the probe tip to the substrate at forward bias. The RR is only *ca.* 1.6 at ±1000 mV suggesting good contact to both ends. The STS plot showed a current of *ca.* -1.4 nA at -1000 mV, comparable to the *ca.* -1.0 nA of **W1** alone at the same voltage. Any difference in magnitude could be the result of different numbers molecules bonding to the tip rather than inherent conductive properties.

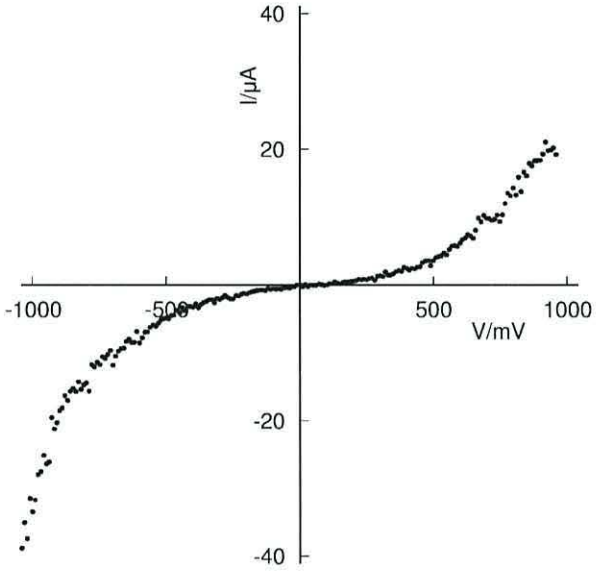

Figure 3.25: I-V curve for **W4** taken using the EMC

The STM result was confirmed using the EMC technique as shown in Figure 3.25. The shape of the graph is virtually identical to the STS plot and exhibits a similar RR of *ca.* 1.4. The current magnitude for the EMC plot is approximately 30,000 times greater, implying a large contact area of *ca.* 0.015 μm^2. The value for the contact area ($A_{contact}$) is found using the following equation:

$$A_{contact} = nA_{molecule} \tag{3.1}$$

where n is the number of molecules between the contacts, found from equation 3.2 which compares EMC and STS currents, assuming that the STS probes

a single molecule, and $A_{molecule}$ is the area per molecule, from QCM studies.

$$n = \frac{I_{EMC}(300mV)}{I_{STS(t)}(300mV)} \tag{3.2}$$

STS(t) was used where possible as a comparison of the EMC and STS(t) techniques is more likely to be valid that comparing EMC and STS(V). In this latter scenario, the contacts are too dissimilar. EMC contacts the molecules directly, whereas the STS(V) method contacts through an air-gap. This introduces another variable to affect the current magnitude. The STS(t) technique is more appropriate for another reason as the statistical analysis involved is more likely to identify the single molecule current than STS(V).

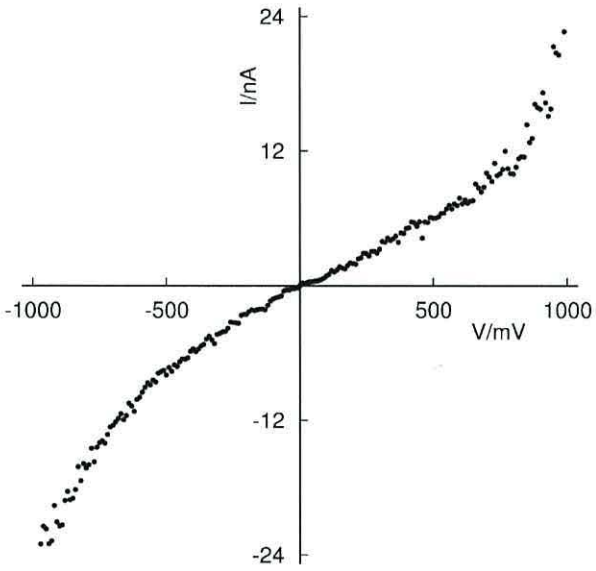

Figure 3.26: I-V curve for **W5** taken using the EMC

The electrical characteristics of **W5** were also studied, formed by extending the **W4** wire with an **M1** unit. The addition of another **M1** molecule creates a wire that is completely symmetrical and, as shown in Figure 3.26, this is reflected in the symmetrical I-V curve. The current in this plot, although it was taken using the EMC method, has a very low magnitude current; a rare instance where a stable, grazing contact has been

achieved. The 24 nA at ±1000 mV is likely to represent contact with only tens of molecules.

3.3.3 Study of the 4.0 nm Long Triple Fluorene Molecule

A long wire, containing **M4**, is crucial to the investigations later in this thesis using the silicon nano-gap devices. The wires investigated in this section use different anchoring units and therefore are unlikely to behave identically. However, the molecule is similar enough to be instructive and provide a useful idea of the current magnitudes to be expected from the devices.

The long and short fluorene molecules are electronically similar, and so the current voltage characteristics were also expected to be similar. Figure 3.27a shows the I-V curve for the long molecule, almost symmetrical but with a slightly lower current in the positive quadrant resulting from marginally different coupling as would be inferred from the presence of the thiol and amine groups. The current magnitude is comparable to the wire with only one fluorene moiety and implies that the conduction is dominated by the contacts rather than the main body of the molecule.

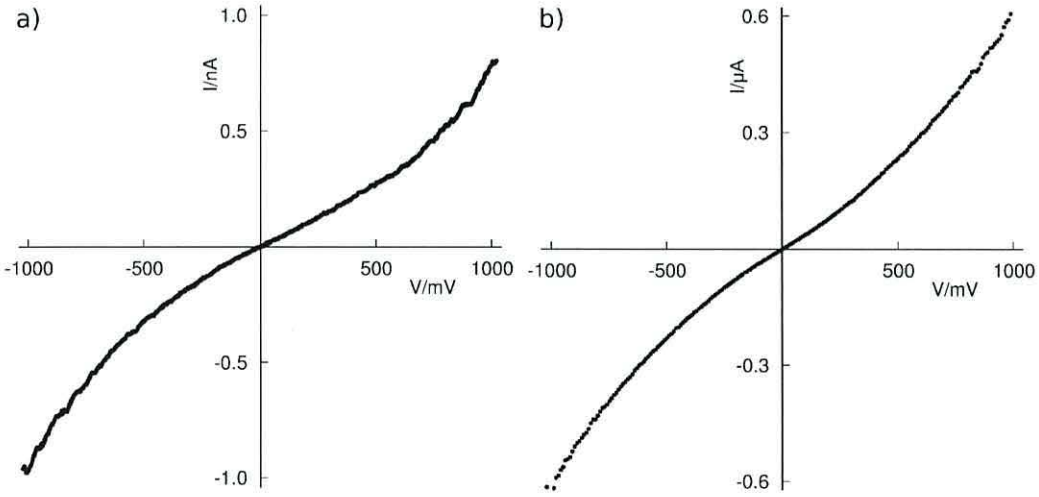

Figure 3.27: IV curve for **W6** taken using: a) STS with set point 400 pA and bias 60 mV averaging over 5 scans and b) the EMC

The same system was studied using the EMC, and the I-V spectra is shown in Figure 3.27b. This plot shows the molecule conducting completely

symmetrically with a gentle s-curve indicating that both ends are coupled equally and the mild donating character of thiol and amine are balanced. Comparison with the STS(t) single molecule current in section 3.4.1 implies that the EMC tip is contacting *ca.* 390 molecules, from which we can infer a contact area of approximately 195 nm^2.

As with the single fluorene, the triple fluorene two-step wire was extended to three steps with an additional **M1** unit to create a symmetrical wire. This wire, **W7** in table 3.2, is approximately 7.5 nm long with a thiol at each end to bond strongly with both the gold substrate and probe tips. The STS spectra is shown in Figure 3.28a. This plot is very similar to the I-V curve without the third layer. The shape is virtually identical, as is the magnitude.

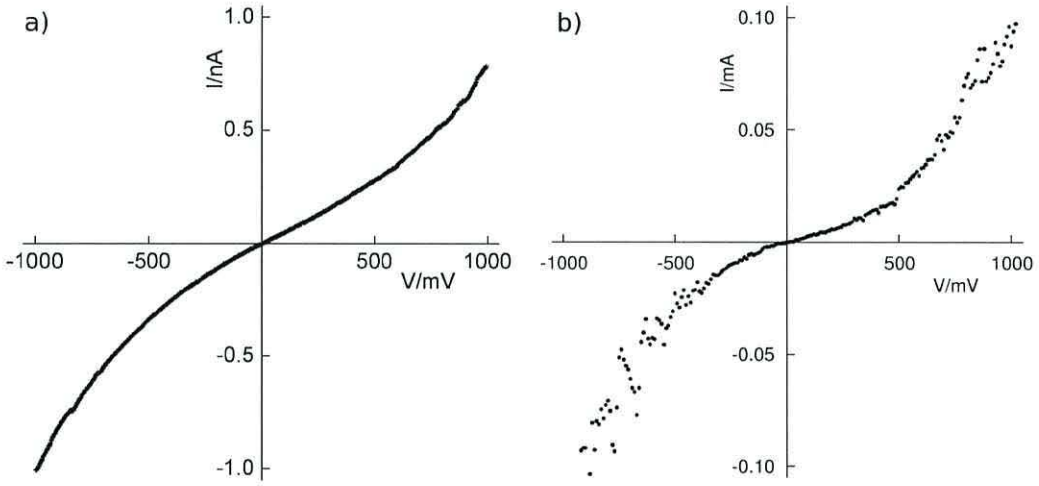

Figure 3.28: IV curve for **W7** taken with: a) STS with set point 400 pA and bias 60 mV averaging over 5 scans and b) the EMC

The same system probed using the EMC produced an I-V characteristic as shown in Figure 3.28b. The magnitude is higher than the two-step system, but from comparison to the STS results from section 3.4.1, this is expected to be due to an increased number of moecules and contact area; *ca.* 61,000 and 0.03 μm^2 respectively. This plot displayed increasing noise at voltages below -500 mV and above 500 mV. This is possibly due to the large contact area, involving a significant amount of interstitial material interacting with the complete molecules, and causing inter-molecular electronic transfer

that disrupts conduction. The noise could also be due to fluctuations in the effective contact area as the greater voltage allows a larger degree of tunnelling to occur, particularly if there are many molecules in grazing contact.

The study of the three-step wire, containing the triple fluorene, has shown that under approximate single-molecule conditions with the STM, that **W7** sustains a current of approximately 1 nA at ±1000 mV. This value provides an order of magnitude guide to use when estimating the number of molecules bridging the silicon nano-gap devices.

3.3.4 Investigation of Many-Step Wires

A study was carried out to investigate what happens as the molecular wire is extended further. **W6** was elongated by two further layers, the bi-substituted terephthalaldehyde and an additional triple-fluorene **M4** unit. The final areas per molecule were generally lower than the molecular cross-section dictated it should be, indicating the presence of interstitial material, but this factor is less important when the layer is examined using the STS technique as shown in Figure 3.29. This wire stands at a length of approximately 10.3 nm, although a relaxed geometry calculation suggests that it will have a large amount of curvature which increases the potential for probing mid-way along the molecule.

The increasing length of the molecule has a negative impact on the conductance of the layer, because although the shape of the curve is similar to the wire with only one **M4** moiety, the current is approximately one order of magnitude lower than before. A current of 0.015 nA at 300mV is lower than the 0.09±0.015 nA value obtained using STS(t) on the same system in section 3.4.2. However, it is within an order of magnitude and consistent with the presence of an air gap in the STS(V) result. The additional noise this time most likely due to the reduced signal to noise ratio of the equipment.

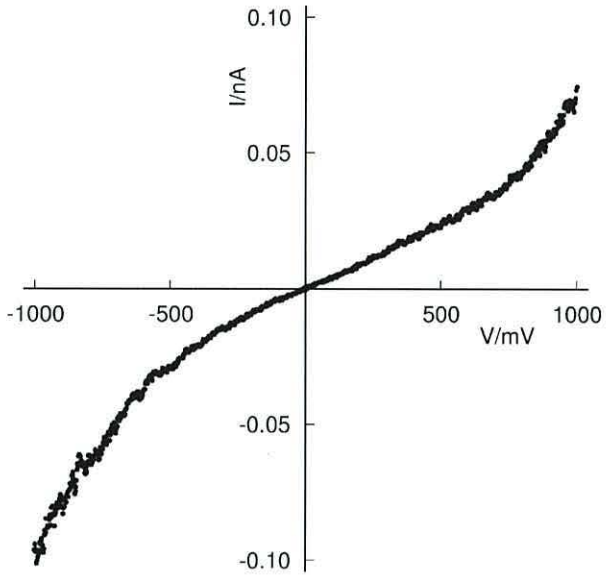

Figure 3.29: IV curve for **W6**+terephthalaldehyde+**M4** wire, taken using STS with set point 400 pA and bias 60 mV, averaging 5 scans

3.4 Current Jumps

An additional technique, used to identify single molecule conduction, was applied to some of the same systems probed using the STS and EMC methods. Known as STS(t) or the current jump technique, it is described in detail in section 2.3.1.1 and utilises the same equipment and basic setup as standard STS measurements. However, instead of probing the current through the molecule as a function of applied voltage, the current is measured as a function of time as the tip is allowed to drift around the surface. In the time domain, the current passing through the tip undergoes occasional sharp increase followed by decrease events, typically lasting milliseconds. These jumps correspond to absorption and desorption of molecules onto the probe tip. Throughout these studies, the measurements were taken at a constant bias of 300 mV. This value is in the low bias range for simplicity; it was the voltage used by other authors during similar studies and allowed comparison.[38,145] The results were all gathered by eye, the probe scanning continually and data recorded when jumps appeared. To reduce the

possibility of experimenter bias, a number of the studies were repeated by colleagues, Dr. Ben Robinson and Dr. Basia Urasinska, and the results combined for the final histograms. However, all studies agreed with respect to the position of the main peak, which increases trust that operator bias is not a significant factor.

3.4.1 7.5 nm Long Triple Fluorene Three-step Wire

The most important system, for which a single molecule current needs to be identified is the triple-fluorene wire that is to be used to bridge the silicon devices. To As a guide, the thiol on gold approximation of this wire was probed at the three stages of its synthesis at a surface.

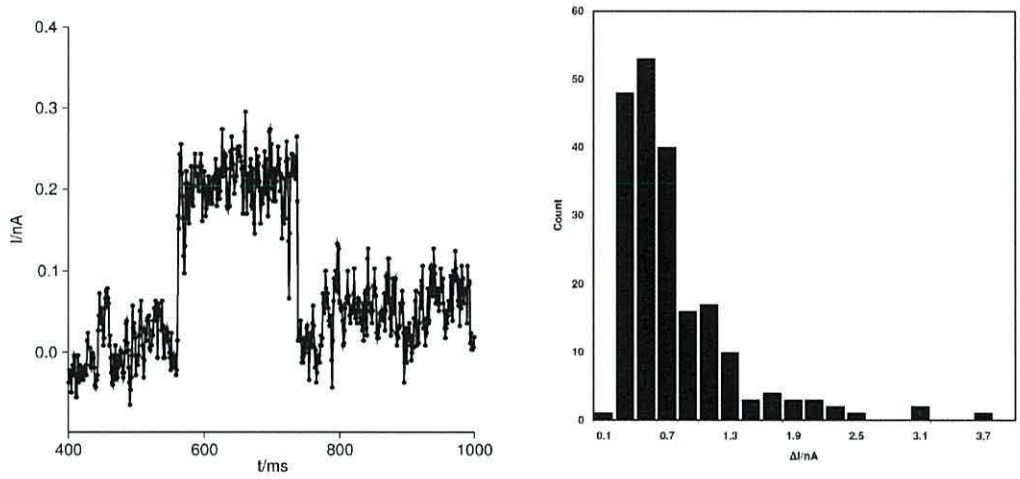

Figure 3.30: An example of a current jump, taken with the STS(t) technique (scanning at 300 mV with rate 0.996 Hz, setpoint 400 pA and bias 60 mV) and a histogram of 205 jumps, all of **W1** on gold-coated quartz crystal. The histogram buckets are 0.2 nA wide, the scale marking their mid-points.

The first stage, **W1** terminates with an aldehyde group, in a tightly packed monolayer. It might be assumed that without a sulphur atom to spontaneously absorb onto the tip, no jumps would occur. However, this was not the case as Figure 3.30 clearly shows. The jump event is clearly visible in the example plot, lasting *ca.* 200 ms, and the resultant histogram of a large sample of current jump data displays evidence of a favoured current

magnitude. The mode jump value is 0.339 nA, which falls just under the most populous bucket at 0.5±0.1 nA. Both these currents are higher than might be expected from the STS(V) data for **W1** in Figure 3.22. From the STS(V) plot, the current at 300 mV is *ca.* 0.05 nA, an order of magnitude lower than the common current jumps found in this study. However, the absorption and desorption event occurs when true physical contact is made by the probe tip whereas the STS(V) method can record a lower current by introducing a tunnelling barrier. Additional evidence, to support the assertion that the 0.5 nA bucket contains the single molecule conduction, comes from the appearance of secondary peaks. These occur at approximate integer multiples of that initial value. Rather than a consistent decline, there are high points centred around 1.1 nA and 1.7 nA. The outliers, 3.1 nA and 3.7 nA also have a difference that fits the general pattern.

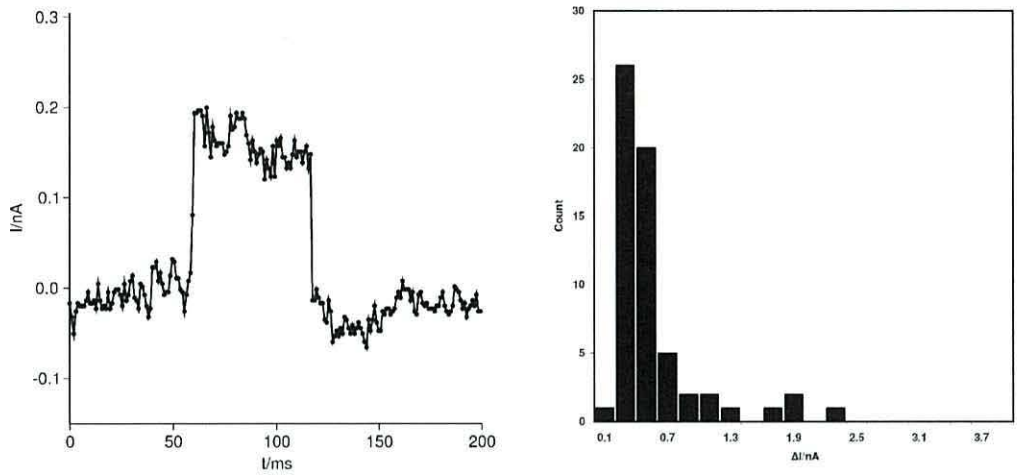

Figure 3.31: An example of a current jump, taken with the STS(t) technique (scanning at 300 mV with rate 0.996 Hz, setpoint 400 pA and bias 60 mV) and a histogram of 61 jumps, all of **W6** on gold-coated quartz crystal. The histogram buckets are 0.2 nA wide, the scale marking their mid-points.

The next stage, with the triple fluorene diamine attached was also probed in the same way as the first layer. A histogram of many current jumps, and an example of one of the jumps used to create the histogram is shown in Figure 3.31. For this longer molecule, the mode current is 0.318 nA which does fall well within the largest bucket, 0.3±0.1 nA. The two buckets encompassing 0.2

to 0.6 nA contain over 75 % of the recorded jumps, indicating very strongly that single molecule conduction is within this range. The equivalent value, taken from the STS(V) data, is 0.18 nA at 300 mV. This again is lower, but is very close to the lower bound of the most popular bucket indicating some agreement. This time there is limited evidence for multiple simultaneous adsorption events. Although the outliers at 1.9 and 2.3 nA have a suitable separation, the pattern does not hold for the entire spectrum and so is too weak to be conclusive.

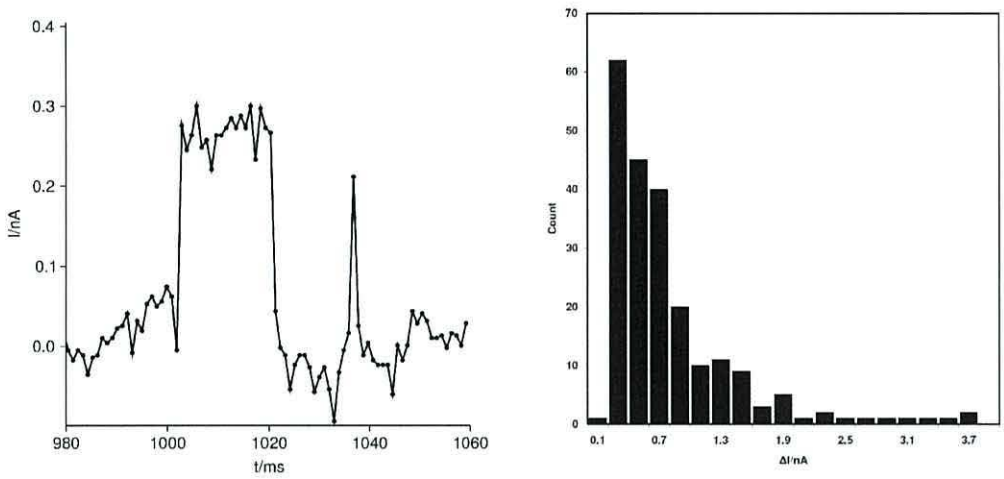

Figure 3.32: An example of a current jump, taken with the STS(t) technique (scanning at 300 mV with rate 0.996 Hz, setpoint 400 pA and bias 60 mV) and a histogram of 217 jumps, all of **W7** on gold-coated quartz crystal. The histogram buckets are 0.2 nA wide, the scale marking their mid-points.

The final step, adding **M1** to create the symmetrical **W7**, forms a molecule with a thiol termination. However, contrary to what might be expected, this did not lead to a different situation and absorption events occurred at a similar rate. One such event, and a histogram summary of several hundred events are shown in Figure 3.32. The mode jump occurs at 0.230 nA, while the bucket at which most events occurred was 0.3±0.1 nA. The current at 300 mV, taken from the STS(V) I-V curve for this molecule, is 0.17 nA, comparable to the most common jump magnitude. Additional evidence for the single molecule conductance value comes again from secondary peaks at integer multiples. The buckets positioned at 0.7,

1.3, 1.9 and 2.3 nA are all higher than would otherwise be expected from the heights of the surrounding buckets.

3.4.2 Investigation of Many-Step Wires

STS(t) studies were also undertaken to ascertain the likely single-molecule current of two very long wires. These were formed by extending **W6** by the small terephthalaldehyde linker and then by the long di-amine **M4**. **W6** + terephthalaldehyde + **M4** produced $\mathbf{W6}_2$, while extending the molecule with the same units again yielded $\mathbf{W6}_3$. The underscore denoting the number of **M4** units present in the molecule. An approximate geometry optimisation suggests that these molecules will be *ca.* 10 nm and 14 nm from sulphur to terminating amine respectively. However, the substantial amount of curvature present limits the relevance of such a calculation. In reality, there is likely to be significant disorder and a correspondingly wide range of lengths.

The current jump histograms for each of the two molecules is shown in Figure 3.33. The **W6** system probed using the STS(t) produced a histogram containing a peak bucket positioned at 0.3±0.1 nA. The $\mathbf{W6}_2$ system peaked at the 0.09±0.015 bucket while the $\mathbf{W6}_3$ system had most jumps in the 0.075±0.015 range. These values are within the bucket width of each other and so are not significantly different. This similarity is a reflection of two effects. Firstly, the reduced length dependence on conduction in long conjugated molecules beyond *ca.* 5 nm means that, even with a perfect single molecule system, the extra 4 nm will not have a dramatic effect on the conductance. Also, the curved molecule and disorder of the system means that the probe tip is likely to be contacting the molecules at a point other than the tips. Therefore, transport lengths will be a random function of tip position rather than favouring the length of the molecule.

3.4.3 Investigation of Current Jump on other systems

Alongside the current jump studies of the various molecules that have been mentioned previously, a number of studies were performed on molecules without an endgroup for attaching to a probe tip and on substrates without

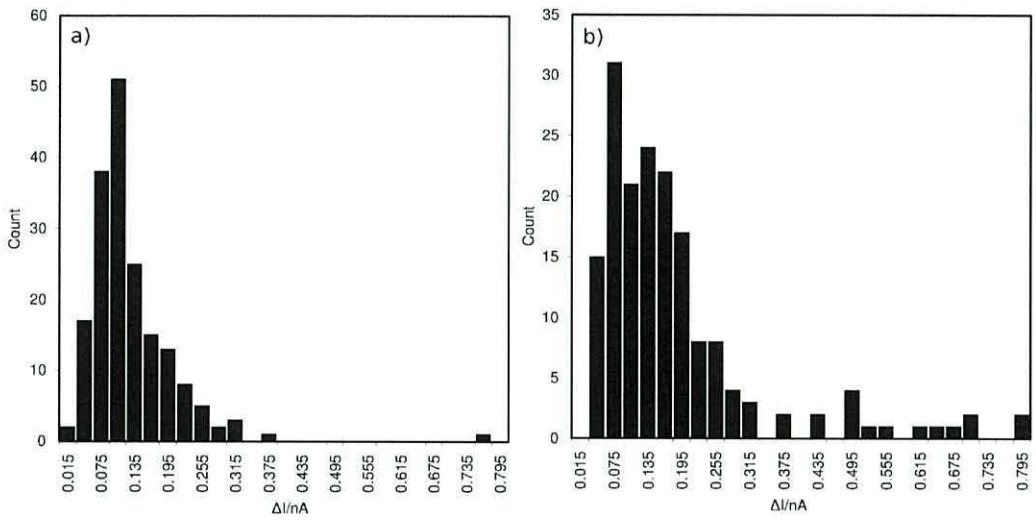

Figure 3.33: Two current jump histograms, taken with the STS(t) technique (scanning at 300 mV with rate 0.996 Hz, setpoint 400 pA and bias 60 mV) of a) $\mathbf{W6}_2$ (184 samples) and b) $\mathbf{W6}_3$ (177 samples) on gold-coated quartz crystal. The histogram buckets are 0.03 nA wide, the scale marking their mid-points.

a molecular layer. This investigation was used to examine the current jump process and in particular the suggestion that all jump events were the result of chemisorption.

3.4.3.1 Thiophenol

The first of these studies used thiophenol, a benzene ring with one thiol group. This molecule was self-assembled onto a gold surface by the sulphur, thereby resulting in a layer of benzene for the STM probe tip to address. The molecule is not long enough or sufficiently flexible to undergo a 'flipping up' adsorption-desorption cycle for a current jump event and has no group at the surface suitable for bonding to a gold probe.

Despite the lack of a moiety to bind to the probe tip, current jumps events occurred often and clearly. The histogram for current jumps on thiophenol-coated gold is shown in Figure 3.34. Several clear peaks are visible. The largest occurs at *ca.* 0.345 nA. However, there is a slightly smaller peak at 0.225 nA. As the smaller peak is at a lower current, it is likely that this represents tunnelling through a single molecule. The larger current, although

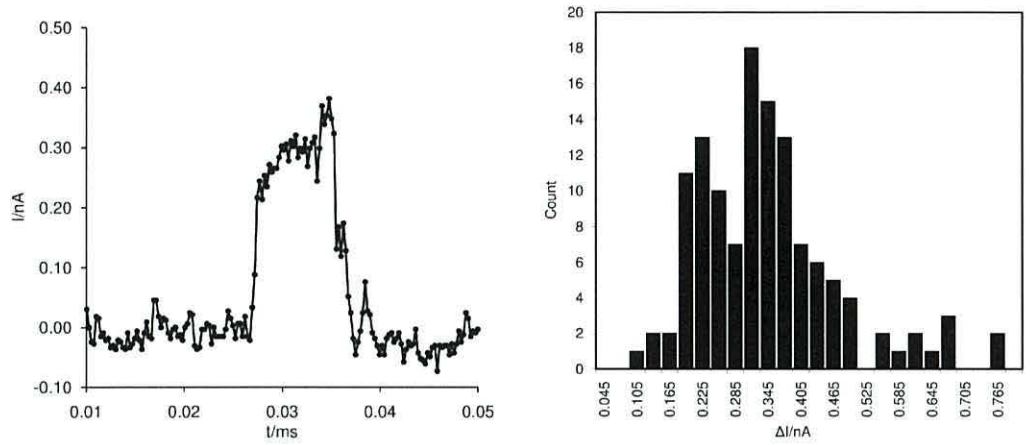

Figure 3.34: An example jump, taking using the STS(t) method, sampling at 300 mV and a histogram of 133 current jumps, taken with the STS(t) technique (scanning at 300 mV with rate 1.993 Hz, setpoint 400 pA and bias 60 mV) on a gold-coated quartz crystal coated with Thiophenol. The histogram buckets are 0.03 nA wide, the scale marking their mid-points.

not a precise integer multiple of the fundamental peak is probably the result of two molecules being probed simultaneously. The fact that the tip probes the π-system randomly, rather than a terminating group, does not broaden the peaks so much when the molecules are so small. All positions are similar, in contrast to the long multi-step wires examined in section 3.4.2.

3.4.3.2 Uncoated Gold

When current jumps appearing on systems without a 'crocodile-clip' terminating group, the next study extended this idea to see if the STS(t) technique would produce current jumps on uncoated surfaces. The first substrate used was a quartz crystal coated with (111) gold. These were thoroughly washed, dried and plasma-cleaned to ensure the surface was free from larger debris and molecular contaminants. Again, jump events were in evidence and a histogram of their magnitudes is shown in Figure 3.35, alongside an example jump. The histogram showed a fairly broad peak, with the largest bucket at 0.25 nA but other maxima around 0.45 nA, 0.75 nA, and 1.05 nA suggesting the possibility of multi-atom tunnelling. Different sized clusters of gold atoms can combine to produce different sized current jumps, both in the

tip or on the surface. It is also possible that conduction could be occurring *via* contaminants in the air that have assembled onto the surface between the cleaning and measuring phases. Therefore, conduction through multiple adventitious molecules cannot be ruled out.

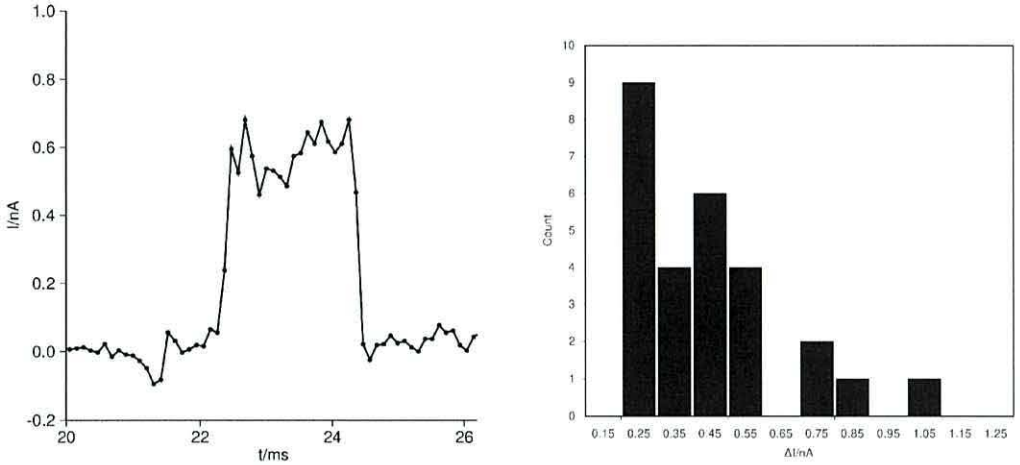

Figure 3.35: An example jump, taking using the STS(t) method, sampling at 300 mV and a Histogram of 28 current jumps, taken with the STS(t) technique (scanning at 300 mV with rate 0.996 Hz, setpoint 400 pA and bias 40 mV) on gold-coated quartz. The histogram buckets are 0.3 nA wide, the scale marking their mid-points.

3.4.3.3 Uncoated Silicon

With a gold planar surface producing jump events, a non-metallic surface was next to be investigated. Planar silicon wafers were available and so these were used for an STS(t) study. The substrates were subjected to the same washing and plasma cleaning cycles as the gold to ensure a pure oxide layer at the surface for probing. Figure 3.36 shows one of the resultant jumps taken from this study and a histogram of all the jumps.

The bias voltage for this study had to be increased dramatically for the tip to land on the surface and successfully take readings. However, with the tip in close proximity to the substrate, clear jumps appeared. The main peak of the histogram at 0.125 nA is very strong, containing almost 58 % of the jumps. A secondary peak appears at 0.325 nA suggesting the possibility

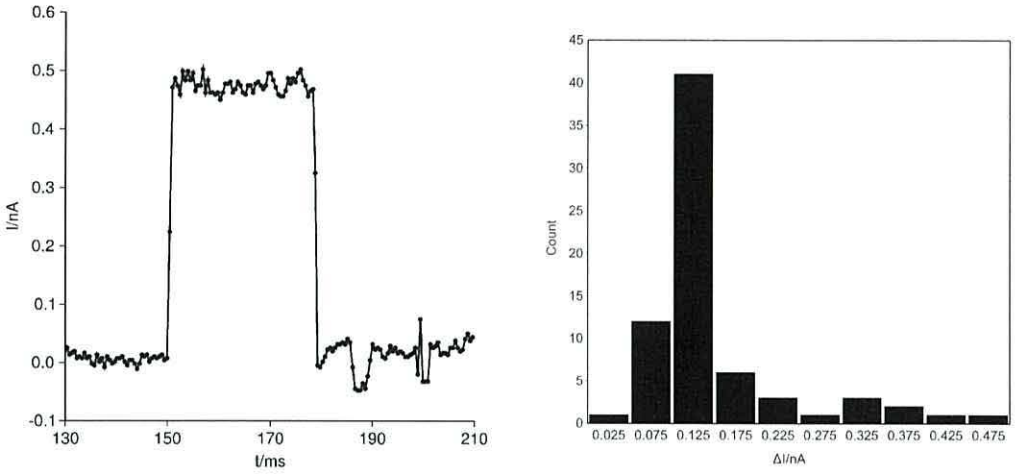

Figure 3.36: An example jump, taking using the STS(t) method, sampling at 300 mV and a Histogram of 71 current jumps, taken with the STS(t) technique (scanning at -1000 mV with rate 1.24 Hz, setpoint 700 pA and bias -1500 mV) on a silicon wafer. The histogram buckets are 0.05 nA wide, the scale marking their mid-points.

of some multi-atom tunnelling events occurring simultaneously without the presence of molecules *via*, for example, two surface atoms equidistant from the tip. However, this is less pronounced than the gold substrate, but this is to be expected due to the much flatter silicon surface and the high mobility of surface gold atoms. Also, the silicon dioxide surface is highly un-reactive and so will be very unlikely to pick up contaminant molecules to aid the production of jumps and multi-jumps.

The many situations in which current jumps can occur establishes the fact that the absorption and desorption event due to flexible molecules bending up and down is only one possible way for contact to be made. The ease with which it is possible to find jumps of bare, uncoated substrates indicates that a more common mechanism is tip drift. This movement could be perpendicular, towards the substrate or laterally along it in combination with a shelf, or similar protrusion from the surface. Corrections are made periodically by the feedback loop, but in between the adjustments, the tip is free to move under the influence of thermally induced drift and vibrations.

3.5 Nano-gap Silicon Devices

The stepwise synthesis developed in this work, is now used to bridge the electrodes of silicon nanogap structures as shown in Figure 3.37. It is the first time that a silicon nanogap has been bridged by a molecular wire, although Tour et al. have bridged electrodes by C_{60} deposits[200] and gold nanoparticles.[201] This development is significant because the molecular wires are covalently bonded to the silicon electrodes and the stepwise growth technique has been used, with assistance from surface roughness, to exactly match the electrode gap.

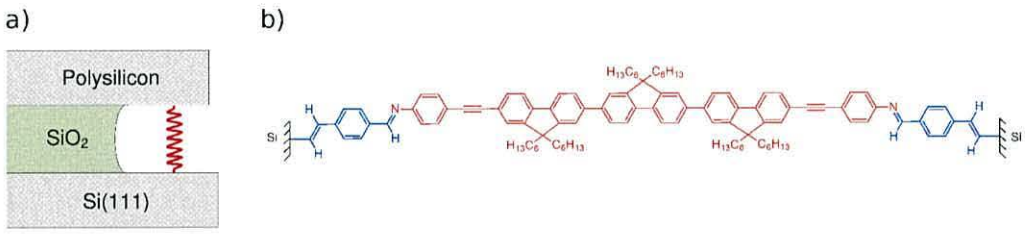

Figure 3.37: The stepwise bridging process: a) a schematic of the SND, showing the top and bottom electrode made of polysilicon and Si(111) respectively; separated by an oxide layer. The molecule, shown in red, assembles between the electrodes and b) the molecular structure of a complete bridging molecule. The anchoring molecule, 4-ethynylbenzaldehyde (in blue) is thermally grafted onto both hydrogenated electrodes in its diethylacetal derivative form. Then, the amino-terminated linking molecule connects both sides *via* an imino-formation reaction.

This section brings together the previous elements to look at the question highlighted in the introduction, when it was asked if organic molecular electronics can become a viable extension to existing silicon electronic devices. Self-assembly and stepwise synthesis at a surface have been established as powerful and versatile tools for creating functional molecules. In the following work, this modular approach is adapted to form bridging units that span silicon nanogaps. As described in section 3.5, vertical nanogap structures had been fabricated by an industrial partner, QinetiQ. They feature two highly doped silicon microelectrodes with a nominal separation of 7 nm. The aim of this study was to insert a single molecule between the electrodes. However, to limit the number of bridges, the

molecular lengths are deliberately chosen to be *ca.* 1 nm shorter than the nominal width of the gap. This deliberate mismatch limits the number of working devices but increases the likelihood of bridging the silicon electrodes via either a single molecule or a few molecules. Contact was made to the nanogaps *via* a Wentworth manual probe station and a Keithley Instruments model 6430 sub-femtoamp source meter was used to obtain IV characteristics.

3.5.1 Collapsed Devices

During the investigation of SNDs, a large proportion of the devices were either received as, or subsequently became, 'collapsed'. Evidence for this came from shorting between the electrodes, presumably due to a partial physical collapse of the device or the presence of extraneous matter that connected the electrodes during fabrication and could not be dislodged by subsequent washing.

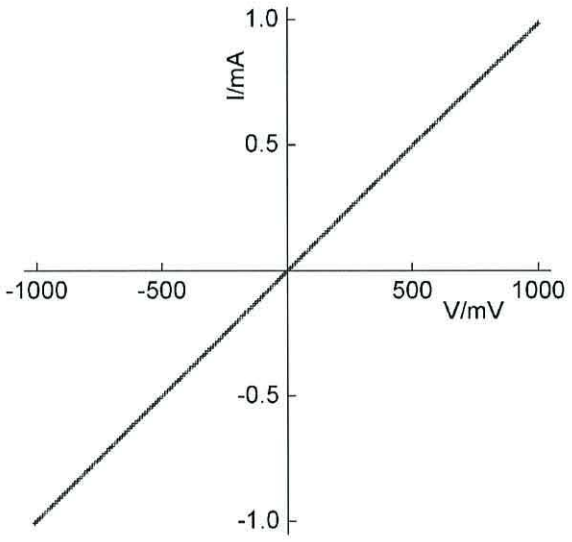

Figure 3.38: I-V curve for collapsed SND

The I-V curve for such a device, as shown in Figure 3.38 shows a highly conducting system behaving Ohmically as would be expected from a device that forms a complete circuit using only the doped silicon. Of

the 675 devices investigated throughout the entire study, 435 displayed characteristics consistent with a shorted connection during the first I-V run. There a several possibilities for creating the short, the most likely being during fabrication where the actions of various etching steps can create debris and unintentional damage, but it was also found that a static discharge can harm the devices and therefore could be responsible for some of the breakdowns.

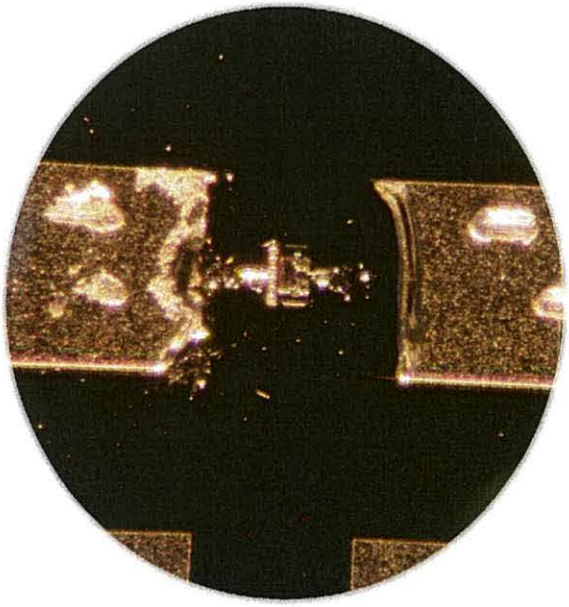

Figure 3.39: Melted device following a catastrophic static discharge event

The photograph in Figure 3.39 was taken after a particularly destructive discharge event. When light is incident on a semiconductor, such as the silicon used to form the SNDs, it can cause charge to build-up due to the photoelectric effect. It was found that when the probe station had made a connection to the device contact pads and the light removed abruptly, the current recorded by the subfemtoamp source meter could surge briefly. The sudden increase in current density would lead to excessive Joule heating. When natural cooling was not sufficient, this effect could melt the device, as shown in the photograph. Ideally, to eliminate any chance of this occurring, the experiment should be performed in complete darkness. However, the

probe station had to be operated manually, and without computer guided positioning of the probes, it was impossible to perform the experiments without some light. Therefore, rather than having strong light to position the probe, followed by complete darkness for the experiments, it was decided to partially cover the probe station with a case. In this way a situation was created whereby there was the minimum necessary light required to work the equipment but no sudden alteration of the light level. After this alteration was implemented, no further surge was observed or any device melting. The devices were studied in both air and an inert nitrogen atmosphere and showed no appreciable difference in the resulting characteristics, therefore it was decided that the simpler air environment would suffice for these experiments.

3.5.2 Empty Devices

The first part of the investigation was to establish a baseline for the devices without any bridging molecules. It was important to find both the character and magnitude of the I-V curve from the device before any bridging occurred so that the change upon insertion of the molecule is unambiguous. The plot in Figure 3.40 shows the current that passes between the electrodes of the SND due to tunnelling across the gap.

The I-V characteristic is symmetrical, and the current is very low. While most of the I-V characteristics are taken between ± 1000 mV, this one was taken out as far as ± 7000 mV to show the full character more clearly. As can be seen from the graph, the current is low level noise until the take-off points of *ca.* ± 3500 mV at which the potential across the electrodes is sufficient to allow significant tunnelling to occur. Without knowing the precise nature of the electrodes, it is difficult to relate the current to the width of the gap.

3.5.3 Addition of Benzaldehyde Linker

Following the grafting of 4-ethynlybenzaldehyde anchoring linker molecules to the sides of the gap, the devices were probed again, to see how the current changed with the smaller gap and altered electrodes.

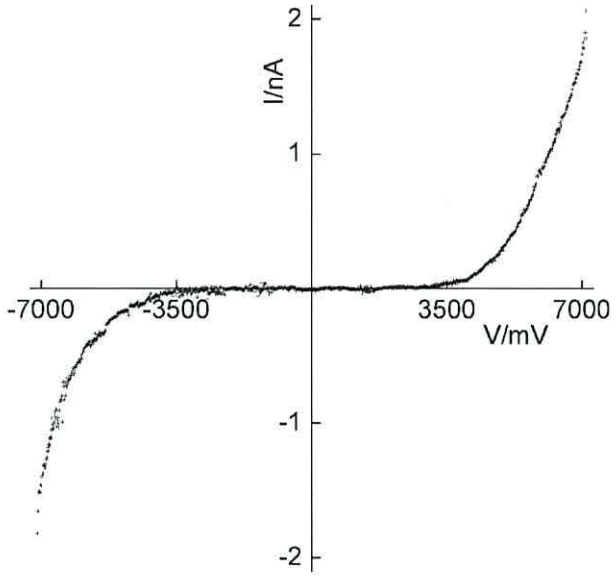

Figure 3.40: I-V curve for completely empty SND

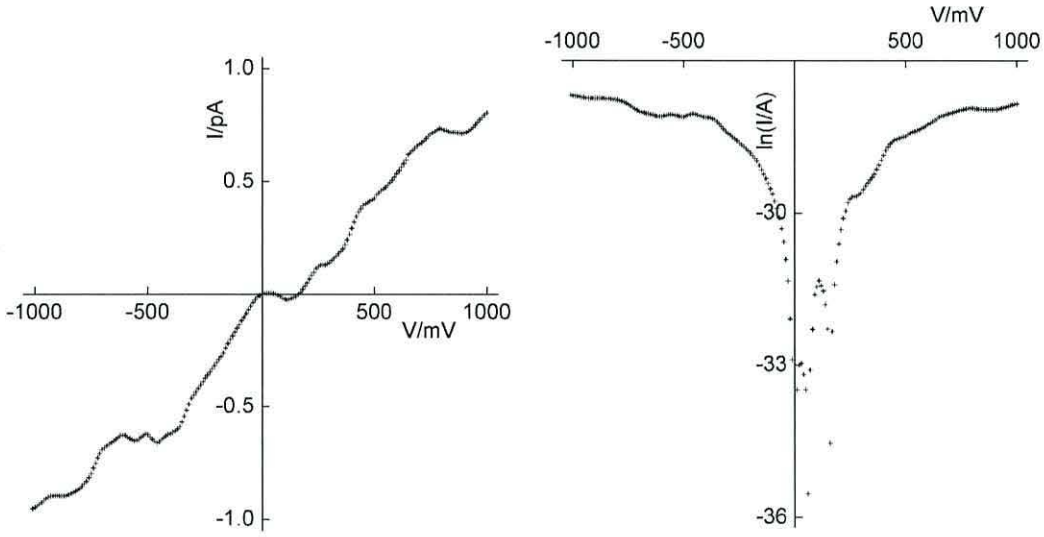

Figure 3.41: I-V and Log plot for SND with 4-ethynylbenzaldehyde linker-group coating

The plot in Figure 3.41 shows one of the many current characteristics taken of SND with the linker coating. The current magnitude is picoamps, consisting of noise dictated by the settings of the source-meter rather than inherent behaviour of the device. Between ±1000 mV, the potential difference

never becomes high enough for a significant tunnelling current to flow. As the plots were dominated by noise, they varied in appearance; Figure 3.41 showing just one example.

3.5.4 Insertion of Aniline

With the aldehyde terminated anchor molecules grafted in the nanogaps, a control chip was immersed several times in a 0.1 mg ml^{-1} solution of aniline, in ethanol for times ranging from 10 minutes to 64 hours. Aniline was chosen as it is mono-substituted and much smaller than the nominal gap size for the devices, therefore it should not be able to bridge the gaps. Many of the devices broke down on repeated measurement to *ca.* milliamp currents, indicating a shorted device. Of the remainder, the initially picoamp currents stayed at this magnitude, confirming the necessity for a larger bi-substituted molecule to span the gap successfully.

3.5.5 Insertion of Large Fluorene Linker

The main study of bridging in the nanogaps used a molecule that has already been under considerable investigation. The very long triple-fluorene diamine **M4** molecule is 4 nm in length and chosen to be marginally shorter than the nominal distance between the anchoring aldehyde terminating molecules assembled on either side of the gap. Therefore, using natural surface roughness, it should be possible to reduce the number of suitable bridging sites and maximise the probability of creating a single molecule device.

Before the bridging molecules were inserted, an I-V characteristic was taken of the device with only the linker coating. This step helped eliminate the nanogaps that had collapsed or shorted and to provide evidence that they were initially conducting only pA at ± 1000 mV. Next, the chips were immersed in chloroform solutions of concentrations varying from 0.005 to 0.1 mg ml^{-1} for periods of time ranging from 5 minutes to 53 hours. The change in immersion time and solution concentration was due to the fact that initial efforts focused on bridging the gap at all whereas latter studies decreased the exposure to attempt that creation of a single-molecule

device. Of the 240 devices that initially showed pA noise, 50 shorted on being immersed in solution and retested. The shorts could be due to the action of solvent molecules dislodging parts of the device or manufacturing defects requiring multiple voltage scans before succumbing to failure. Of the remainder, 166 showed no change in electrical properties implying that these devices contained no sites matching the length requirements for bridging while a further 24 nanogaps exhibited currents indicative of molecular bridging.

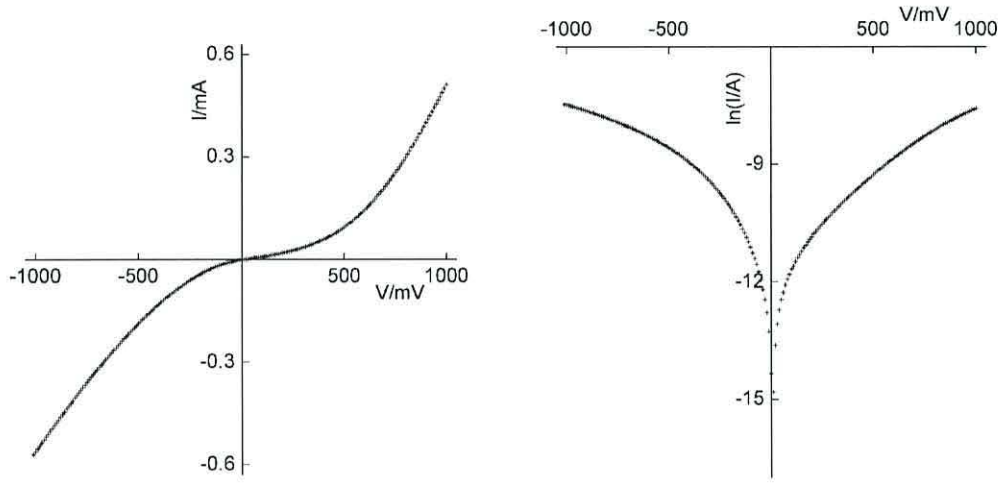

Figure 3.42: I-V curve and log plot for **M4** bridging the SND

The chips were immersed for varying lengths of time with the assumption that the number of linkages formed, and therefore the magnitude of the current, should be proportional to the time the devices spent in solution. However, although there was some correlation in this regard, it was very weak and therefore it can be inferred that the bridging process is dominated by the availability of sites rather than availability of reactant molecule.

The I-V and its corresponding log plot of a silicon device bridged by the **M4** dialdehyde after a 53 hour immersion in a 0.05 mg ml^{-1} chloroform solution is shown in Figure 3.42. The curve shows a relatively high current of *ca.* 0.6 mA at $\pm$1000 mV. The character of the curve at forward and reverse bias is slightly different, possibly indicating an effect from the slightly

altered bonding arrangement for the poly-silicon and Si(111) lower and upper electrodes.

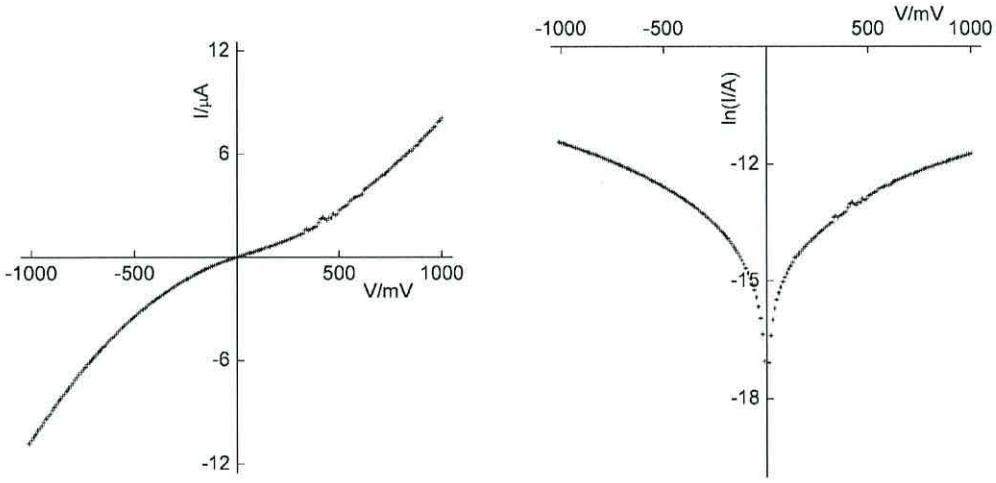

Figure 3.43: I-V curve and log plot for **M4** bridging the SND

The device that produced the curve in Figure 3.43 was on the same chip as that in Figure 3.42 and was therefore subjected to exactly the same conditions. However, the current produced, 12 μA at $\pm$1000 mV is significantly smaller than before. Part of the explanation could be due to the differing electrode areas. Figure 3.43 was produced by the smallest, whereas the device used for Figure 3.42 had a larger area. However, the order of magnitude difference in current is significantly larger, which implies that there were more sites close to the ideal *ca.* 6 nm in the higher current device, allowing a larger number of bridges to form.

Exposing a different device to 5 minutes of the 0.005 mg ml^{-1} **M4** in chloroform solution resulted in the I-V plot shown in Figure 3.44. The current is several orders of magnitude lower than the previous study, suggesting that either there are significantly fewer available bridging sites or the exposure to the connecting molecule is sufficiently limited to connect only a proportion of the sites. Comparing this curve with the analogue deposited on gold and probed using STS in Figure 3.28a, it is clear that the shape of the curves are very similar and the magnitude suggests the silicon system has been bridged

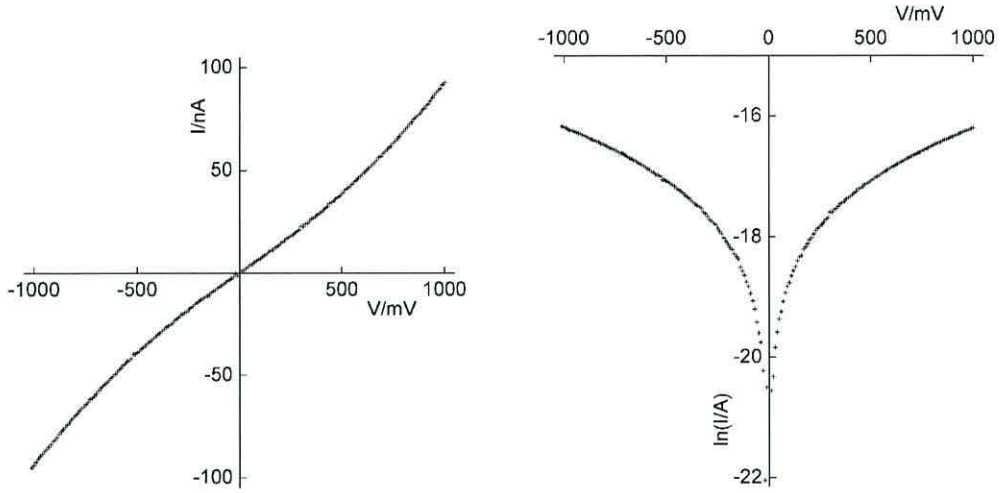

Figure 3.44: I-V curve and log plot for **M4** bridging the SND

by not more than 100 wires.

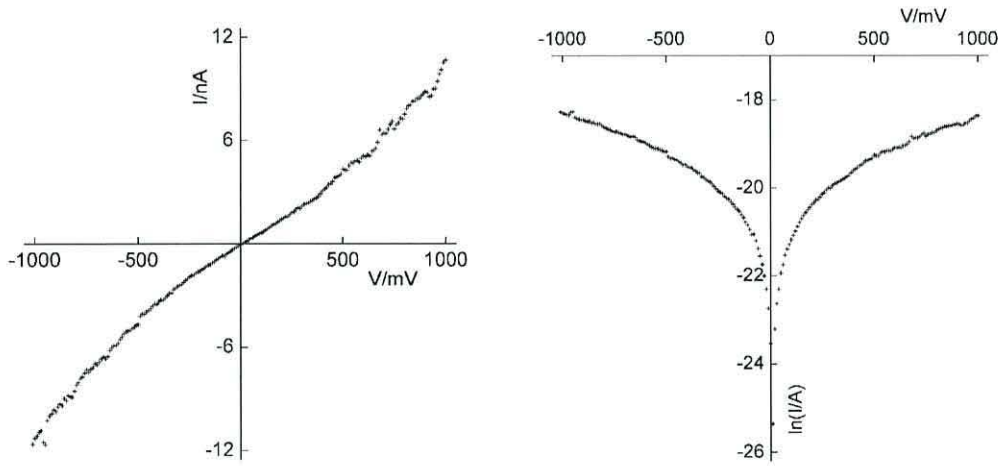

Figure 3.45: I-V curve and log plot for **M4** bridging the SND

The lowest currents achieved during these experiments were all similar to that shown in Figure 3.45. Again the shape of the curve very closely follows that of the system measured using STS in Figure 3.28a. In this instance, however, the magnitude of the current is *ca.* 10 nA at ±1000 mV, approaching single molecular conduction. Comparison with both the STS

result from **W7** and the theoretical study suggest bridging by no more than of the order of 10 molecules.

3.5.5.1 Theoretical study of the large triple-fluorene linker bridging the SND

Theoretical work, carried out by Prof. Colin Lambert's group at Lancaster University,[202] examined the same molecular system as was inserted between the nanogap electrodes. The *ab initio* transport code SMEAGOL[203] and the density functional (DFT) code SIESTA[204] were used to examine the system. The relaxed geometry of the molecule, and the optimum binding arrangement was established using DFT. The nanogap electrodes were incorporated into the system by including 6 layers of 5×5 Si(111), which were attached to infinite periodic leads. Periodic boundary conditions were imposed perpendicular to the axis of transmission and the leads were chosen to have a finite density of states at the Fermi energy in order to mimic the doped nature of the actual electrodes. The SMEAGOL code was then used to calculate the zero bias electron transmission coefficient, T(E), shown in Figure 3.46a. Here, the Fermi energy is situated closer to the LUMO resonance and there is an approximate 2 eV energy gap between the resonances. The IV characteristic, as shown in Figure 3.46b, could then be obtained using equation 3.3.

$$I = \frac{2e}{h} \int_{eV/2}^{-eV/2} T(E)\,\mathrm{d}E. \tag{3.3}$$

Although the general shape of the theoretical curve is similar to the experimental data, there are two differences. The first is that the theoretical curve shows a more pronounced reverse S-shape whereas the experimental IV curve is more gentle and closer to a straight line. This discrepancy may be due to effects caused by higher voltage which were not taken into account by the equilibrium calculation. Also, the conductance is over an order of magnitude lower than the experimentally determined limiting value in the silicon gap although it is close to the gold STM based analogue. The lower current may be due to the experimental system containing more than a single molecule or from well known problems associated with the use of DFT to estimate

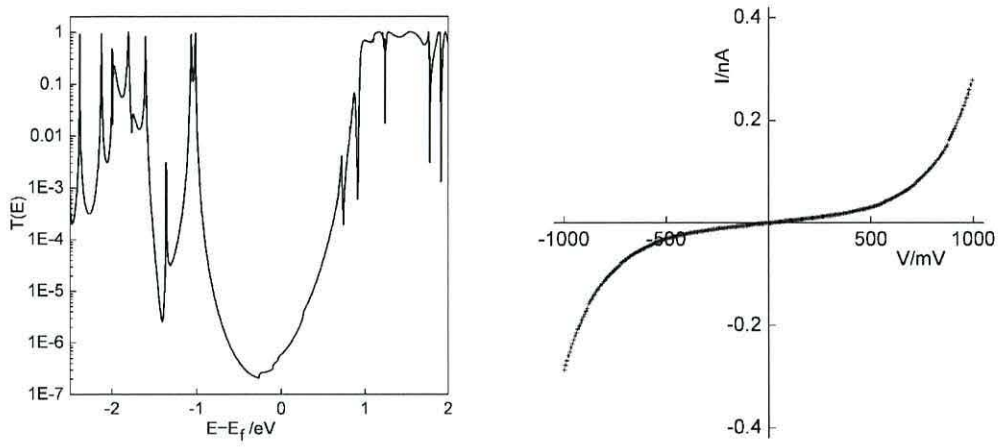

Figure 3.46: Theoretical transport properties of the bridged SND *via* **M4**: a) zero bias transmission coefficient of the molecular wire contacted by silicon leads as a function of $E - E_F$ where E_F is the Fermi energy and E is the energy of the transmitted electrons b) the resultant I-V curve obtained *via* equation 3.3 from the transmission coefficient

the HOMO-LUMO gap and position of the Fermi energy. Furthermore, because the nanogap electrodes are highly doped and asymmetric, there are difficulties in simulating the device characteristics. The upper and lower surfaces, consisting of polycrystalline Si and Si(111) respectively, introduce additional unknown parameters that are difficult to model accurately.

3.5.5.2 Summary

Molecular bridging of silicon nanogaps has been achieved *via in-situ* stepwise synthesis. The lowest, limiting current of *ca.* 10 nA at ±1000 mV, when compared to a theoretical value of *ca.* 0.3 nA at the same voltage, is likely to be the result of a small number of bridging molecules. However, a single molecule device cannot be ruled out as there were unknown factors due to the presence of arsenic doping in the electrodes of the experimental study that could not be accurately replicated in the theory.

3.5.6 Insertion of Diaminoanthraquinone Linker

After the successful bridging of the silicon nanogap with the triple fluorene diamino, a similar experiment was performed with the smallest diamine linker studied during this thesis; 2,6-diaminoanthra-9,10-quinone. This linking molecule is approximately 1 nm long and, when coupled between the 4-ethynylbenzaldehyde anchoring units assembled on the silicon electrodes, the total length of the molecular wire is only 2.85 nm, less than half of the nominal electrode spacing. However, as in the previous study, coupling both sides of the diamine linker with the aldehyde terminating anchor units relies on surface roughness to match the separation. Therefore, it is still possible that there will be sites to match the molecules. In addition, due to the smaller size of the central molecule, there are more geometries possible to form a complete coupling of one electrode to the other. For example, two **M2** diamino linker units could join on to both sides and be close enough in the centre for their π-systems to interact and conduct. Also, by alternating the depositing solution between **M2** and another molecule that is bi-substituted with aldehyde units, in this case terephthaldehyde, the stepwise sequential synthesis methodology should allow a wider variety of gap widths to be spanned. As with all immersions, the chips were subject to washing with copious amounts of pure solvent after each deposition to eliminate any trapped molecular build-up that could result in electrical conduction.

Initially, in each case, data were obtained from the SNDs containing only the self-assembled anchoring molecules. An example of the pA magnitude noise produced by the empty devices has been shown previously in Figure 3.41. These studies used identical devices and so this plot is equally relevant. This baseline of pA noise was consistently present in all the devices, prior to reaction with a linker molecule, which would be subsequently examined for evidence of linkage formation.

Immersing a chip of SNDs in a 0.1 mg ml^{-1} **M2** solution in THF, with catalytic traces of acetic acid, for 5 minutes yielded several shorted devices and the one shown in Figure 3.47. This magnitude of current likely corresponds to a small number of covalently bonded bridges. With exposure

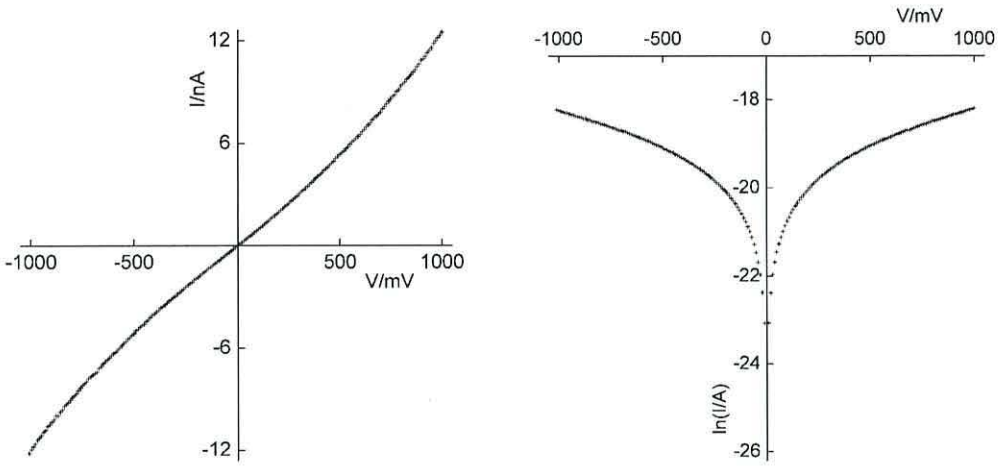

Figure 3.47: I-V curve and log plot for **M2** bridging the SND

only to the amino-terminated **M2**, the only possibility for complete bridging is the simplest case shown in Figure 3.48a, although it is not possible to rule out an interdigitating or partially bridged scenario such as that in Figure 3.48b.

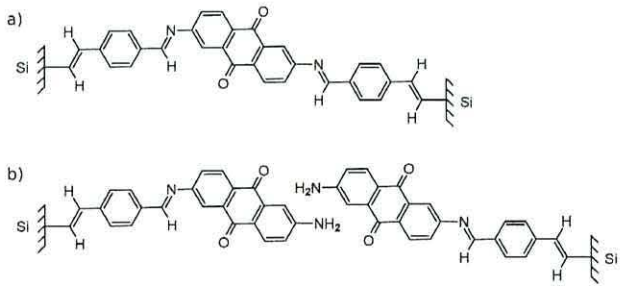

Figure 3.48: Possible bridging geometries for the **M2** molecule in a SND: a) complete bridging b) interdigitating

However, as will be shown in a later study, there is a lower limit for the current believed to be the result of incomplete bridging which implies that the I-V plot shown here is the result of a complete covalent molecular connection of the electrodes. Comparing this I-V plot with the theoretical curve of the same system in Figure 3.51b suggests approximately 17 molecules, assuming each molecule conducts independently and the currents sums linearly.

The chip containing the device in Figure 3.47 was subject to an extensive study involving multiple alternating immersions in THF solutions of both **M2** and terephthalaldehyde. The concentrations used were 0.1 mg ml^{-1} for **M2** and 0.05 mg ml^{-1} for the terephthalaldehyde, both in THF with catalytic traces of acetic acid. The immersion times began with 5 minutes, but were gradually increased until 16 hour depositions were used. However, there was no discernible change observed to either the current magnitude or the shape of the I-V curve from the original device after two immersions in terephthalaldehyde and two further **M2** immersions. Several other devices collapsed to high, 1 mA, Ohmic currents while the remainder showed only pA noise. The IV characteristics were stable when cycled between ±1000 mV over the length of the study which took a fortnight and involved many immersions and I-V cycles. This suggests that it is possible for a molecular-wire inserted SND system to be durable for a significant time period. The invariability casts doubt over the significance of interdigitating arrangements however, because the overlap of molecules due to the stepwise build-up of either side should increase the resultant current.

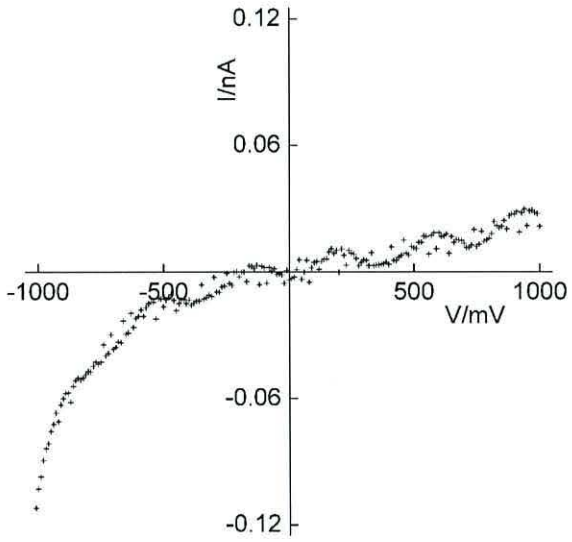

Figure 3.49: I-V curve for an SND bridged by **M2** after it has been washed out

Further evidence for the conduction mechanism of this system being of molecular origin comes from Figure 3.49. After a 16 hour immersion in a 0.05 mg ml^{-1}, acidified solution of terephthalaldehyde in THF, the current characteristic of the device altered significantly. The magnitude of the current reduced by two orders of magnitude and there was evidence of some asymmetry. The current is still significantly higher than the pA exhibited by a device without bridging and therefore it is to be assumed that this represents a partial bridging geometry with the slight electrical asymmetry due to the presence of the electron-accepting linker, located at one of the electrodes. Higher current occurs when the bottom electrode is acting as the cathode and therefore may be explained by the electron-accepting **M2** moiety being attached to the lower electrode. The precise nature of the bridge between the electrodes after this 'washing-out' has occurred is impossible to determine, but it does provide compelling evidence that the I-V curve of 12 nA at ±1000 mV is not an experimental artefact but due to the molecular assembly attached between the silicon electrodes.

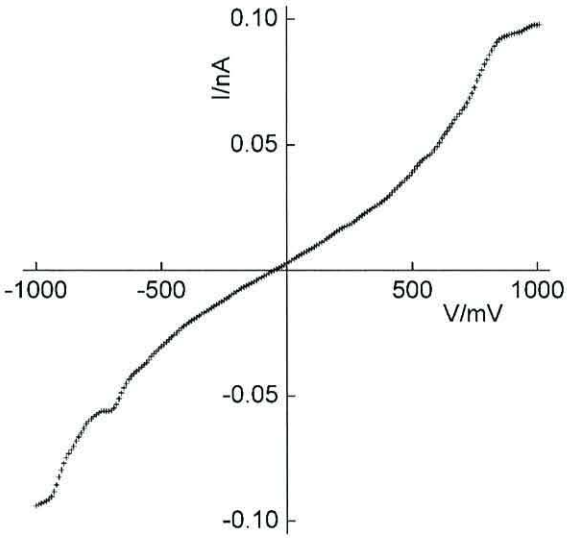

Figure 3.50: Theoretical I-V curve for an SND bridged by **M2**

On a different chip, subjected first to a one hour de-protecting wash of 2:1 mixture of THF:formic acid followed by 30 minutes immersion in a

0.01 mg ml^{-1} solution of **M2** in THF with a catalytic trace of acetic acid produced several collapsed devices and one that indicated the presence of bridging. The resultant I-V curve, shown in Figure 3.50, is a factor of 7 lower than the current magnitude derived from theoretical model of the system. Also, while much of the curve is the common smooth reverse-S shape, there are several places where the sweep is distorted suggesting secondary effects influencing conduction. The lower current magnitude implies an incomplete bridging arrangement with a narrow tunnelling gap between the molecular strands assembled on either electrode. With each molecule free to rotate around some of the bonds, the anomalous distortions could be the result of relative motion of the molecules altering the size of the gap between them.

3.5.6.1 Theoretical study of the 2,6-diaminoanthra-9,10-quinone linker bridging the SND

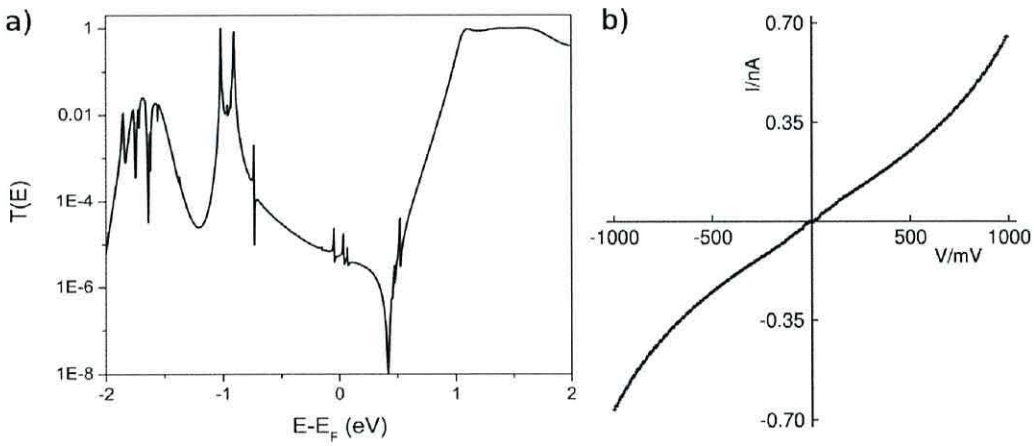

Figure 3.51: Theoretical transport properties of the bridged SND *via* **M2**: a) zero bias transmission coefficient of the molecular wire contacted by silicon leads as a function of $E - E_F$ where E_F is the Fermi energy and E is the energy of the transmitted electrons b) the resultant I-V curve obtained *via* equation 3.3 from the transmission coefficient

A theoretical study was also carried out on the 2.85 nm system examined experimentally in the previous section. *Ab-initio* transport code SMEAGOL[203] and density functional (DFT) code SIESTA[204] were used to simulate the electrical properties of the molecules covalently bonded between

silicon electrods. DFT calculations were used to find the relaxed geometry of the molecule itself and the optimum binding position when it is attached with the anchoring units to the silicon. Contact pads comprising 6 layers of 5×5 atoms of Si(111) were added to each end of the molecule. As before, periodic boundary conditions and a finite density of states at the Fermi energy completed the simulation of infinite leads with doped behaviour. Figure 3.51a and 3.51b show the zero bias electron transmission coefficient, T(E), as calculated by the SMEAGOL code and the I-V characteristic of the molecule computed using the formula in equation 3.3.

The shape of both the I-V curves from experiment and theory are very similar although their magnitudes differ by a factor of 17. The incongruity might the be result of problems with using DFT to calculate a value for Fermi energy and the size of the HOMO-LUMO gap. Also, the electrical characteristics of highly doped, asymmetric contacts are very complex to simulate reliably, especially with small devices. These theoretical problems may also be the result of the experimental device containing more than one bridging molecule.

3.5.6.2 Summary

Silicon nanogap devices have been reliably bridged by a 2.85 nm long molecular wire and subsequently detached. The nature of the surface roughness present in the gap electrodes has been used to match molecule lengths in order to facilitate very low density bridging. Stable contact was formed to a small number of molecules that remained connected to the electrodes for two weeks during multiple further immersions before finally being washed out by a weak, acidified solution. This study has verified the molecular origin of the enhanced conduction over the pA noise observed from empty devices and has demonstrated that it is possible to form a stable quasi single molecule organic-silicon hybrid device.

Chapter 4

Conclusions

It has been shown that by assembling molecular wires using a multi-step modular approach, it is possible to build up long wires consisting of many component units.

The presence of layers on gold has been verified using a Sauerbrey analysis of quartz crystal microbalance data. These results yield limiting areas per molecule that closely match the molecular cross-sections taken from van der waals radii. This suggests the formation of generally close-packed, upright, homogeneous layers. Any variation from expectation tends towards an excess, due to a proportion of interstitial impurities and physisorbed material. Evidence for the stepwise extension of the wire has also been provided by QCM. Again these data indicate generally good coverage of closely packed layers. However, physisorption is also in evidence, particularly as the wire grows long with the larger molecules that contain alkane-chain side-arms and the very small molecules, including solvent molecules, that can become trapped between.

X-ray photo-electron spectroscopy data have confirmed the presence of the the various components in the stepwise-formed wire systems. The substituent elements and their sub-environments, particularly nitrogen and sulphur, closely match the molecular formula of the constituent compounds. Importantly, the nitrogen regions of the spectra have verified that imino formation is the mechanism by which wires are extended.

A simple method of contacting a monolayer has been developed, using an electromagnetic cantilever. This technique has been applied to a number of systems and produces results with similar characteristics to the scanning tunnelling spectroscopy measurements. Electrical measurements of the two-part wire, **W2**, demonstrate weak rectifying characteristics with a current ratio of 4 at ± 1 V. Other systems investigated, comprising up to seven components, produce symmetrically conducting wires. Current magnitudes through these wires are *ca.* 1 nA at ± 1V. This suggests that electrons rely on a weakly length-dependant hopping mechanism to traverse the wires due to the high degree of conjugation and energy available at room temperature. Only when the wire is extended to beyond 10 nm is the conductance attenuated significantly.

The main result is the molecular bridging of silicon nanogaps, which had never been reported previously. It was achieved *via in-situ* stepwise synthesis. Empty devices exhibit leakage currents in the sub-picoampere range for ≤ 1 V, only rising to *ca.* 2 nA when tunnelling between contacts becomes significant at ± 7 V. Coating the contacts with the 4-ethynlybenzaldehyde anchoring layer does not change the electrical character of the gap as the molecule is too small to influence the properties of a gap that is nominally 7 nm wide. Similarly, inserting the mono-substituted aniline did not result in a bridged gap. Although some devices showed increased current, the very high and ohmic nature of the I-V characteristics were attributed to device collapse and connecting electrodes. However, bridged devices did form after the insertion of **M4**, the large, 4 nm long, amino-terminated linker; specifically chosen to be slightly smaller than the gap width. Surface roughness was relied on to match the length of the assembled molecule. The lowest, limiting current found for this system was 10 nA at ± 1 V. This was higher than the theoretical value of 0.3 nA at the same voltage, and is likely to be the result of a small number of bridging molecules. However, it is not possible to rule out a single molecule bridge due to a variety of unknown factors in the modelling process. The presence of arsenic doping in the electrodes of the experimental study could not be accurately replicated by the theoretical calculations and could alter the result significantly.

Silicon nanogap devices have also been bridged using the **M2** molecule. Surface roughness was again essential to the success of bridging. The nominal 7 ± 1 nm gap should result in very few sites appropriate for a 2.85 nm long molecule. This restriction was ideal to facilitate very low density bridging. Stable contact resulted for a small number of molecules, producing a smooth I-V curve of 12 nA at ± 1 V. The device remained bridged for two weeks during multiple further immersions before finally being washed out by a weak, acidified solution. Returning to a low leakage current verifies the molecular origin of the enhanced conduction. It also demonstrated that a stable, covalently bonded, molecular organic-silicon hybrid device is possible, even without encapsulation.

4.1 Further Work and Outlook

The work in this thesis has gone a long way to demonstrate the potential of molecular electronics for integration with silicon systems *via* self-assembly and stepwise synthesis and elongation. However, more is needed before useful devices are realised.

It is important that studies are performed at a range of temperatures. The weak length dependence of conduction strongly indicates a hopping regime, with little tunnelling character. Examining the temperature dependence will allow this to be confirmed conclusively and decay factors, β, extracted. Also, molecules in the silicon devices should be able to act as sensing devices. The limited supply of device structures meant that it was not possible to investigate this application during this thesis. However, if long-term stability was achieved regularly, sensing should prove a fruitful avenue of research.

Several of the silicon nanogap devices have been bridged by what appears to be single molecules, or just a few molecules within the uncertainty of the contact environment. However, further work could help verify this using weaker solutions and shorter immersions times or by first depositing a small mono-substituted capping moiety. This technique could work in a similar way as the matrix isolation method for examining a small number of molecules with a scanning probe tip. The capping molecules would block many of the

potential bridging sites and provide a more restricted device to be bridged by a bi-substituted molecule. Unfortunately, without moving away from a method dependant on statistical chance, it will be difficult to establish, with complete certainty, a single-molecule device.

Ideally, the equipment could also be modified in order to perform the investigation of silicon nanogap devices in the dark. Although the addition of a case eliminated catastrophic static discharge events, it would still be useful to examine the systems without any potential photoelectric interference. A computer controlled probe station would allow the chips to be enclosed completely in darkness throughout the entire investigation.

Molecular electronics has the potential to be a disruptive technology, bringing a bottom-up approach to the top-down dominated world of silicon processing architecture. It has been shown that organic molecular electronics and silicon architecture can combine to create hybrid devices that approach single molecule electronics. However, before this breakthrough becomes commercially viable, three issues need to be addressed.

The first is that, for reliable behaviour, the devices must be formed identically. For molecular devices, this requires both a consistency with regard to the number and arrangement of the molecules. The simplest way to achieve this restriction is single molecules in identical architectures. The nanogap devices investigated during this thesis are unlikely to be suitable for consistent single-molecule electronics. Creating the undercut using etching, forms rough surfaces on the molecular scale. The requirement of an electrode area comparable to the cross-sectional area of the molecule, with the electrodes separated by the molecule length, is too difficult to achieve with the nanogap architecture. A more appropriate candidate is the crossbar structure. This is a particularly useful construct if carbon nanotubes are used, as these can be made with a diameter comparable to molecular dimensions. This will limit electrode areas to that of a single molecule cross-section, thus ensuring single-molecule connections.

The second issue is device density. While the smallest current devices produced in this thesis contained only a few molecules, the silicon architecture itself was *ca.* 50 μm across (neglecting macroscopic contact pads). There is

the potential to reduce this by three orders of magnitude, to approach the molecular scale.

Finally, as has already been mentioned, stability is a key issue. Computing devices must be capable of lasting many years and undergoing countless actuations, without degrading or altering their behaviour. As more is learnt about single molecule devices, certain geometry and molecule combinations may be found that perform sufficiently well. Alternatively, the answer may lie in encapsulation.

If these issues can be overcome, there is great potential in molecular electronics to make a significant contribution to the technological landscape.

References

1. T. Theis, D. Parr, P. Binks, J. Ying, K. E. Drexler, E. Schepers, K. Mullis, C. Bai, J. J. Boland, R. Langer, P. Dobson, C. N. R. Rao, and M. Ferrari. nan'o.tech.nol'o.gy *n.* *Nature Nanotechnology*, 1(1):8, 2006.

2. G. M. Whitesides. Nanoscience, nanotechnology, and chemistry. *Small*, 1(2):172, 2005.

3. R. A. L. Jones. The future of nanotechnology. *Physics World*, (August):25, 2004.

4. R. A. L. Jones. New materials, old challenges. *Nature Nanotechnology*, 2(8):453, 2007.

5. C. N. R. Rao and A. K. Cheetham. Science and technology of nanomaterials: current status and future prospects. *Journal of Materials Chemistry*, 11(12):2887, 2001.

6. R. P. Feynman. There's plenty of room at the bottom. Available at `http://www.zyvex.com/nanotech/feynman.html`. Accessed Dec 2009.

7. C. Tourney. Apostolic Succession. *Engineering and Science*, 68(1):16, 2005.

8. D. M. Eigler and E. K. Schweizer. Positioning single atoms with a scanning tunnelling microscope. *Nature*, 344(6266):524, 1990.

9. T. O. Yeates and J. E. Padilla. Designing supramolecular protein assemblies. *Current Opinion in Structural Biology*, 12(4):464, 2002.

10. M. Meister, S. R. Caplan, and H. C. Berg. Dynamics of a tightly coupled mechanism for flagellar rotation. bacterial motility, chemiosmotic coupling, protonmotive force. *Biophysical Journal*, 55(5):905, 1989.

11. N. C. Seeman. An overview of structural DNA nanotechnology. *Molecular Biotechnology*, 37(3):246, 2007.

12. H. van Zalinge, D. J. Schiffrin, A. D. Bates, W. Haiss, J. Ulstrup, and R. J. Nichols. Single-molecule conductance measurements of single- and double-stranded DNA oligonucleotides. *ChemPhysChem*, 7(1):94, 2006.

13. Y. Shirai, A. J. Osgood, Y. Zhao, K. F. Kelly, and J. M. Tour. Directional control in thermally driven single-molecule nanocars. *Nano Letters*, 5(11):2330, 2005.

14. K. E. Drexler. *Engines of Creation: The Coming Era of Nanotechnology.* 1986.

15. R. A. L. Jones. *Soft Machines: Nanotechnology and Life.* Oxford University Press, 1 edition, 2004.

16. G. E. Moore. Cramming more components onto integrated circuits. *Electronics*, 38(8), 1965.

17. W. Zulehner. Czochralski growth of silicon. *Journal of Crystal Growth*, 65(1-3):189, 1983.

18. J. S. Kilby. The integrated circuit's early history. *Proceedings of the IEEE*, 88(1):109, 2000.

19. R. Noyce. Semiconductor switching device. U.S. Patent 2,971,139, June 1959.

20. P. Hahn. The 300 mm silicon wafer - a cost and technology challenge. *Microelectronic Engineering*, 56(1-2):3, 2001.

21. C. G. Willson and B. J. Roman. The future of lithography: SEMATECH litho forum 2008. *ACS Nano*, 2(7):1323, 2008.

22. J. Bjorkholm. EUV lithography - the successor to optical lithography? *Intel Technology Journal*, Q3(1):1, 1998.

23. C. W. Gwyn. Extreme ultraviolet lithography. *Journal of Vacuum Science & Technology B: Microelectronics and Nanometer Structures*, 16(6):3142, 1998.

24. R. Ito and S. Okazaki. Pushing limits of lithography. *Nature*, 406(6799):1027, 2000.

25. R. H. French, W. Qiu, M. K. Yang, R. C. Wheland, M. F. Lemon, A. L. Shoe, D. J. Adelman, M. K. Crawford, H. V. Tran, J. Feldman, S. J. McLain, and S. Peng. Second generation fluids for 193nm immersion lithography. *Proceedings of SPIE*, 6154:418, 2006.

26. P. Zimmerman. Double patterning lithography: double the trouble or double the fun? *SPIE Newsroom*, 2009.

27. The International Technology Roadmap for Semiconductors: 2007 Edition. Available at `http://www.itrs.net/Links/2007ITRS/Home2007.htm`. Accessed Dec 2009.

28. E. P. Gusev, E. Cartier, D. A. Buchanan, M. Gribelyuk, M. Copel, H. Okorn-Schmidt, and C. D'Emic. Ultrathin high-κ metal oxides on silicon: processing, characterization and integration issues. *Microelectronic Engineering*, 59(1-4):341, 2001.

29. K. Maex, M. R. Baklanov, D. Shamiryan, F. lacopi, S. H. Brongersma, and Z. S. Yanovitskaya. Low dielectric constant materials for microelectronics. *Journal of Applied Physics*, 93(11):8793, 2003.

30. B. Yu, L. Chang, S. Ahmed, H. Wang, S. Bell, C.-Y. Yang, C. Tabery, C. Ho, Q. Xiang, T.-J. King, J. Bokor, C. Hu, M.-R. Lin, and D. Kyser. FinFET scaling to 10 nm gate length. In *Electron Devices Meeting, 2002. IEDM '02. Digest. International*, page 251.

31. Y.-C. Yeo, T.-J. King, and C. Hu. MOSFET gate leakage modeling and selection guide for alternative gate dielectrics based on leakage considerations. *IEEE Transactions on Electron Devices*, 50(4):1027, 2003.

32. P. Raha, S. Ramaswamy, and E. Rosenbaum. Heat flow analysis for EOS/ESD protection device design in SOI technology. *IEEE Transactions on Electron Devices*, 44(3):464, 1997.

33. D. Divins. Simulate MOSFET Heating Caused by Inrush Currents. *Power Electronics Technology*, June:34, 2007.

34. L. Tang, K. Pey, C. Tung, M. Radhakrishnan, and W. Lin. Gate dielectric-breakdown-induced microstructural damage in MOSFETs. *IEEE Transactions on Device and Materials Reliability*, 4(1):38, 2004.

35. P. E. Blöchl and J. H. Stathis. Aspects of defects in silica related to dielectric breakdown of gate oxides in MOSFETs. *Physica B: Condensed Matter*, 273:1022, 1999.

36. M.-H. Chiang, C.-N. Lin, and G.-S. Lin. Threshold voltage sensitivity to doping density in extremely scaled MOSFETs. *Semiconductor Science and Technology*, 21(2):190, 2006.

37. The International Technology Roadmap For Semiconductors: 2010 Update. Available at `http://www.itrs.net/Links/2010ITRS/Home2010.htm`. Accessed May 2010.

38. G. J. Ashwell, B. Urasinska, C. Wang, M. R. Bryce, I. Grace, and C. J. Lambert. Single-molecule electrical studies on a 7 nm long molecular wire. *Chemical Communications*, (45):4706, 2006.

39. G. J. Ashwell, B. Urasinska, and W. D. Tyrrell. Molecules that mimic Schottky diodes. *Physical Chemistry Chemical Physics*, 8(28):3314, 2006.

40. G. Snider, P. Kuekes, and R. S. Williams. CMOS-like logic in defective, nanoscale crossbars. *Nanotechnology*, 15(8):881, 2004.

41. C. P. Collier, E. W. Wong, M. Belohradsky, F. M. Raymo, J. F. Stoddart, P. J. Kuekes, R. S. Williams, and J. R. Heath. Electronically configurable molecular-based logic gates. *Science*, 285(5426):391, 1999.

42. M. Leclerc. Polyfluorenes: Twenty years of progress. *Journal of Polymer Science Part A: Polymer Chemistry*, 39(17):2867, 2001.

43. M. T. Bernius, M. Inbasekaran, J. O'Brien, and W. Wu. Progress with light-emitting polymers. *Advanced Materials*, 12(23):1737, 2000.

44. J. Collet and D. Vuillaume. Nano-field effect transistor with an organic self-assembled monolayer as gate insulator. *Applied Physics Letters*, 73(18):2681, 1998.

45. J. Collet, O. Tharaud, A. Chapoton, and D. Vuillaume. Low-voltage, 30 nm channel length, organic transistors with a self-assembled monolayer as gate insulating films. *Applied Physics Letters*, 76(14):1941, 2000.

46. R. S. Mulliken. Quantum-mechanical methods and the electronic spectra and structure of molecules. *Chemical Reviews*, 41(2):201, 1947.

47. N. S. Hush. An overview of the first half-century of molecular electronics. *Annals of the New York Academy of Sciences*, 1006(1):1, 2003.

48. A. Szent-Györgyi. The study of energy-levels in biochemistry. *Nature*, 148(3745):157, 1941.

49. A. Aviram and M. Ratner. Molecular rectifiers. *Chemical Physics Letters*, 29(2):277, 1974.

50. F. L. Carter. The molecular device computer: point of departure for large scale cellular automata. *Physica*, 10D:175, 1984.

51. F. L. Carter. Molecular level fabrication techniques and molecular electronic devices. *Microelectronic Engineering*, 2(1-3):11, 1984.

52. F. L. Carter. Chemistry and microstructures: fabrication at the molecular size level. *Superlattices and Microstructures*, 2(2):113, 1986.

53. A. Ghosh and S. Datta. Molecular conduction: Paradigms and possibilities. *Journal of Computational Electronics*, 1(4):515, 2002.

54. J. M. Seminario. Molecular electronics: approaching reality. *Nature Materials*, 4(2):111, 2005.

55. H. Shirakawa, E. J. Louis, A. G. MacDiarmid, C. K. Chiang, and A. J. Heeger. Synthesis of electrically conducting organic polymers: halogen derivatives of polyacetylene, $(CH)_x$. *Journal of the Chemical Society, Chemical Communications*, (16):578, 1977.

56. H. Shirakawa. Nobel lecture: The discovery of polyacetylene film—the dawning of an era of conducting polymers. *Reviews of Modern Physics*, 73(3):713, 2001.

57. A. MacDiarmid. Synthetic metals: A novel role for organic polymers. *Reviews of Modern Physics*, 73(3):701, 2001.

58. A. J. Heeger. Semiconducting and metallic polymers: the fourth generation of polymeric materials. *The Journal of Physical Chemistry B*, 105(36):8475, 2001.

59. G.-P. Tang, Z.-Q. Fan, X.-J. Zhang, Y. Ren, and K.-Q. Chen. Negative differential resistance behaviour in OPE molecular devices with semiconductor electrodes. *Journal of Physics D: Applied Physics*, 42(17):175104, 2009.

60. J. M. Tour, M. Kozaki, and J. M. Seminario. Molecular scale electronics: a synthetic/computational approach to digital computing. *Journal of the American Chemical Society*, 120(33):8486, 1998.

61. R. M. Metzger. The unimolecular rectifier: unimolecular electronic devices are coming .... *Journal of Materials Chemistry*, 9(9):2027, 1999.

62. R. M. Metzger. Unimolecular rectifiers and proposed unimolecular amplifier. *Annals of the New York Academy of Sciences*, 1006(1):252, 2003.

63. G. J. Ashwell, J. R. Sambles, A. S. Martin, W. G. Parker, and M. Szablewski. Rectifying characteristics of Mg—($C_{16}H_{33}$-Q3CNQ LB film)—Pt structures. *Chemical Communications*, (19):1374, 1990.

64. C. M. Finch, S. Sirichantaropass, S. W. Bailey, I. M. Grace, V. M. García-Suárez, and C. J. Lambert. Conformation dependence of molecular conductance: chemistry versus geometry. *Journal of Physics: Condensed Matter*, 20(2):022203, 2007.

65. G. J. Ashwell and A. Mohib. Improved molecular rectification from self-assembled monolayers of a sterically hindered dye. *Journal of the American Chemical Society*, 127(46):16238, 2005.

66. C. P. Collier. A [2]catenane-based solid state electronically reconfigurable switch. *Science*, 289(5482):1172, 2000.

67. M. A. Reed and J. M. Tour. Computing with molecules. *Scientific American*, 282(6):86, 2000.

68. F. Jiang. First-principles study of phenyl ethylene oligomers as current-switch. *Physics Letters A*, 359(5):487, 2006.

69. D. Nozaki and G. Cuniberti. Silicon-based molecular switch junctions. *Nano Research*, 2(8):648, 2009.

70. K. Wang, N. L. Rangel, S. Kundu, J. C. Sotelo, R. M. Tovar, J. M. Seminario, and H. Liang. Switchable molecular conductivity. *Journal of the American Chemical Society*, 131(30):10447, 2009.

71. S. Kolliopoulou, P. Dimitrakis, P. Normand, H.-L. Zhang, N. Cant, S. D. Evans, S. Paul, C. Pearson, A. Molloy, M. C. Petty, and D. Tsoukalas. Hybrid silicon–organic nanoparticle memory device. *Journal of Applied Physics*, 94(8):5234, 2003.

72. J.-S. Lee, J. Cho, C. Lee, I. Kim, J. Park, Y.-M. Kim, H. Shin, J. Lee, and F. Caruso. Layer-by-layer assembled charge-trap memory devices with adjustable electronic properties. *Nature Nanotechnology*, 2(12):790, 2007.

73. W. R. Dichtel, J. R. Heath, and J. F. Stoddart. Designing bistable [2]rotaxanes for molecular electronic devices. *Philosophical Transactions of The Royal Society A*, 365(1855):1607, 2007.

74. W. Clegg, C. Gimenez-Saiz, D. A. Leigh, A. Murphy, A. M. Z. Slawin, and S. J. Teat. "smart" rotaxanes: shape memory and control in tertiary amide peptido[2]rotaxanes. *Journal of the American Chemical Society*, 121(17):4124, 1999.

75. Y. Chen, G.-Y. Jung, D. A. A. Ohlberg, X. Li, D. R. Stewart, J. O. Jeppesen, K. A. Nielsen, J. F. Stoddart, and R. S. Williams. Nanoscale molecular-switch crossbar circuits. *Nanotechnology*, 14(4):462, 2003.

76. Z. Liu, A. A. Yasseri, J. S. Lindsey, and D. F. Bocian. Molecular memories that survive silicon device processing and real-world operation. *Science*, 302(5650):1543, 2003.

77. P. Qi, A. Javey, M. Rolandi, Q. Wang, E. Yenilmez, and H. Dai. Miniature organic transistors with carbon nanotubes as quasi-one-dimensional electrodes. *Journal of the American Chemical Society*, 126(38):11774, 2004.

78. J. Tang, E. Depoortere, J. Klare, C. Nuckolls, and S. Wind. Single-molecule transistor fabrication by self-aligned lithography and *in situ* molecular assembly. *Microelectronic Engineering*, 83(4-9):1706, 2006.

79. T. Shimazaki. A theoretical study of molecular conduction: IV. a three-terminal molecular device. *Nanotechnology*, 18(42):424012, 2007.

80. H. Weber, J. Reichert, F. Weigend, R. Ochs, D. Beckmann, M. Mayor, R. Ahlrichs, and H. Lohneysen. Electronic transport through single conjugated molecules. *Chemical Physics*, 281(2-3):113, 2002.

81. A. Nitzan and M. A. Ratner. Electron transport in molecular wire junctions. *Science*, 300(5624):1384, 2003.

82. M. Brandbyge, J.-L. Mozos, P. Ordejón, J. Taylor, and K. Stokbro. Density-functional method for nonequilibrium electron transport. *Physical Review B*, 65(16):165401, 2002.

83. H. Ohnishi, Y. Kondo, and K. Takayanagi. Quantized conductance through individual rows of suspended gold atoms. *Nature*, 395(6704):780, 1998.

84. X. D. Cui, A. Primak, X. Zarate, J. Tomfohr, O. F. Sankey, A. L. Moore, T. A. Moore, D. Gust, L. A. Nagahara, and S. M. Lindsay. Changes in the electronic properties of a molecule when it is wired into a circuit. *The Journal of Physical Chemistry B*, 106(34):8609, 2002.

85. X. D. Cui, X. Zarate, J. Tomfohr, O. F. Sankey, A. Primak, A. L. Moore, T. A. Moore, D. Gust, G. Harris, and S. M. Lindsay. Making electrical contacts to molecular monolayers. *Nanotechnology*, 13(1):5, 2001.

86. W. Wang, T. Lee, and M. A. Reed. Electronic transport in self-assembled alkanethiol monolayers. *Physica E*, 19(1-2):117, 2003.

87. E. A. Weiss, M. R. Wasielewski, and M. A. Ratner. Molecules as wires: Molecule-assisted movement of charge and energy. In *Molecular Wires and Electronics*, volume 257 of *Topics in Current Chemistry*, pages 103–133. Springer Berlin, 2005.

88. R. H. Goldsmith, L. E. Sinks, R. F. Kelley, L. J. Betzen, W. Liu, E. A. Weiss, M. A. Ratner, and M. R. Wasielewski. Wire-like charge transport at near constant bridge energy through fluorene oligomers. *Proceedings of the National Academy of Sciences of the United States of America*, 102(10):3540, 2005.

89. L. Luo and C. D. Frisbie. Length-dependent conductance of conjugated molecular wires synthesized by stepwise 'click' chemistry. *Journal of the American Chemical Society*, 132(26):8854, 2010.

90. A. Nitzan, J. Jortner, J. Wilkie, A. L. Burin, and M. A. Ratner. Tunneling time for electron transfer reactions. *The Journal of Physical Chemistry B*, 104(24):5661, 2000.

91. Y. Selzer and D. L. Allara. Single-molecule electrical junctions. *Annual Review of Physical Chemistry*, 57:593, 2006.

92. D. Segal, A. Nitzan, W. B. Davis, M. R. Wasielewski, and M. A. Ratner. Electron transfer rates in bridged molecular systems 2. A steady-state analysis of coherent tunneling and thermal transitions. *The Journal of Physical Chemistry B*, 104(16):3817, 2000.

93. E. A. Weiss, M. J. Ahrens, L. E. Sinks, A. V. Gusev, M. A. Ratner, and M. R. Wasielewski. Making a molecular wire: charge and spin transport through para-phenylene oligomers. *Journal of the American Chemical Society*, 126(17):5577–84, 2004.

94. E. A. Weiss, M. J. Tauber, R. F. Kelley, M. J. Ahrens, M. A. Ratner, and M. R. Wasielewski. Conformationally gated switching between superexchange and hopping within oligo-*p*-phenylene-based molecular wires. *Journal of the American Chemical Society*, 127(33):11842, 2005.

95. Q. Lu, K. Liu, H. Zhang, Z. Du, X. Wang, and F. Wang. From tunneling to hopping: a comprehensive investigation of charge transport mechanism in molecular junctions based on oligo(*p*-phenylene ethynylene)s. *ACS Nano*, 3(12):3861, 2009.

96. R. J. Hamers, J. S. Hovis, S. Lee, H. Liu, and J. Shan. Formation of ordered, anisotropic organic monolayers on the Si(001) surface. *The Journal of Physical Chemistry B*, 101(9):1489, 1997.

97. P. T. Hurley, E. J. Nemanick, B. S. Brunschwig, and N. S. Lewis. Covalent attachment of acetylene and methylacetylene functionality to Si(111) surfaces: scaffolds for organic surface functionalization while retaining Si-C passivation of Si(111) surface sites. *Journal of the American Chemical Society*, 128(31):9990, 2006.

98. R. J. Hamers. Formation and characterization of organic monolayers on semiconductor surfaces. *Annual Review of Analytical Chemistry (2008)*, 1(1):707, 2008.

99. N. P. Guisinger, N. L. Yoder, and M. C. Hersam. Probing charge transport at the single-molecule level on silicon by using cryogenic ultra-high vacuum scanning tunneling microscopy. *Proceedings of the National Academy of Sciences of the United States of America*, 102(25):8838, 2005.

100. V. Meunier, W. Lu, J. Bernholc, and B. G. Sumpter. Electron transport in molecular systems. *Journal of Physics: Conference Series*, 16:283, 2005.

101. N. P. Guisinger, R. Basu, A. S. Baluch, and M. C. Hersam. Molecular electronics on silicon: An ultrahigh vacuum scanning tunneling microscopy study. *Annals of the New York Academy of Sciences*, 1006(1):227, 2003.

102. M. J. Sailor, F. L. Klavetter, R. H. Grubbs, and N. S. Lewis. Electronic properties of junctions between silicon and organic conducting polymers. *Nature*, 346(6280):155, 1990.

103. A. Vilan, O. Yaffe, A. Biller, A. Salomon, A. Kahn, and D. Cahen. Molecules on Si: electronics with chemistry. *Advanced Materials*, 22(2):140, 2010.

104. W. Lu, V. Meunier, and J. Bernholc. Nonequilibrium quantum transport properties of organic molecules on silicon. *Physical Review Letters*, 95(20), 2005.

105. N. Saito, K. Hayashi, H. Sugimura, and O. Takai. Microstructured π-conjugated organic monolayer covalently attached to silicon. *Langmuir*, 19(26):10632, 2003.

106. J. Basu, S. Hazra, and M. Sanyal. Growth mechanism of Langmuir-Blodgett films. *Physical Review Letters*, 82(23):4675, 1999.

107. A. Ulman. Formation and structure of self-assembled monolayers. *Chemical Reviews*, 96(4):1533, 1996.

108. J. H. Fendler. Chemical self-assembly for electronic applications. *Chemistry of Materials*, 13(10):3196, 2001.

109. H. B. Akkerman, P. W. M. Blom, D. M. de Leeuw, and B. de Boer. Towards molecular electronics with large-area molecular junctions. *Nature*, 441(7089):69, 2006.

110. N. R. Champness. Surface chemistry: building with molecules. *Nature Nanotechnology*, 2(11):671, 2007.

111. J. C. Love, L. A. Estroff, J. K. Kriebel, R. G. Nuzzo, and G. M. Whitesides. Self-assembled monolayers of thiolates on metals as a form of nanotechnology. *Chemical Reviews*, 105(4):1103, 2005.

112. W. Bigelow, D. Pickett, and W. Zisman. Oleophobic monolayers I. films adsorbed from solution in non-polar liquids. *Journal of Colloid Science*, 1(6):513, 1946.

113. R. G. Nuzzo and D. L. Allara. Adsorption of bifunctional organic disulfides on gold surfaces. *Journal of the American Chemical Society*, 105(13):4481, 1983.

114. R. B. Pontes, F. D. Novaes, A. Fazzio, and A. J. R. da Silva. Adsorption of benzene-1,4-dithiol on the Au(111) surface and its possible role in molecular conductance. *Journal of the American Chemical Society*, 128(28):8996, 2006.

115. E. Cortés, A. A. Rubert, G. Benitez, P. Carro, M. E. Vela, and R. C. Salvarezza. Enhanced stability of thiolate self-assembled monolayers (SAMs) on nanostructured gold substrates. *Langmuir*, 25(10):5661, 2009.

116. R. Desikan. Effect of chain length on nanomechanics of alkanethiol self-assembly. *Nanotechnology*, 18(42):424028, 2007.

117. B. Kersting. Self-assembly of organo-sulfur, selenium and tellurium compounds *via* π stacking and hydrogen bonding interactions. *Zeitschrift für Naturforschung*, 57(b):1115, 2002.

118. M. F. Calhoun, J. Sanchez, D. Olaya, M. E. Gershenson, and V. Podzorov. Electronic functionalization of the surface of organic semiconductors with self-assembled monolayers. *Nature Materials*, 7(1):84, 2008.

119. S. Gupta. Self-assembled and electrochemically deposited mono/multilayers for molecular electronics applications. *Applied Surface Science*, 256(2):407, 2009.

120. J. S. Schumm, D. L. Pearson, L. Jones II, R. Hara, and J. M. Tour. Potential molecular wires and molecular alligator clips. *Nanotechnology*, 7(4):430, 1999.

121. C. Shen, M. Buck, J. D. E. T. Wilton-Ely, T. Weidner, and M. Zharnikov. On the importance of purity for the formation of self-assembled monolayers from thiocyanates. *Langmuir*, 24(13):6609, 2008.

122. G. E. Poirier and E. D. Pylant. The self-assembly mechanism of alkanethiols on Au(111). *Science*, 272(5265):1145, 1996.

123. J. Zhang, J. Zhao, H. Zhang, H. Li, and Z. Liu. Effect of the molecular interaction on molecular packing and orientation in azobenzene-functionalized self-assembled monolayers on gold. *Thin Solid Films*, 327-329:195, 1998.

124. Y. Qi, X. Liu, B. L. M. Hendriksen, V. Navarro, J. Y. Park, I. Ratera, J. M. Klopp, C. Edder, F. J. Himpsel, J. M. J. Fréchet, E. E. Haller, and M. Salmeron. Influence of molecular ordering on electrical and friction properties of ω-(trans-4-stilbene)alkylthiol self-assembled monolayers on Au(111). *Langmuir*, 26(21):16522, 2010.

125. D. J. Lavrich, S. M. Wetterer, S. L. Bernasek, and G. Scoles. Physisorption and chemisorption of alkanethiols and alkyl sulfides on Au(111). *The Journal of Physical Chemistry B*, 102(18):3456, 1998.

126. M. Roper, M. Skegg, C. Fisher, J. Lee, V. Dhanak, D. Woodruff, and R. G. Jones. Atop adsorption site of sulphur head groups in gold-thiolate self-assembled monolayers. *Chemical Physics Letters*, 389(1-3):87, 2004.

127. P. Maksymovych, D. C. Sorescu, and J. T. Yates. Methanethiolate adsorption site on Au(111): a combined STM/DFT study at the single-molecule level. *Journal of Physical Chemistry B*, 110(42):21161, 2006.

128. P. Maksymovych and J. T. Yates. Au adatoms in self-assembly of benzenethiol on the Au(111) surface. *Journal of the American Chemical Society*, 130(24):7518, 2008.

129. I. Langmuir. The constitution and fundamental properties of solids and liquids. part i. solids. *Journal of the American Chemical Society*, 38(11):2221, 1916.

130. C. A. Widrig, C. Chung, and M. D. Porter. The electrochemical desorption of n-alkanethiol monolayers from polycrystalline Au and Ag electrodes. *Journal of Electroanalytical Chemistry and Interfacial Electrochemistry*, 310(1-2):335, 1991.

131. S. Coe-Sullivan, J. S. Steckel, W.-K. Woo, M. G. Bawendi, and V. Bulović. Large-area ordered quantum-dot monolayers *via* phase separation during spin-casting. *Advanced Functional Materials*, 15(7):1117, 2005.

132. A. J. Steckl and R. Birkhahn. Visible emission from Er-doped GaN grown by solid source molecular beam epitaxy. *Applied Physics Letters*, 73(12):1700, 1998.

133. G. Decher, Y. Lvov, and J. Schmitt. Proof of multilayer structural organization in self-assembled polycation-polyanion molecular films. *Thin Solid Films*, 244(1-2):772, 1994.

134. C. F. J. Faul. Ionic self-assembled molecular receptor-based liquid crystals with tripeptide recognition capabilities. *Journal of Materials Chemistry*, 18(25):2962, 2008.

135. G. J. Ashwell, J. Ewington, and B. J. Robinson. Organic rectifying junctions fabricated by ionic coupling. *Chemical Communications*, (6):618, 2006.

136. J. Tang, Y. Wang, C. Nuckolls, and S. J. Wind. Chemically responsive molecular transistors fabricated by self-aligned lithography and chemical self-assembly. *Journal of Vacuum Science and Technology B*, 24(6):3227, 2006.

137. J. Tang, Y. Wang, J. E. Klare, G. S. Tulevski, S. J. Wind, and C. Nuckolls. Encoding molecular-wire formation within nanoscale sockets. *Angewandte Chemie International Edition*, 46(21):3892, 2007.

138. J. E. Klare, G. S. Tulevski, and C. Nuckolls. Chemical reactions with upright monolayers of cruciform π-systems. *Langmuir*, 20(23):10068, 2004.

139. P. W. Loscutoff, H. Zhou, S. B. Clendenning, and S. F. Bent. Formation of organic nanoscale laminates and blends by molecular layer deposition. *ACS Nano*, 4(1):331, 2010.

140. K. Slowinski, R. V. Chamberlain, R. Bilewicz, and M. Majda. Evidence for inefficient chain-to-chain coupling in electron tunneling through liquid alkanethiol monolayer films on mercury. *Journal of the American Chemical Society*, 118(19):4709, 1996.

141. K. Slowinski, H. K. Y. Fong, and M. Majda. Mercury–mercury tunneling junctions 1. electron tunneling across symmetric and asymmetric alkanethiolate bilayers. *Journal of the American Chemical Society*, 121(31):7257, 1999.

142. E. A. Weiss, R. C. Chiechi, G. K. Kaufman, J. K. Kriebel, Z. Li, M. Duati, M. A. Rampi, and G. M. Whitesides. Influence of defects on the electrical characteristics of mercury-drop junctions: self-assembled monolayers of n-alkanethiolates on rough and smooth silver. *Journal of the American Chemical Society*, 129(14):4336, 2007.

143. N. Néel. Conductance of single atoms and molecules studied with a scanning tunnelling microscope. *Nanotechnology*, 18(4):044027, 2007.

144. M. C. Petty. *Molecular Electronics: From Principles to Practice.* John Wiley & Sons Ltd., 2007.

145. W. Haiss, R. J. Nichols, H. van Zalinge, S. J. Higgins, D. Bethell, and D. J. Schiffrin. Measurement of single molecule conductivity using the spontaneous formation of molecular wires. *Physical Chemistry Chemical Physics*, 6(17):4330, 2004.

146. W. Haiss. Thermal gating of the single molecule conductance of alkanedithiols. *Faraday Discussions*, 131:253, 2006.

147. C. Xu, H. van Zalinge, J. L. Pearson, A. Glidle, J. M. Cooper, D. R. S. Cumming, W. Haiss, J. Yao, D. J. Schiffrin, M. Proupín-Pérez, R. Cosstick, and R. J. Nichols. A combined top-down bottom-up approach for introducing nanoparticle networks into nanoelectrode gaps. *Nanotechnology*, 17(14):3333, 2006.

148. W. Haiss, C. Wang, R. Jitchati, I. Grace, S. Martín, A. S. Batsanov, S. J. Higgins, M. R. Bryce, C. J. Lambert, P. S. Jensen, and R. J. Nichols. Variable contact gap single-molecule conductance determination for a series of conjugated molecular bridges. *Journal of Physics: Condensed Matter*, 20(37):374119, 2008.

149. D. S. Seferos, S. A. Trammell, G. C. Bazan, and J. G. Kushmerick. Probing π-coupling in molecular junctions. *Proceedings of the National Academy of Science of the United States of America*, 102(25):8821, 2005.

150. G. J. Ashwell, P. Wierzchowiec, C. J. Bartlett, and P. D. Buckle. Molecular electronics: connection across nano-sized electrode gaps. *Chemical Communications*, (12):1254, 2007.

151. A. S. Blum, J. G. Kushmerick, S. K. Pollack, J. C. Yang, M. Moore, J. Naciri, R. Shashidhar, and B. R. Ratna. Charge transport and scaling in molecular wires. *The Journal of Physical Chemistry B*, 108(47):18124, 2004.

152. J. J. Kushmerick, S. K. Pollack, J. C. Yang, J. Naciri, D. B. Holt, M. A. Ratner, and R. Shashidhar. Understanding charge transport in molecular electronics. *Annals of the New York Academy of Sciences*, 1006(1):277, 2003.

153. E. H. Huisman, M. L. Trouwborst, F. L. Bakker, B. de Boer, B. J. van Wees, and S. J. van der Molen. Stabilizing single atom contacts by molecular bridge formation. *Nano Letters*, 8(10):3381, 2008.

154. F. O. Hadeed. Controlled fabrication of 1–2 nm nanogaps by electromigration in gold and gold-palladium nanowires. *Applied Physics Letters*, 91(12):123120, 2007.

155. A. K. Mahapatro, S. Ghosh, and D. B. Janes. Nanometer scale electrode separation (nanogap) using electromigration at room temperature. *IEEE Transactions on Nanotechnology*, 5:232, 2006.

156. L. Ke. Breakdown of a gold nanowire between electrodes. *Nanotechnology*, 18(42):424002, 2007.

157. Q. Pu. Molecular simulations of stretching gold nanowires in solvents. *Nanotechnology*, 18(42):424007, 2007.

158. A. Thiess, Y. Mokrousov, S. Blügel, and S. Heinze. Theory and application of chain formation in break junctions. *Nano Letters*, 8(8):2144, 2008.

159. J. van Ruitenbeek, E. Scheer, and H. B. Weber. Contacting individual molecules using mechanically controllable break junctions. In *Introducing Molecular Electronics*, volume 680 of *Lecture Notes in Physics*, chapter 9, page 253. Springer Berlin, 2006.

160. L. Romaner, G. Heimel, M. Gruber, J.-L. Brédas, and E. Zojer. Stretching and breaking of a molecular junction. *Small*, 2(12):1468, 2006.

161. M. A. Reed, C. Zhou, C. Muller, T. Burgin, and J. Tour. Conductance of a molecular junction. *Science*, 278(5336):252, 1997.

162. J. Reichert, R. Ochs, D. Beckmann, H. Weber, M. Mayor, and H. Löhneysen. Driving current through single organic molecules. *Physical Review Letters*, 88(17):176804, 2002.

163. D. R. Strachan, D. E. Smith, D. E. Johnston, T.-H. Park, M. J. Therien, D. A. Bonnell, and A. T. Johnson. Controlled fabrication of nanogaps in ambient environment for molecular electronics. *Applied Physics Letters*, 86(4):043109, 2005.

164. J. Park. Wiring up single molecules. *Thin Solid Films*, 438-439:457, 2003.

165. Y. Noguchi, T. Nagase, T. Kubota, T. Kamikado, and S. Mashiko. Fabrication of Au–molecule–Au junctions using electromigration method. *Thin Solid Films*, 499(1-2):90, 2006.

166. R. Sordan. Coulomb blockade phenomena in electromigration break junctions. *Applied Physics Letters*, 87(1):013106, 2005.

167. K. O'Neill, E. A. Osorio, and H. Zant. Self-breaking in planar few-atom Au constrictions for nm-spaced electrodes. *Applied Physics Letters*, 90(13):133109, 2007.

168. Y. S. Park, A. C. Whalley, M. Kamenetska, M. L. Steigerwald, M. S. Hybertsen, C. Nuckolls, and L. Venkataraman. Contact chemistry and single-molecule conductance: a comparison of phosphines, methyl sulfides, and amines. *Journal of the American Chemical Society*, 129(51):15768, 2007.

169. J. Hihath and N. Tao. Rapid measurement of single-molecule conductance. *Nanotechnology*, 19(26):265204, 2008.

170. Z. Huang, F. Chen, P. A. Bennett, and N. Tao. Single molecule junctions formed *via* Au-thiol contact: stability and breakdown mechanism. *Journal of the American Chemical Society*, 129(43):13225, 2007.

171. N. Zhitenev, H. Meng, and Z. Bao. Conductance of small molecular junctions. *Physical Review Letters*, 88(22), 2002.

172. Y. Otsuka, Y. Naitoh, T. Matsumoto, W. Mizutani, H. Tabata, and T. Kawai. A simple fabrication method of nanogap electrodes for top-contacted geometry: application to porphyrin nanorods and a DNA network. *Nanotechnology*, 15(11):1639, 2004.

173. G. J. Ashwell, L. J. Phillips, B. J. Robinson, B. Urasinska-Wojcik, C. J. Lambert, I. M. Grace, M. R. Bryce, R. Jitchati, M. Tavasli, T. I. Cox, I. C. Sage, R. P. Tuffin, and S. Ray. Molecular bridging of silicon nanogaps. *ACS Nano*, 4(12):7401, 2010.

174. G. Ashwell, L. Phillips, B. Robinson, S. Barnes, A. Williams, C. Lambert, I. Grace, T. Cox, and I. Sage. Silicon nanogap bridged by a 2.85 nm long molecular wire. *Angewandte Chemie International Edition*, under submission.

175. G. J. Ashwell, B. Urasinska-Wojcik, and L. J. Phillips. *In Situ* stepwise synthesis of functional multijunction molecular wires on gold electrodes and gold nanoparticles. *Angewandte Chemie International Edition*, 49(20):3508, 2010.

176. H. Amekura, N. Umeda, and N. Kishimoto. Near-surface sensitive infrared reflection spectroscopy on SiO_2 implanted with high-flux negative ions. *Vacuum*, 74(3-4):549, 2004.

177. G. Dufour, F. Rochet, F. Stedile, C. Poncey, M. De Crescenzi, R. Gunnella, and M. Froment. SiC formation by reaction of Si(001) with acetylene: Electronic structure and growth mode. *Physical Review B*, 56(7):4266, 1997.

178. R. Hofman, J. G. F. Westheim, I. Pouwel, T. Fransen, and P. J. Gellings. FTIR and XPS studies on corrosion-resistant SiO_2 coatings as a function of the humidity during deposition. *Surface and Interface Analysis*, 24(1):1, 1996.

179. K. D. Schierbaum, T. Weiss, E. U. van Veizen, J. F. Engbersen, D. N. Reinhoudt, and W. Göpel. Molecular recognition by self-assembled monolayers of cavitand receptors. *Science*, 265(5177):1413, 1994.

180. A. Stanchev, V. Ignatova, and C. Ghelev. A novel approach to angular-resolved X-ray photoelectron spectroscopy depth-profiling. *Nuclear Instruments and Methods in Physics Research Section B*, 166-167:350, 2000.

181. D. Langstaff, A. Bushell, T. Chase, and D. Evans. A fully integrated multi-channel detector for electron spectroscopy. *Nuclear Instruments and Methods in Physics Research Section B*, 238(1-4):219, 2005.

182. D. A. Evans, O. R. Roberts, A. R. Vearey-Roberts, D. P. Langstaff, D. J. Twitchen, and M. Schwitters. Direct observation of Schottky to Ohmic transition in Al-diamond contacts using real-time photoelectron spectroscopy. *Applied Physics Letters*, 91(13):132114, 2007.

183. D. J. Wold and C. D. Frisbie. Fabrication and characterization of metal–molecule–metal junctions by conducting probe atomic force microscopy. *Journal of the American Chemical Society*, 123(23):5549, 2001.

184. T. W. Kelley, E. Granstrom, and C. D. Frisbie. Conducting probe atomic force microscopy: A characterization tool for molecular electronics. *Advanced Materials*, 11(3):261, 1999.

185. G. J. Ashwell, A. T. Williams, S. A. Barnes, S. L. Chappell, L. J. Phillips, B. J. Robinson, B. Urasinska-Wojcik, P. Wierzchowiec, I. R. Gentle, and B. J. Wood. Self-assembly of amino–thiols *via* gold–nitrogen links and consequence for *in situ* elongation of molecular wires on surface-modified electrodes. *The Journal of Physical Chemistry C*, 115(10):4200, 2011.

186. D. Neher. Polyfluorene homopolymers: Conjugated liquid-crystalline polymers for bright blue emission and polarized electroluminescence. *Macromolecular Rapid Communications*, 22(17):1365, 2001.

187. U. Scherf and E. List. Semiconducting polyfluorenes - towards reliable structure-property relationships. *Advanced Materials*, 14(7):477, 2002.

188. A. Donat-Bouillud, I. Lévesque, Y. Tao, M. D'Iorio, S. Beaupré, P. Blondin, M. Ranger, J. Bouchard, and M. Leclerc. Light-emitting diodes from fluorene-based π-conjugated polymers. *Chemistry of Materials*, 12(7):1931, 2000.

189. S. Bettington, M. Tavasli, M. R. Bryce, A. Beeby, H. Al-Attar, and A. P. Monkman. Tris-cyclometalated iridium(III) complexes of carbazole(fluorenyl)pyridine ligands: synthesis, redox and photophysical properties, and electrophosphorescent light-emitting diodes. *Chemistry - A European Journal*, 13(5):1423, 2007.

190. F. B. Dias, S. Pollock, G. Hedley, L.-O. Pålsson, A. Monkman, I. I. Perepichka, I. F. Perepichka, M. Tavasli, and M. R. Bryce. Intramolecular charge transfer assisted by conformational changes in the excited state of fluorene-dibenzothiophene-S,S-dioxide co-oligomers. *Journal of Physical Chemistry B*, 110(39):19329, 2006.

191. L. Lafferentz, F. Ample, H. Yu, S. Hecht, C. Joachim, and L. Grill. Conductance of a single conjugated polymer as a continuous function of its length. *Science*, 323(5918):1193, 2009.

192. C. Wang, M. R. Bryce, J. Gigon, G. J. Ashwell, I. Grace, and C. J. Lambert. Synthesis and properties of functionalized 4 nm scale molecular wires with thiolated termini for self-assembly onto metal surfaces. *Journal of Organic Chemistry*, 73(13):4810, 2008.

193. T. Papadopoulos, I. Grace, and C. Lambert. Control of electron transport through fano resonances in molecular wires. *Physical Review B*, 74(19), 2006.

194. M. H. Schoenfisch and J. E. Pemberton. Air stability of alkanethiol self-assembled monolayers on silver and gold surfaces. *Journal of the American Chemical Society*, 120(18):4502, 1998.

195. G. E. Poirier, T. M. Herne, C. C. Miller, and M. J. Tarlov. Molecular-scale characterization of the reaction of ozone with decanethiol monolayers on Au(111). *Journal of the American Chemical Society*, 121(41):9703, 1999.

196. J. Kim, E. Samano, and B. E. Koel. CO adsorption and reaction on clean and oxygen-covered Au(211) surfaces. *Journal of Physical Chemistry B*, 110(35):17512, 2006.

197. M. J. Tarlov, D. R. F. Burgess, and G. Gillen. UV photopatterning of alkanethiolate monolayers self-assembled on gold and silver. *Journal of the American Chemical Society*, 115(12):5305, 1993.

198. C. D. Bain and G. M. Whitesides. Attenuation lengths of photoelectrons in hydrocarbon films. *The Journal of Physical Chemistry*, 93(4):1670, 1989.

199. G. J. Ashwell, P. Wierzchowiec, L. J. Phillips, C. J. Collins, J. Gigon, B. J. Robinson, C. M. Finch, I. R. Grace, C. J. Lambert, P. D. Buckle, K. Ford, B. J. Wood, and I. R. Gentle. Functional molecular wires. *Physical Chemistry Chemical Physics*, 10(14):1859, 2008.

200. D. A. Corley, T. He, and J. M. Tour. Two-terminal molecular memories from solution-deposited C_{60} films in vertical silicon nanogaps. *ACS Nano*, 4(4):1879, 2010.

201. S. W. Howell, S. M. Dirk, K. Childs, H. Pang, M. Blain, R. J. Simonson, J. M. Tour, and D. R. Wheeler. Mass-fabricated one-dimensional silicon nanogaps for hybrid organic/nanoparticle arrays. *Nanotechnology*, 16(6):754, 2005.

202. I. M. Grace, S. W. Bailey, J. Jefferson, and C. J. Lambert. Electron transport through single molecular wires. *Materials Science-Poland*, 22(4):509, 2004.

203. A. Rocha, V. García-Suárez, S. Bailey, C. Lambert, J. Ferrer, and S. Sanvito. Spin and molecular electronics in atomically generated orbital landscapes. *Physical Review B*, 73(8), 2006.

204. J. M. Soler, E. Artacho, J. D. Gale, A. García, J. Junquera, P. Ordejón, and D. Sánchez-Portal. The SIESTA method for *Ab Initio* order-N materials simulation. *Journal of Physics: Condensed Matter*, 14(11):2745, 2002.